

NASA  
CR  
3544  
c.1

# NASA Contractor Report 3544

LOAN COPY: RETURN TO  
NASA TECHNICAL LIBRARY  
Kirtland AFB, NM



TECH LIBRARY KAFB, NM

## Goertler Instability in Compressible Boundary Layers Along Curved Surfaces With Suction and Cooling

LOAN COPY: RETURN TO  
NASA TECHNICAL LIBRARY  
Kirtland AFB, NM

Nabil El-Hady and Alok K. Verma

GRANT NSG-1645  
APRIL 1982

FOR EARLY DOMESTIC DISSEMINATION  
Because of its significant early commercial potential, this information, which has been developed under a U.S. Government program, is being disseminated within the United States in advance of general publication. This information may be duplicated and used by the recipient within the United States limitation that it not be published. Release of this information to other domestic parties by the recipient shall be made subject to these limitations.  
Foreign release may be made only with the approval and appropriate export licenses by the recipient of this information. This legend shall be marked on any reproduction of this information in whole or in part.

Review for general release

April 30, 1983

NASA



0062199

## NASA Contractor Report 3544

# Goertler Instability in Compressible Boundary Layers Along Curved Surfaces With Suction and Cooling

Nabil El-Hady and Alok K. Verma

*Old Dominion University  
Norfolk, Virginia*

Prepared for  
Langley Research Center  
under Grant NSG-1645



National Aeronautics  
and Space Administration

**Scientific and Technical  
Information Office**

1982



## TABLE OF CONTENTS

LIST OF FIGURES .....	v
NOMENCLATURE .....	viii
CHAPTER	
I. INTRODUCTION .....	1
II. PROBLEM FORMULATION .....	8
2.1 The Mean Flow .....	9
2.2 The Disturbance Flow .....	11
III. COMPUTATIONAL AND NUMERICAL PROCEDURE .....	17
3.1 Eigenvalues and Eigenvectors .....	20
3.2 Boundary Conditions .....	22
3.3 Numerical Procedure .....	22
3.4 Adjoint Problem .....	23
IV. NUMERICAL RESULTS AND DISCUSSION .....	24
4.1 Effect of Compressibility on the Neutral Curve .....	24
4.2 Growth Rates of Goertler Vortices .....	26
4.3 Effect of Thermal Disturbance Boundary Condition at the Wall on the Stability Characteristics .....	28
4.4 Effect of Compressibility on Eigenfunctions .....	29
4.5 Effect of Compressibility on the Amplitude Ratio ...	30
4.6 Effect of Suction on Stability .....	32
4.7 Effect of Wall Cooling on Stability .....	34

V. CONCLUSIONS .....	39
REFERENCES .....	42
FIGURES .....	48
APPENDIX A -- Dimensional Field Equations for Compressible Flow ..	82
APPENDIX B -- Compressible Boundary Layer Equations .....	84
APPENDIX C -- Eigenvector Matrix when $\lambda_2$ and $\lambda_6$ are repeated .....	85
APPENDIX D -- Eigenvector Matrix when $\lambda_1$ , $\lambda_2$ , $\lambda_3$ , and $\lambda_4$ are repeated	86
APPENDIX E -- Eigenvector Matrix for the Adjoint Problem .....	87
APPENDIX F -- FORTRAN Program for the Stability Analysis .....	89

## LIST OF FIGURES

<u>FIG. NO.</u>	<u>FIGURE TITLE</u>	
1	Body oriented coordinate system. . . . .	48
2	Coordinate system based on streamlines and potential lines. . . . .	48
3	Goertler vortices in a flow along a concave wall. . . . .	49
4	Effect of compressibility on neutral stability curve. . . . .	50
5	Effect of mean density, mean viscosity, and disturbance viscosity on minimum critical Goertler number. . . . .	51
6	Variation of mean density and viscosity in the boundary layer. . . . .	52
7	Contours of constant growth rates at $M_{\infty}=0$	53
8	Contours of constant growth rates at $M_{\infty}=1$ .	54
9	Contours of constant growth rates at $M_{\infty}=2$ .	55
10	Contours of constant growth rates at $M_{\infty}=3$	56
11	Contours of constant growth rates at $M_{\infty}=4$ .	57
12	Contours of constant growth rates at $M_{\infty}=5$ .	58
13	Effect of compressibility on the variation of vortex growth rate with Goertler number.	59
14	Effect of compressibility on local stability.	60
15	Effect of the wall boundary condition of the thermal disturbance on stability characteristics.	61

16	Effect of compressibility on the shape of eigenfunctions for a disturbance having a wave-number 0.3 and a growth rate 5.	62
17	Effect of compressibility on the maximum amplitude ratio calculated along a growth path of constant wavelength $\Lambda$ .	63
18	Effect of compressibility on the amplitude ratio calculated along the locus of maximum growth rates.	64
19	Neutral stability curves for different values of the suction parameter at $M_\infty=0.8$ .	65
20	Neutral stability curves for different values of the suction parameter at $M_\infty=3.0$ .	66
21	Effect of suction on critical Goertler number at different Mach numbers.	67
22	Contours of constant growth rates at $M_\infty=3$ and suction parameter $\gamma=-1.2$ .	68
23	Contours of constant growth rates at $M_\infty=3$ and suction parameter $\gamma=-1.6$ .	69
24	Effect of suction on the amplitude ratio calculated along the locus of maximum growth rates at $M_\infty=3$ .	70
25	Effect of suction on the amplitude ratio at $G=20$ for different Mach numbers.	71
26	Effect of suction at $M_\infty = 3$ on the shape of the eigenfunctions for a disturbance having wave-number 0.3 and zero growth rate.	72
27	Neutral stability curves for different cooling rates at $M_\infty=3$ .	73

28	Contours of constant growth rates at $M_{\infty}=3$ and $\theta_w/\theta_{ad}=0.75.$	74
29	Contours of constant growth rates at $M_{\infty}=3$ and $\theta_w/\theta_{ad}=0.25.$	75
30	Contours of constant growth rates at $M_{\infty}=3$ and $\theta_w/\theta_{ad}=0.15.$	76
31	Effect of cooling on local stability.	77
32	Effect of cooling on the amplitude ratio calculated along the locus of maximum growth rates at $M_{\infty}=3.$	78
33	Effect of cooling on the amplitude ratio at $G=20$ for different Mach numbers.	79
34	Variation of mean density and viscosity for different cooling rates , at $M_{\infty} = 3.$	80
35	Effect of cooling at $M_{\infty} = 3$ on the shape of eigenfunctions for a disturbance having a wavenumber 0.3 and zero growth rate..	81

## NOMENCLATURE

<u>Symbol</u>	<u>Explanation</u>
$a_{mn}$	Variable coefficient matrix
$a^*_{mn}$	Constant coefficient matrix
$c_n$	Arbitrary constant vector
$D_{mn}$	Characteristic eigenvector matrix
$G$	Goertler number; $G = Rk$
$G_c$	Critical Goertler number
$h$	Metric coefficient
$K$	Wall curvature; $K^* = 1/r^*$
$k$	Small curvature parameter; $k = (L^*K^*)^{1/2}$
$L$	Characteristic length
$M$	Mach number
$P$	Mean flow pressure
$p$	Disturbance pressure
$R$	Reynolds number; $R = U_\infty^* L^* / v_\infty^*$
$r$	Radius of curvature
$U$	Streamwise component of mean velocity
$V$	Normal component of mean velocity
$W$	Spanwise component of mean velocity
$u$	Streamwise component of disturbance velocity
$v$	Normal component of disturbance velocity
$w$	Spanwise component of disturbance velocity

<u>Symbol</u>	<u>Explanation</u>
X	Coordinate in the streamwise direction
Y	Coordinate normal to the wall
Z	Coordinate in the spanwise direction
$\frac{l_n}{a_0}$	Amplitude ratio
v	Kinematic viscosity
$\epsilon$	Small viscous parameter; $\epsilon = 1/R$
$\gamma$	Suction parameter; $\gamma = \frac{(\rho^* v^*)_w}{(\rho^* U^*)_\infty} R$
$\bar{\rho}$	Mean flow density
$\rho$	Disturbance density
$\theta$	Nondimensional mean flow temperature (See Appendix B)
$\theta'$	Disturbance temperature
$\Gamma$	Prandtl number
$\mu$	Viscosity
$\tilde{\mu}$	Derivative of mean flow viscosity with respect to mean temperature
$\beta$	Nondimensional wave number in the spanwise direction
$\sigma$	Spatial growth rate
$\lambda n$	Eigenvalue
$\delta_1$	Displacement thickness
$\delta_2$	Momentum thickness
$\lambda$	Wavelength of vortices (See Figure 3)

<u>Symbol</u>	<u>Explanation</u>
$\Lambda$	Nondimensional wavelength parameter $\Lambda = \frac{U_\infty \lambda}{v_\infty} (\frac{\lambda}{r})^{1/2}$
$\theta_w/\theta_{ad}$	Wall cooling parameter

### Superscripts

*	Dimensional quantity
^	Amplitude of disturbance quantity (Eq. 15) or total disturbance quantity (Eq. 6)

### Subscripts

$\infty$	Free-stream conditions
e	Boundary layer edge conditions
w	Wall conditions
x	Derivative in the streamwise direction
y	Derivative in the normal direction
z	Derivative in the spanwise direction

## CHAPTER I

### INTRODUCTION

Instability of viscous flows along concave surfaces, like that between rotating concentric cylinders, is controlled by the balance of induced centrifugal forces and other forces acting on the flow. The criteria for instability for such systems was first postulated by Rayleigh (1916) for inviscid flows, and examined both theoretically and experimentally by Taylor (1923) for circular Couette flow, while Goertler (1954) investigated the mode of motion in a boundary layer along a concave surface. Centrifugal forces induced by curvature effects in these systems lead to the instability of the flow in the form of counter-rotating, vortex-like disturbances.

Earlier transition measurements in the incompressible boundary layer next to a concave surface, indicate a steady three-dimensional vortex-like disturbance with a spanwise periodicity which develops according to the linearized theory. Gregory and Walker (1956) were the first to observe traces of these vortices by using the China-Clay technique, followed by Aihara (1962) and Tani and Sakagami (1962) using colored liquids and smoke threads, and Aihara (1961) and Tani (1961) using hot-wire measurements. Wortmann (1964) used the telurium method to visualize these vortices in a water tunnel. Bippes (1978) and Bippes and Goertler (1972) presented detailed observations of these vortices using the hydrogen-bubble technique. At compressible speeds, evidence of the vortex-like disturbances has been observed by Persen (1968) and Ginoux (1970) in quasi two-dimensional flows in regions of separated flow reattachments. Zakkay and Calarese (1972) observed the presence of these vortices in a hypersonic turbulent

boundary layer over an axisymmetric configuration with adverse pressure gradient. In their experiments in two Mach 5 nozzles, Beckwith and Holley (1981) showed by using oil flow patterns that these vortices persisted to the nozzle exit and that the vortices were involved in the transition process.

Available experimental evidence has shown that the counter-rotating vortices affect indirectly the transition from laminar to turbulent flow on a concave surface. As steady vortices, they may not lead to transition by themselves, but when their growth becomes strong enough, they do cause transition by an unknown mechanism. Transition over a concave surface occurs at Reynolds numbers that are lower than those for flow over a convex or flat surfaces (Clauser and Clauser, 1937). Moreover, the Goertler number (the nondimensional parameter of interest in this type of problems) has to reach a certain critical value before transition takes place over a constant curvature surface (Liepmann, 1945). Tani indicated that, although their growth is small these vortices cause spanwise variation in the velocity field, thus modifying the development of unstable waves. Wortmann (1969) concluded that transition was lead by a secondary instability that he observed following the appearance of the counter-rotating vortices. On the other hand, the observations of Bippes (1978) and Aihara (1976) of a sinusoidal motion of the vortex axes before turbulence sets in lead Aihara to correlate that with a nonlinear theory. Nayfeh (1979) studied the effect of these vortices on Tollmien-Schlichting waves, and showed that these vortices have a strong tendency to amplify three-dimensional waves having a spanwise wavelength that is twice the wavelength of the vortices.

The instability of boundary layer flow on curved surfaces was first

demonstrated theoretically by Goertler (1954) for incompressible flows, where he showed that a system of counter-rotating vortices were formed parallel and oriented in the streamwise direction. These vortices are referred to as Taylor-Goertler vortices or also as Goertler vortices. In his analysis, Goertler assumed the boundary layer to be parallel, streamwise curvature to be constant with the distance normal to the surface, and the vortices to be confined to the boundary layer. In an attempt to relax these assumptions, several investigators followed Goertler and extended his analysis for incompressible flows. A detailed review of these efforts is given by Herbert (1976) and Floryan and Saric (1979).

Various theoretical investigations were performed to provide an accurate mathematical model of the instability nearer to the physical reality. Various investigators used the body oriented coordinate system 1 with some assumptions regarding the variation of curvature in the direction normal to the flow. The governing equations written in the body oriented coordinate system contain the terms  $(1 - Ky)^{-n}$ , where K is the curvature of the surface, and y is the coordinate normal to the curved surface. These terms present a singularity when  $Ky = 0(1)$ . Goertler (1954) assumed that these terms can be replaced by 1, that is streamline curvature is constant at any normal distance. Smith (1955) and Kahawita and Meroney (1977) expanded these terms binomially and kept the first two terms, i.e.  $(1 + nKy)$ , thus effectively transferring the singularity to infinity. Floryan and Saric (1979) gave a brief description of different approaches used in the past using body oriented coordinate system and utilized a new system of coordinate based on the streamlines and potential lines of the inviscid flow over the curved surface.

A typical illustration of this coordinate system is shown in Fig. 2 for a circular arc. The shape of the streamline is directly related to the system of coordinates. Consequently, different treatments of the streamline curvature are expected to influence the stability characteristics of the flow because they are equivalent to changes in the outer flow conditions. Larger rates of decay of curvature outside the boundary layer causes a reduction of the driving centrifugal forces in the outer flow. A similar situation exists by decreasing the streamwise extent of the curved flow region (see Herbert, 1976). Both factors considerably stabilize the flow.

The effect of boundary-layer growth was introduced by several researchers (e.g. Smith, 1955; Kahawita and Meroney, 1977; Herbert, 1976; Floryan and Saric, 1979; Ragab and Nayfeh, 1980). The inclusion of the normal velocity component of the basic flow in the analysis drastically changes the location of the neutral curve. Moreover, the streamwise variation of the normal velocity component which appears in the leading order stability equations has a strong influence on the stability characteristics. While Smith incorporated the normal velocity component of the basic flow with some of the higher order curvature terms, Floryan and Saric based the scaling of the normal disturbance velocity component on a viscous scale that contributed a leading order effect of the normal velocity component of the basic flow and its streamwise variation on the stability analysis.

In spite of the extensive investigations of Goertler instability in incompressible flows, there have been only a limited number of studies on the effect of compressibility of the basic flow on this type of disturbance. The compressible linear stability theory now available (Hammerlin, Aihara, 1961; and Kobayashi and Kohama, 1977) for the development of these

vortices is not reliable and far from being complete. It 5

neglects the normal velocity component of the basic flow that proved to have a profound effect in reducing the stability of incompressible flows. Existing compressible theories treat only the neutral stability case which is of limited importance regarding vortex development, possible nonlinear interactions, and transition correlation.

In his compressible stability analysis of boundary layer flow along a concave surface, Hammerlin expanded the disturbance equations in power series of the square of the freestream Mach number. He kept terms to  $O(M_\infty^2)$ , and obtained a solution to the disturbance equations which is valid only for  $M_\infty \ll 1$ . He used a power law for the viscosity-temperature relation and kept Prandtl number constant in the calculations. His results indicated that minimum critical Goertler number increases as Mach number increases. Aihara reduced the perturbation equations into two extreme cases of the freestream Mach number, namely,  $M_\infty \ll 1$ , and  $M_\infty \gg 1$ . In his analysis, he assumed constant viscosity and Prandtl number. His results shows that minimum critical Goertler number decreases as Mach number increases, that is, compressibility effect on the stability of the boundary layer is opposite to that predicted by Hammerlin. Kobayashi and Kohama treated the problem over a wide range of Mach numbers. They used Sutherland's formula for the temperature dependence of the viscosity and assumed constant Prandtl number and specific heat. They treated only the neutrally stable disturbances showing that the boundary layer becomes more stable (Goertler number increases) as Mach number increases.

Kobayashi (1972,73,74) was the first to examine the effects of suction on the stability characteristics of a laminar incompressible boundary layer along curved surfaces. Although his analysis excluded the

effect of normal component of mean velocity due to boundary layer growth, it gave insight into the effect of the presence of this velocity component due to suction. Using homogeneous suctions Kobayashi found that the laminar boundary layer is stabilized (critical Goertler number increases). However, the changes in the critical Goertler number remains much less than the changes in the critical Reynolds number for the Tollmien-Schlichting instabilities due to homogeneous suction (Hughes and Reid, 1965). So, Goertler instability will probably predominate in the laminar boundary layer along the concave wall with suction. Floryan and Saric (1979) and Floryan (1980) included the normal component of the mean velocity in their analysis and examined the case of self similar suction and came to the same conclusion.

DiPrima and Dunn (1956) examined the effect of cooling and heating on the stability characteristics of laminar liquid boundary layer over curved surface. Since their analysis was done for liquids, they neglected the viscous dissipation and variations in density and came to a conclusion that heating or cooling has very slight influence on Goertler instability. For compressible boundary layer, Kobayashi and Kohama (1977) found that for isothermal walls the ratios of wall to freestream temperature has less effect on the critical value of Goertler number as Mach number is increased.

In this article, a basic approximation to a compressible linear stability theory is developed for three-dimensional longitudinal type vortices in two-dimensional compressible boundary layers along curved surfaces.

The effect of compressibility on the critical stability limit, growth rates, and amplitude ratios of the vortices is evaluated over a range of Mach numbers from 0 to 5. The effect of boundary layer growth is

included in the analysis. The effect of wall cooling and suction on the development of Goertler velocities in a compressible boundary layer is examined. In Chapter II, a formulation of the stability problem is introduced. In Chapter III, the method of solution and numerical procedures are outlined. A discussion of the numerical results is given in Chapter IV and conclusions are in Chapter V.

## CHAPTER II

PROBLEM FORMULATION

The Spatial three-dimensional stability of laminar incompressible and compressible two-dimensional boundary layers along a slightly curved wall is considered. The wall curvature is in the direction of the flow and its variation is assumed to be weak to avoid a nonuniform Mach number distribution along the wall due to the presence of shock waves that might occur in the case of rapid changes.

The flow field is governed by the Navier-Stokes, energy, continuity and state equations written in an orthogonal curvilinear coordinate system. The local curvature of the streamlines enters the field equations through the appropriate coordinate system. Following Floryan and Saric and Ragab and Nayfeh, a coordinate system ( $x$ ,  $y$ ,  $z$ ) based on the streamlines and potential lines of the inviscid flow over a curved surface is used in this analysis. Here  $x$  and  $y$  are in the direction of stream lines and potential lines, respectively, and  $z$  is the coordinate normal to the  $x$ - $y$  plane. Figure 3 shows the direction of the development of Goertler vortices in this coordinate system. This coordinate system has the advantage of a body oriented coordinate system in the wall region and decays to a rectangular Cartesian coordinate system away from the wall.

The compressible field equations written in this coordinate system are presented in Appendix A. The local curvature of the streamlines enters the field equations through the metric coefficients. They are determined from the definition of the

arc length to be  $h$ ,  $h$  and  $l$  in the  $x$ ,  $y$  and  $z$  directions, respectively. The field equations given in Appendix A are used to formulate the disturbance equations.

We consider the basic state to be two-dimensional, viscous, compressible flow over a slightly curved surface. The field equations are made dimensionless using a reference length

$$L^* = (v_\infty^* x^*/U_\infty^*) \quad (1)$$

and  $U_\infty^*$  as reference velocity and  $(\rho^* U^{*2})_\infty$  as reference pressure, where \* indicates a dimensional quantity, and  $v$  is the kinematic viscosity of the fluid. The thermodynamic and transport properties of the fluid are made dimensionless using their corresponding free stream values. With these definitions the characteristic Reynolds number becomes

$$R = (U_\infty^* L^* / v_\infty^*) \quad (2)$$

We define a small viscous parameter  $\epsilon$ , and a small curvature parameter  $k$  as

$$\epsilon = 1/R, k = (L^* K^*)^{1/2} \quad (3)$$

where  $K^*$  is the curvature of the wall. The metric coefficient  $h$  is related to the curvature parameter  $k$  by

$$k^2 = -h_y/h^2 \text{ at } y = 0 \quad (4)$$

## 2.1 The Mean Flow

Van Dyke (1960,62) using a body oriented coordinate system, showed for incompressible and compressible flows that the leading

order approximation of the boundary layer equations is the familiar boundary layer equations on a flat plate.

In terms of the small parameters  $\epsilon$  and  $k$ , Floryan (1980) showed that for incompressible flows the leading order approximation of the boundary layer equations (terms of order  $\epsilon^0$  and  $k^0$ ), when  $\epsilon$  and  $k$  are of the same order, is the conventional boundary layer equations over a flat plate. Modification of the boundary layer profiles due to the curvature comes mainly through the normal pressure gradient. This pressure gradient is  $O(k)$  and it will enter higher order boundary layer.

Because the aim of this study is to provide a basic approximation for the stability of a compressible boundary layer over a curved surface, therefore the basic approximation for the mean flow is required. The compressible boundary layer flow over a flat plate is considered to provide a basic approximation for the stability of the compressible boundary layer over a curved surface. The mean flow profiles are calculated for an adiabatic or isothermal flat plate. In case of suction, a similar suction parameter  $\gamma$  is defined as

$$\gamma = \frac{(\rho^* v^*)_w}{(\rho^* U^*)_\infty} R \quad (5)$$

and is introduced to the boundary layer equations (see Appendix B). Here  $w$  indicates wall conditions, and  $R$  is given in Eq. (2). The fluid is considered to be a perfect gas with all the thermodynamic and transport properties function of temperature. The mean viscosity is related to mean temperature through Sutherland formula. The flow stagnation temperature is kept constant and equal to 310K for all Mach numbers under study.

## 2.2 The Disturbance Flow

A steady three-dimensional small disturbance is superposed on each mean-flow quantity in the following form

$$\hat{u}(x,y,z) = U(x,y) + u(x,y,z) \quad (6a)$$

$$\hat{v}(x,y,z) = V(x,y) + v(x,y,z) \quad (6b)$$

$$\hat{w}(x,y,z) = 0 + w(x,y,z) \quad (6c)$$

$$\hat{p}(x,y,z) = P(x,y) + p(x,y,z) \quad (6d)$$

$$\hat{\theta}(x,y,z) = \Theta(x,y) + \theta(x,y,z) \quad (6e)$$

$$\hat{\rho}(x,y,z) = \bar{\rho}(x,y) + \rho(x,y,z) \quad (6f)$$

$$\hat{\mu}(x,y,z) = \mu(\theta) + \frac{d\mu}{d\theta} \theta(x,y,z) \quad (6g)$$

In the above equations the order of magnitude of the normal mean velocity  $V$  is smaller than  $U$  by the Reynolds number  $R$ , and the disturbance quantities are made dimensionless using

$$\begin{aligned} u &= u^*/U_\infty^*, \quad v = v^*/RU_\infty^*, \quad w = w^*/RU_\infty^*, \\ p &= p^*/R\rho^*U_\infty^{*2}, \quad \theta = \theta^*/\Theta_\infty^*, \quad \rho = \rho^*/\bar{\rho}_\infty^* \end{aligned} \quad (7)$$

The order of magnitude of the disturbance quantities  $v$  and  $w$  differ from the disturbance  $U$  by the Reynolds number  $R$ . The need for different disturbance velocity scaling was recognized by DiPrima and Stuart and observed by Bippes, Bippes and Goertler, and Wortmann in their experiments. Floryan and Saric and Ragab and Nayfeh used this type of scaling and as a result the normal velocity component of the mean flow affected the leading order stability analysis. With this scaling the disturbance motion varies in the

x coordinate according to a new scale.

$$x = x^*/RL^* \quad (8)$$

Boundary-layer theory combined with the assumed scales, gives the x variation of mean-flow quantities in terms of the new scale.

Substituting Eq. (6) into the dimensionless field equations, subtracting the mean flow, linearizing the equations, and keeping the leading order terms, that is terms  $O(1)$ , the following disturbance equations are obtained:

x-momentum

$$\frac{1}{\theta}(\bar{U}u)_x - \mu u_{zz} + \frac{V}{\theta}u_y - (\mu u_y)_y + \frac{1}{\theta}Uv \\ - \left[ \frac{1}{\theta^2}(UU_x + VU_y) + (\tilde{\mu}U_y)_y \right] \theta - \tilde{\mu}U_y \theta_y = 0 \quad (9)$$

y-momentum

$$\frac{1}{\theta}(V_x + 2UG^2)u - c\mu_y u_x - (c+1)\mu u_{yx} - \mu_x u_y \\ + \frac{1}{\theta}(Vv)_y + \frac{U}{\theta}v_x - \mu v_{zz} - (c+2)(\mu v_y)_y + p_y \\ - \left[ \frac{1}{\theta^2}(UV_x + VV_y + U^2G^2) + (c+1)\tilde{\mu}U_{yx} + c\tilde{\mu}_y U_x \right. \\ \left. + (c+2)(\tilde{\mu}V_y)_y + \tilde{\mu}_x U_y \right] \theta - \tilde{\mu}U_y \theta_x - \left[ c\tilde{\mu}U_x \right. \\ \left. + (c+2)\tilde{\mu}V_y \right] \theta_y - c\mu_y w_z - (c+1)\mu w_{yz} = 0 \quad (10)$$

z-momentum

$$\mu_x u_z + (c+1)\mu u_{xz} + \mu_y v_z + (c+1)\mu v_{yz} - p_z \\ + c\tilde{\mu}(U_x + V_y)\theta_z - \frac{U}{\theta}w_x + (c+2)\mu w_{zz} - \frac{V}{\theta}w_y \\ + (\mu w_y)_y = 0 \quad (11)$$

Continuity

$$\left(\frac{u}{\theta}\right)_x + \left(\frac{v}{\theta}\right)_y + \left(\frac{w}{\theta}\right)_z + \frac{1}{\theta^2} \left( \frac{2u}{\theta} \theta_x + \frac{2v}{\theta} \theta_y - u_x - v_y \right) \theta - \frac{1}{\theta^2} (u \theta_x + v \theta_y) = 0 \quad (12)$$

Energy

$$\begin{aligned} \frac{1}{\theta} \theta_x u - 2(\gamma - 1) M_\infty^2 \mu u_y u_y + \frac{1}{\theta} \theta_y v - \left[ \frac{1}{\theta^2} (u \theta_x + v \theta_y) \right. \\ \left. + (\gamma - 1) M_\infty^2 \tilde{\mu} (u_y)^2 + \frac{1}{\Gamma} (\tilde{\mu} \theta_y)_y \right] \theta + \frac{u}{\theta} \theta_x - \frac{u}{\Gamma} \theta_{zz} \\ + \left( \frac{v}{\theta} - \frac{1}{\Gamma} \tilde{\mu} \theta_y \right) \theta_y - \frac{1}{\Gamma} (\mu \theta_y)_y = 0 \end{aligned} \quad (13)$$

By keeping the leading order terms in the disturbance equations, the parameters  $\epsilon$  and  $k$  appear only implicitly in the so called Goertler number  $G$  and consequently Eqs. (9) - (13) are configuration independent at this level of approximation. The parameters  $\epsilon$  and  $k$  will appear explicitly in a higher order stability analysis. The Goertler number  $G$  is defined by

$$G = Rk \quad (14)$$

The other parameters that appear in Eqs. (9) - (13) are the free stream Mach number  $M_\infty$ , Prandtl number  $\Gamma$ , and  $\tilde{\mu} = d\mu/d\theta$ . The density disturbance is eliminated by using the equation of state.

Equations (9) - (13) constitute a system of homogeneous linear partial differential equations with variable coefficients. The type of disturbance considered in this analysis is periodic in the z-coordinate, thus the dependence on z can be eliminated from the equations. The scale x may also be separated from the equations by considering the mean flow to be quasi parallel. Then the form of the disturbance and flow characteristics suggest the normal mode approach. The disturbance variables can be written as

$$u = \hat{u}(y) \cos(\beta z) \exp(\sigma dx) \quad (15a)$$

$$v = \hat{v}(y) \cos(\beta z) \exp(\sigma dx) \quad (15b)$$

$$w = \hat{w}(y) \sin(\beta z) \exp(\sigma dx) \quad (15c)$$

$$p = \hat{p}(y) \cos(\beta z) \exp(\sigma dx) \quad (15d)$$

$$\theta = \hat{\theta}(y) \cos(\beta z) \exp(\sigma dx) \quad (15e)$$

where  $\beta$  is the dimensionless wave number in z-coordinate, and  $\sigma$  is the spatial growth rate. The variables  $\hat{u}$ ,  $\hat{v}$ ,  $\hat{w}$ ,  $\hat{p}$ , and  $\hat{\theta}$  should not be confused with the total flow variables defined in Eq. (6) which will not be referred to later on.

Substituting Eq. (15) into Eqs. (9) - (13) we obtain

x-momentum

$$\left[ \frac{1}{\theta} (\sigma U + U_x) + \mu \beta^2 \right] \hat{u} + \left( \frac{V}{\theta} - \mu_y \right) \hat{u}_y - \mu \hat{u}_{yy} + \frac{1}{\theta} U_y \hat{v} - \left[ \frac{1}{\theta^2} (U U_x + V U_y) + (\tilde{\mu} U_y)_y \right] \hat{\theta} - \tilde{\mu} U_y \hat{\theta}_y = 0 \quad (16)$$

y-momentum

$$\begin{aligned}
 & \left[ \frac{1}{\theta} (v_x + 2UG^2) - c\sigma\mu_y \right] \hat{u} - \left[ (c+1)\sigma\mu + \mu_x \right] \hat{u}_y \\
 & + \frac{1}{\theta} (v_y + \sigma U + \mu\beta^2) \hat{v} + \left[ \frac{v}{\theta} - (c+2)\mu_y \right] \hat{v}_y \\
 & - (c+2)\mu\hat{v}_{yy} - c\mu_y\beta\hat{w} - (c+1)\mu\beta\hat{w}_y + \hat{p}_y \\
 & - \left[ \frac{1}{\theta^2} (UV_x + VV_y + U^2G^2) + (c+1)\tilde{\mu}U_{xy} + c\tilde{\mu}_y U_x \right. \\
 & \left. + (c+2)(\tilde{\mu}V_y)_y + \tilde{\mu}_x U_y + \sigma\tilde{\mu}U_y \right] \hat{\theta} - \left[ c\tilde{\mu}U_x \right. \\
 & \left. + (c+2)\tilde{\mu}V_y \right] \hat{\theta}_y = 0
 \end{aligned} \tag{17}$$

z-momentum

$$\begin{aligned}
 & \beta \left[ (c+1)\sigma\mu + \mu_x \right] \hat{u} + \beta\mu_y \hat{v} + (c+1)\beta\mu\hat{v}_y + \left[ (c+2)\beta^2\mu \right. \\
 & \left. + \frac{\sigma U}{\theta} \right] \hat{w} - (\mu_y - \frac{v}{\theta}) \hat{w}_y - \mu w_{yy} - \beta\hat{p} + c\beta\tilde{\mu}(U_x \\
 & + V_y) \hat{\theta} = 0
 \end{aligned} \tag{18}$$

Continuity

$$\begin{aligned}
 & \frac{1}{\theta} (\sigma - \frac{1}{\theta} \theta_x) \hat{u} - \frac{1}{\theta^2} \theta_y \hat{v} + \frac{1}{\theta} \hat{v}_y + \frac{\beta}{\theta} \hat{w} + \frac{1}{\theta^2} (\frac{2U}{\theta} \theta_x + \frac{2V}{\theta} \theta_y) \\
 & - (U_x - V_y - \sigma U) \hat{\theta} - \frac{V}{\theta^2} \hat{\theta}_y = 0
 \end{aligned} \tag{19}$$

Energy

$$\begin{aligned}
 & \frac{1}{\theta} \theta_x \hat{u} - 2(\gamma - 1)M_\infty^2 \mu U_y \hat{u}_y + \frac{1}{\theta} \theta_y \hat{v} - \left[ \frac{1}{\theta^2} (U\theta_x + V\theta_y) \right. \\
 & \left. + (\gamma - 1)M_\infty^2 \tilde{\mu} (U_y)^2 + \frac{1}{\Gamma} (\tilde{\mu}\theta_y)_y - \frac{\sigma U}{\theta} + \frac{\beta^2\mu}{\Gamma} \right] \hat{\theta} \\
 & + (\frac{V}{\theta} - \frac{1}{\Gamma} \tilde{\mu}\theta_y - \frac{1}{\Gamma} \mu_y) \hat{\theta}_y - \frac{1}{\Gamma} \mu \hat{\theta}_{yy} = 0
 \end{aligned} \tag{20}$$

In the limiting case of  $M_\infty = 0$  the above equations reduce to the incompressible equations developed by Floryan and Saric, and reduce to the basic system of equations developed by Ragab and Nayfeh. The above equations also reduce to the compressible equations of Kobayashi and Kohama for the neutral stability case ( $\sigma = 0$ ) and when all normal velocity and streamwise variations of the mean flow are disregarded.

Eq. (16) - (20) are supplemented with the appropriate boundary conditions, which are

$$\hat{u} = \hat{v} = \hat{w} = 0, \text{ and}$$

$$\hat{\theta}_y + B\hat{\theta} = 0 \text{ at } y = 0 \quad (21)$$

$$\hat{u}, \hat{v}, \hat{w}, \hat{\theta} \rightarrow 0 \text{ as } y \rightarrow \infty \quad (22)$$

The function  $B$  in the condition (21) depends on the thermal properties of both the solid surface and the fluid, as well as the wave length of the disturbance. For an adiabatic surface the case where  $B \rightarrow 0$  ( $\hat{\theta}_y = 0$  at  $y = 0$  that is to consider "adiabatic disturbance") is considered. However, for cases involving surface cooling the case where  $B \rightarrow \infty$  ( $\hat{\theta} = 0$  at  $y = 0$ ) is considered. The effect of using the thermal boundary condition  $\hat{\theta}_y(0) = 0$  on the stability characteristics of the boundary layer over an adiabatic surface is discussed in section 4.3.

CHAPTER III  
COMPUTATIONAL AND NUMERICAL PROCEDURE

Equations (16 - 22) constitute an eighth-order system of homogeneous linear differential equations with homogeneous boundary conditions. This forms an eigenvalue problem for the parameters  $\beta$ ,  $\sigma$ , and  $G$ . Equations (16 - 22) are reduced to eight first-order equations in the form

$$(Z_m)_y - \sum_{n=1}^8 a_{mn} Z_n = 0 \quad m = 1, 2, \dots, 8 \quad (23)$$

$$Z_1 = Z_3 = Z_5 = Z_7 = 0 \quad \text{at } y = 0, \text{ for isothermal wall} \quad (24)$$

$$\text{or } Z_1 = Z_3 = Z_6 = Z_7 = 0 \quad \text{at } y = 0, \text{ for adiabatic wall} \quad (25)$$

$$Z_1, Z_3, Z_5, Z_7 \rightarrow 0 \quad \text{as } y \rightarrow \infty \quad (26)$$

where  $Z$ 's are defined as

$$\begin{aligned} Z_1 &= \hat{u}, \quad Z_2 = \hat{u}_y, \quad Z_3 = \hat{v}, \quad Z_4 = \hat{p} \\ Z_5 &= \hat{\theta}, \quad Z_6 = \hat{\theta}_y, \quad Z_7 = \hat{w}, \quad Z_8 = \hat{w}_y \end{aligned} \quad (27)$$

and  $a_{mn}$  is a variable coefficient matrix, whose nonzero elements are

$$a_{12} = 1$$

$$a_{21} = \frac{1}{\mu\Theta} (U_x + \sigma U) + \beta^2$$

$$a_{22} = \frac{1}{\mu} \left( \frac{V}{\Theta} - \mu_y \right)$$

$$a_{23} = \frac{1}{\mu\Theta} U_y$$

$$a_{25} = -\frac{1}{\mu} \left[ \frac{1}{\Theta^2} (UU_x + VU_y) + \tilde{\mu}U_{yy} + \tilde{\mu}_y U_y \right]$$

$$a_{26} = -\frac{\tilde{U}}{\mu} U_y$$

$$a_{31} = \frac{1}{\theta} \theta_x - \sigma$$

$$a_{33} = \frac{1}{\theta} \theta_y$$

$$a_{35} = \frac{\sigma U}{\theta} + \frac{1}{\theta}(U_x + V_y) - \frac{2}{\theta^2}(U\theta_x + V\theta_y)$$

$$a_{36} = \frac{V}{\theta}$$

$$a_{37} = \beta$$

$$a_{41} = -\frac{1}{\theta} \left[ 2UG^2 + 2\sigma\mu_y + V_x + \frac{V}{\theta} \theta_x - \sigma V - (c+2)(-\sigma\mu + \theta_x\mu_y + \frac{\Gamma V}{\theta} \theta_x + \theta_{xy}\mu) \right]$$

$$a_{42} = -\sigma\mu + \mu_x + \frac{c+2}{\theta} \left[ \theta_x - 2(\gamma-1)M_\infty^2 \Gamma V U_y \right]$$

$$a_{43} = -\frac{1}{\theta} \left[ \sigma U + \mu\theta\beta + V_y + \frac{V}{\theta} \theta_y - (c+2)(\theta_y\mu_y + \mu\theta_{yy} + \frac{\Gamma V}{\theta} \theta_y) \right]$$

$$\begin{aligned} a_{45} = & \frac{U^2 G^2}{\theta^2} + \frac{c+2}{\theta} \mu (\sigma U_y - \frac{U}{\theta} \theta_y) + \sigma \tilde{\mu} U_y \\ & + (c+2) \left[ (\tilde{\mu} V_y)_y - \frac{V}{\theta} (\tilde{\mu} \theta_y)_y \right] + \frac{1}{\theta^2} (UV_x + VV_y) \\ & + (c+1)\tilde{\mu}\mu_{xy} + \tilde{\mu}_x U_y + c\tilde{\mu}_y U_x + \frac{1}{\theta} \left[ \frac{2}{\theta} (V\theta_y \right. \\ & \left. + U\theta_x) - U_x - V_y - \sigma U \right] \left[ \frac{V}{\theta} - (c+2)(\mu_y + \frac{1}{\theta^2} \mu \theta_y) \right] \\ & - \frac{(c+2)\Gamma V}{\theta^2} \left[ \frac{1}{\theta} (V\theta_y + U\theta_x) - \sigma U + (\gamma-1)M_\infty^2 \tilde{\mu} \theta (U_y)^2 \right. \\ & \left. + \frac{\mu\theta}{\Gamma} \beta^2 \right] - \frac{(c+2)}{\theta^2} \left[ 2V\theta_{yy} + 2U\theta_{xy} + 3\theta_y V_y \right. \\ & \left. + 2\theta_x U_y - \frac{4V}{\theta} (\theta_y)^2 - \frac{4U}{\theta} \theta_y \theta_x + \theta_y U_x - \theta U_{xy} - \theta V_{yy} \right] \end{aligned}$$

$$a_{46} = \frac{(c+2)\mu}{\theta} \left[ \sigma U - \frac{2V}{\theta} \Theta_y - \frac{2U}{\theta} \Theta_x + U_x + 2V_y + \frac{\Gamma V^2}{\theta \mu} \right. \\ \left. - \frac{V}{\mu} \mu_y - \frac{\tilde{\mu}V}{\mu} \Theta_y \right] - \frac{V^2}{\theta^2} + \frac{(c+2)V}{\theta} \mu_y + c \tilde{\mu} U_x \\ + (c+2) \tilde{\mu} V_y$$

$$a_{47} = -2\beta \mu_y + \frac{1}{\theta} \left[ \beta V - (c+2)\beta \mu \Theta_y \right]$$

$$a_{48} = \beta \mu$$

$$a_{56} = 1$$

$$a_{61} = \frac{\Gamma}{\mu \theta} \Theta_x$$

$$a_{62} = 2(\gamma - 1) M_\infty^2 \Gamma U_y$$

$$a_{63} = \frac{\Gamma}{\mu \theta} \Theta_y$$

$$a_{65} = \beta^2 - \frac{1}{\mu} (\tilde{\mu} \Theta_y)_y + \frac{\Gamma}{\mu} \left[ \frac{\sigma U}{\theta} - \frac{1}{\theta^2} (U \Theta_x + V \Theta_y) \right. \\ \left. - (\gamma - 1) M_\infty^2 \tilde{\mu} (U_y)^2 \right]$$

$$a_{66} = \frac{1}{\mu} \left( \frac{\Gamma V}{\theta} - \mu_y - \tilde{\mu} \Theta_y \right)$$

$$a_{78} = 1$$

$$a_{81} = \beta \left( \frac{1}{\mu} \mu_x + \frac{c+1}{\theta} \Theta_x \right)$$

$$a_{83} = \beta \left( \frac{1}{\mu} \mu_y + \frac{c+1}{\theta} \Theta_y \right)$$

$$a_{84} = -\frac{\beta}{\mu}$$

$$a_{85} = \frac{c+1}{\theta} \beta \left[ \sigma U + U_x + V_y - \frac{2}{\theta} (V \Theta_y + U \Theta_x) \right] \\ + \frac{c \tilde{\mu} \beta}{\mu} (U_x + V_y)$$

$$a_{86} = \frac{c+1}{\theta} \beta V$$

$$a_{87} = \beta^2 + \frac{\sigma U}{\mu \theta}$$

$$a_{88} = \frac{1}{\mu} \left( \frac{V}{\theta} - \mu_y \right)$$

The reduction of the governing equations to a system of eight first-order equations requires only the second derivatives of the basic-flow quantities. In the work of Kobayashi and Kohama the disturbance equations for neutral stability were reduced to three coupled equations, the first of second order in  $\hat{u}$ , the second of fourth order in  $\hat{v}$ , and the third of second order in  $\hat{\theta}$ , and then solved numerically by finite difference. The coefficients in their equations contain fourth-order derivatives of the basic flow, which requires a higher accuracy of the basic flow solution than the method used here.

### 3.1 Eigenvalues and Eigenvectors

Outside the boundary layer, i.e. at  $y \geq y_e$  ( $e$  indicates the edge of the boundary layer), the coefficients in equations (23) become constant since  $U = \mu = \Theta = 1$ ,  $\mu = \mu_e = \text{constant}$ ,  $V = V_e = \text{constant}$ ,  $\Gamma = \Gamma_e = \text{constant}$  and the  $x$  and  $y$  derivatives of all mean-flow quantities are zero except  $V_x$ . The nonzero elements of the constant coefficient matrix

$a_{mn}^*$  are:

$$a_{12}^* = 1$$

$$a_{21}^* = \sigma + \beta^2$$

$$a_{22}^* = V_e$$

$$a_{31}^* = -\sigma$$

$$a_{35}^* = \sigma$$

$$a_{36}^* = V_e$$

$$a_{37}^* = -\beta$$

$$a_{41}^* = [2G^2 + V_{xe} - \sigma V_e]$$

$$a_{42}^* = -\sigma$$

$$a_{43}^* = -(\sigma + \beta^2)$$

$$a_{45}^* = G^2 + V_{xe} - \sigma V_e + \frac{(C + 2)\Gamma_e V_e}{\Gamma_e} (\beta^2 + \sigma)$$

$$a_{46}^* = (C + 2)(\sigma + \Gamma_e V_e^2) - V_e^2$$

$$a_{47}^* = \beta V_e$$

$$a_{48}^* = -\beta$$

$$a_{56}^* = 1$$

$$a_{65}^* = \beta^2 + \Gamma_e \sigma$$

$$a_{66}^* = \Gamma_e V_e$$

$$a_{78}^* = 1$$

$$a_{84}^* = -\beta$$

$$a_{85}^* = (C + 1) \beta \sigma$$

$$a_{86}^* = (C + 1) \beta V_e$$

$$a_{87}^* = \beta^2 + \sigma$$

$$a_{88}^* = V_e$$

Equation (23) with the constant coefficient matrix  $a_{mn}^*$  has a solution that can be expressed in the form

$$Z_m = \sum_{n=1}^8 D_{mn} c_n \exp(\lambda_n y) \quad m = 1, 2, \dots, 8, \quad y=y_e \quad (28)$$

where  $D_{mn}$  is the characteristic eigenvector matrix,  $c_n$  is arbitrary constant vector, and  $\lambda_n$  are the eigenvalues of the matrix  $a_{mn}^*$ . They are:

$$\begin{aligned}\lambda_1 &= -\beta \\ \lambda_2 &= \lambda_3 = -\frac{1}{2}\{-V_e + [V_e^2 + 4(\sigma + \beta^2)]^{1/2}\} \\ \lambda_4 &= -\frac{1}{2}\{-\Gamma_e V_e + [\Gamma_e^2 V_e^2 + 4(\sigma \Gamma_e + \beta^2)]^{1/2}\} \\ \lambda_5 &= \beta \\ \lambda_6 &= \lambda_7 = \frac{1}{2}\{V_e + [V_e^2 + 4(\sigma + \beta^2)]^{1/2}\} \\ \lambda_8 &= \frac{1}{2}\{\Gamma_e V_e + [\Gamma_e^2 V_e^2 + 4(\sigma \Gamma_e + \beta^2)]^{1/2}\}\end{aligned} \quad (29)$$

We consider the case in which  $\lambda_1, \lambda_2, \lambda_3$  and  $\lambda_4$  are negative real numbers whereas the other four are positive real numbers. Only negative signs satisfy the boundary conditions (26).

It should be noted that the eigenvalues  $\lambda_2$  and  $\lambda_6$  are repeated. Also in the special case when  $\sigma = \beta V_e$  four eigenvalues are repeated, i.e.

$$\begin{aligned}\lambda_1 &= \lambda_2 = \lambda_3 = \lambda_4 = -\beta \\ \lambda_5 &= \lambda_6 = \lambda_7 = \lambda_8 = \beta\end{aligned} \quad (30)$$

Evaluation of the eigenvectors requires special care when the multiplicity of the roots is equal to or greater than two. Eigenvectors corresponding to the eigenvalues (29) are given in Appendix C and those corresponding to the eigenvalues (30) are given in Appendix D. Eigenvectors are checked by reducing the constant coefficient matrix  $a^*$  to a Jordan canonical form using the similarity transformation

$$J = D^{-1} a^* D \quad (31)$$

(where  $D^{-1}$  is the inverse of the eigenvector matrix  $D$ ).

When  $\lambda_n$  are distinct (which is not the case here), the resulting matrix

$J$  is a diagonal matrix with the diagonal elements as eigenvalues. In case of repeated roots, elements of the super diagonals corresponding to the repeated roots are nonzeros.

### 3.2 Boundary Conditions

The asymptotic boundary condition (26) as  $y \rightarrow \infty$  demand that the constants  $c_5 - c_8$  be zero in the solution (28). This can be expressed as

$$\sum_{n=1}^8 D_{mn}^{-1} Z_m = 0 \quad m = 5, 6, 7, 8 \quad y = y_e \quad (32)$$

The boundary condition at the wall (24) or (25) can be written in the form

$$\sum_{n=1}^8 e_{mn} Z_n = 0 \quad m = 1, 2, 3, 4, \quad y = 0 \quad (33)$$

where the elements of the  $4 \times 8$  matrix  $e_{mn}$  are all zeros except  $e_{11} = e_{23} = e_{36} = e_{47} = 1$  in case of adiabatic wall, and  $e_{11} = e_{23} = e_{35} = e_{47} = 1$  in case of isothermal wall.

### 3.3 Numerical Procedures

Equations (23) with boundary conditions (32) and (33) form a two point boundary value problem which is solved numerically. We assign values for two of the parameters  $\beta$ ,  $\sigma$  and  $G$ , guess the third one, and use the boundary condition (32) to construct a linear combination of the general solution (28). A variable stepsize integrator, written by Scott and Watts (1977), based on the Runge Kutta-Fehlburg fifth-order formulas, coupled with orthonormalization is used to integrate equations (23) from  $y = y_e$  to the wall. At the wall, the values of the independent solution vectors are linearly combined to satisfy all but one of the wall boundary conditions. The last wall boundary condition can only be satisfied by this combined solution when the exact

eigenvalue has been found. A Newton-Raphson procedure is used to determine this eigenvalue. In the results presented here, a value is always assigned to  $\sigma$  to locate contours of constant growth rate use either  $\beta$  or  $G$  as an eigenvalue and determine it to  $0(10^{-4})$ . A FORTRAN computer program for the stability analysis is given in Appendix F.

### 3.4 Adjoint Problem

The system of equations adjoint to (23) are formed to check the eigenvalue. The adjoint system of equations can be written as

$$(Z_m^*)_y + \sum_{n=1}^8 a_{nm} Z_n^* = 0 \quad m = 1, 2, \dots, 8 \quad (34)$$

$$Z_2^* = Z_4^* = Z_5^* = Z_8^* = 0 \quad \text{at } y = 0, \text{ for adiabatic wall} \quad (35)$$

$$\text{or } Z_2^* = Z_4^* = Z_6^* = Z_8^* = 0 \quad \text{at } y = 0, \text{ for isothermal wall} \quad (36)$$

$$Z_2^*, Z_4^*, Z_6^*, Z_8^* \rightarrow 0 \quad \text{as } y \rightarrow \infty \quad (37)$$

Equations (34) - (37) are solved using the same procedures used to solve the regular equations (23) - (26). The eigenvectors of the adjoint problem are given in Appendix E.

Eigenvalues calculated by Equations (23) and its adjoint (34) were checked, and found to agree to  $0(10^{-4})$ , and both were found to be independent of the value of  $y_e$ . However, the value of  $y_e$  used for the adjoint problem (34) to achieve the required accuracy was always higher than the value of  $y_e$  used for the regular problem (23). It was also necessary to increase  $y_e$  as Mach number increases. For example for the regular problem  $y_e = 10, 12, 14, 16, 18$  and  $20$  for  $M_\infty = 0, 1, 2, 3, 4$ , and  $5$ , respectively. The shape of the eigenfunctions was checked in order to avoid calculations of higher modes.

## CHAPTER IV

NUMERICAL RESULTS AND DISCUSSION

The results of stability analysis are usually presented as curves of Goertler number versus wave number for constant growth rate. Neutral stability curve ( $\sigma = 0$ ) separates the stable from unstable regions and increasing growth rate is akin to moving downstream with the vortices. Goertler number which represents viscous and curvature effects can be associated with a particular geometry and flow conditions.

Effect of compressibility of the mean flow on Goertler instability is investigated for a range of Mach numbers from 0 to 5. These results are reported by El-Hady and Verma (1981a) and discussed in details in sections 4.1 and 4.2. An attempt is made in section 4.1 to evaluate the effect of the mean density and mean viscosity on the stability characteristics of the boundary layer. The effect of using different thermal disturbance wall boundary conditions is examined in section 4.3. Effect of compressibility of the mean flow on the shape of the eigenfunctions is discussed in section 4.4, while its effects on the amplitude ratio of Goertler vortices is given in section 4.5. The effect of suction and cooling of the boundary layer on the development of these vortices is given in section 4.6 and 4.7, respectively.

#### 4.1 Effect of Compressibility on the Neutral Curve

Figure 4 shows the neutral stability curves for different Mach numbers. Instability of the boundary layer sets in at higher Goertler number as Mach number increases for all wavenumbers higher than 0.1. The critical value of G below which the flow is stable for any disturbance wavenumber increases as Mach number increases. The stabilizing

effect of compressibility is qualitatively in agreement with the results of Kobayashi and Kohama, but differs quantitatively due to the effect of the boundary layer growth that is included in the present analysis. It is worth noting that the incompressible limit,  $M_\infty = 0$ , of the neutral stability curve agrees with the results of Floryan and Saric and Ragab and Nayfeh.

The rate of heat transfer between the fluid and the wall and the subsequent development of a thermal boundary layer in addition to the velocity boundary layer, play an important role in a compressible flow. The mean-density and the mean-viscosity variations inside the boundary layer have different roles in shaping the stability characteristics of the flow. Figure 5 shows the variation of the critical Goertler number with  $M_\infty$  for a neutrally stable disturbance. The mean density is shown by curve 3 to locally destabilize the flow (curve 3 is calculated with constant mean viscosity). This effect can be predicted from Rayleigh criterion for inviscid flows with curved streamlines. His criterion for instability modified for a case with density variation is  $\bar{\rho}_y/\bar{\rho} + (r^* U_\infty)_y/(r^* U_\infty) > 0$ , where  $r^*$  is the radius of curvature of the surface. This criterion shows that positive density gradient seems to destabilize the boundary layer. A compressible mean flow along an adiabatic flat plate has a positive density gradient as shown in Fig. 6. The figure shows the variation of the mean density and mean viscosity in the boundary layer for different Mach numbers. The effect of the mean viscosity is shown by curve 2 in Fig. 5 (calculated with constant mean density). The mean viscosity has a stabilizing effect compared to the mean-density variation. The exclusion of the disturbance viscosity, shown by curve 4, has a profound destabilizing effect on the boundary layer. It is worth noting that the conditions of

curve 4 are similar to the assumptions taken by Aihara in his calculations. In spite of that, curve 4 indicates that critical Goertler number is increasing as Mach number increases which is opposite to that predicted by Aihara. It may be concluded that the stabilizing influence of the mean viscosity is more dominant than the opposite influence of the mean density, resulting in a more stable boundary layer as Mach number increases.

#### 4.2 Growth Rates of the Goertler Vortices

The calculation of the initial point of instability or the minimum critical Goertler number as a function of mean flow or disturbance parameters is not that useful quantity regarding transition dependence. The growth of the vortices and not its initial point of instability is the decisive factor. It is one of the goals of this investigation to study the effect of Mach number on the growth rates of Goertler vortices and to present design charts for a range of Mach numbers.

Figures 7-12 show contours of constant growth rates plotted in the G- $\beta$  plane for a range of Mach numbers from 0 to 5. The stable region below  $\sigma = 0$  curve is increasing as Mach number increases. The growth rate curves posses minimum which indicate a trend to higher wavenumbers at higher growth rates. They form a locus of the maximum growth rates of different wavenumber components. As Mach number increases, Figs.7-12 indicate that maximum growth rates occur at lower wavenumbers and higher Goertler numbers. The locus of the maximum growth rates shifts up and to the left of the chart as Mach number increases.

Figure 7 ( $M_\infty = 0$ ) and Fig. 10 ( $M_\infty = 3$ ) show constant growth rate curves calculated by excluding all terms due to the growth of the

boundary layer. These terms greatly influence the neutral stability curve specially at high Mach number. The effect of these terms diminishes as the growth rate of the disturbance increases.

For different Mach numbers, Fig.13 shows the variation of the vortex growth rate with the Goertler number. The values plotted in Fig. 13 correspond to the minimum of the growth rate curves. The figure indicates that the vortex becomes more sensitive (its growth rate) to changes in Goertler number as Mach number increases. The influence of compressibility on reducing the growth rates is very small at high Goertler numbers. Fig.13 also shows that compressibility has its maximum stabilizing influence when the vortex is weak. This conclusion is best illustrated by Fig. 14 where the parameter  $(G_{oc} - G_c)/G_{oc}$  is used as ordinate to indicate the stabilizing effect (increase of critical Goertler number) as Mach number increases compared with  $G_{oc}$ , the critical Goertler number at  $M_\infty = 0$  at the corresponding value of the growth rate  $\sigma$ .

It should be reminded that the present definition of Goertler number is based on the reference length  $L^*$  defined in Eq.(1), whereas the original parameter identified by Goertler is based on the momentum thickness of the boundary layer. For the purpose of comparison with data referenced to the displacement thickness  $\delta_1$  or the momentum thickness  $\delta_2$ , the following relations are used:

$$G_n = G_L \Delta_n^{3/2} \quad \beta_n = \beta_L \Delta_n \quad \sigma_n = \sigma_L \Delta_n^2$$

where the subscript L denotes data based on the reference length  $L^*$ , and n denotes data based on the displacement thickness  $\delta_1$ , or the momentum thickness  $\delta_2$  as reference length. The following table gives values

for the conversion factor  $\Delta_n$  for different Mach numbers, and freestream stagnation temperature of 310 K, where  $\Delta_1 = \delta_1/L$ ,  $\Delta_2 = \delta_2/L$

$M_\infty$	0	1	2	3	4	5
$\Delta_1$	1.720	2.129	3.365	5.48	8.504	12.393
$\Delta_2$	0.663	0.656	0.643	0.641	0.645	0.646

#### 4.3 Effect of the Wall Boundary Condition of the Thermal Disturbance on The Stability Characteristics

All the results presented so far are for an adiabatic wall. The wall boundary condition of the temperature disturbance requires a solution of the heat conduction equation very close to the surface. This leads to a boundary condition in the form of Eq. (21), that should be applied to a particular solid and a specified disturbance wavenumber. A detailed study of this boundary condition, with its two extreme cases of  $B \rightarrow 0$  ( $\theta_y = 0$ , the wall is a perfect insulator), and  $B \rightarrow \infty$  ( $\theta = 0$ , the wall is a perfect conductor), leads to the conclusion that local stability near to the neutral region is dependent on the temperature fluctuation and the boundary condition imposed on it in a compressible boundary layer. At  $M_\infty = 3$ , Fig.15a shows a comparison between neutral stability curves calculated using the wall condition  $\theta_y(0) = 0$  and  $\theta(0) = 0$ . Apart from the differences in the value of the critical Goertler number, large discrepancies also appear for disturbances having low wavenumbers. The reason is that for low wavenumber disturbances the thermal fluctuation can penetrate large distances into the solid wall, and hence, the wall temperature cannot remain at the wall

temperature of the mean boundary layer. Figure 15b shows the effect of the thermal wall boundary condition on critical Goertler numbers of neutrally stable disturbances. The wall condition  $\theta_y(0) = 0$  shows always a locally stabilizing effect in a compressible boundary layer compared to the condition  $\theta(0) = 0$ , regarding the neutral stability curve. Using the full thermal boundary condition, Eq. 21, the actual neutral stability characteristics will lie, probably, somewhere between the curves presented in Figs. 15a and 15b. It is of interest to notice that the effect of the thermal boundary condition vanishes with the growth of the disturbance. Figure 15c shows that for  $M_\infty = 3$  which is typical for all the range of Mach numbers under investigation.

#### 4.4 Effect of Compressibility on Eigenfunctions

Figures 16a-16d give a comparison of the shape of the eigenfunctions of  $\hat{u}$ ,  $\hat{v}$ ,  $\hat{w}$ , and  $\hat{\theta}$ , respectively at different Mach numbers for a disturbance having a waveumber  $\beta = 0.3$  and a growth rate  $\sigma = 5$ . The corresponding Goertler numbers are  $G = 13.4637, 12.9289, 12.0844, 11.5310, 11.4786$ , and  $11.7611$  at  $M_\infty = 1, 2, 3, 4$ , and  $5$ , respectively. The values of  $\hat{u}$ ,  $\hat{v}$ ,  $\hat{w}$ , and  $\hat{\theta}$  are normalized with the maximum of the  $\hat{u}$  component at the corresponding  $M_\infty$ . Figure 16 shows that the location of  $\hat{u}_{\max}$ ,  $\hat{v}_{\min}$ ,  $\hat{w}_{\max}$ , and  $\hat{\theta}_{\min}$  move away from the wall as Mach number increases. The case of neutral stability (not shown) indicates a persistence of the disturbance outside the boundary layer that increases as Mach number increases. At  $M_\infty = 3$ , Fig. 16a shows the shape of the eigenfunction  $\hat{u}$  when terms due to boundary layer growth are neglected for a neutrally stable as well as a growing disturbance of  $\sigma = 5$ . The effect of the boundary layer growth is to move the location of  $\hat{u}_{\max}$  away from the wall leading to a slow decay of the disturbance outside the boundary layer.

In their study on the influence of suction or cooling on Goertler instability in compressible boundary layers, El-Hady and Verma (1981b) showed that high suction or cooling rates bring the location of  $\hat{u}_{\max}$ ,  $\hat{v}_{\min}$ ,  $\hat{w}_{\max}$ , and  $\hat{\theta}_{\min}$  nearer to the wall and result in stabilizing the boundary layer. The stabilizing mechanism here is different from that due to compressibility. The effect of suction and cooling is further discussed in secs. 4.6 & 4.7.

#### 4.5 Effect of Compressibility on the Amplitude Ratio

In this section, the growth of the measured by the amplitude ratio is considered since the growth rate alone is of little help in correlating transition. The logarithmic derivative of the amplitude of any disturbance quantity  $q$  in Eq. (15) is

$$(\ln q)_x = \sigma \quad (38)$$

In terms of  $G$  instead of  $x$  and introducing  $a$  for  $q$

$$\ln (a/a_0) = (4/3) \int_{G_0}^G (\sigma/G) dG \quad (39)$$

where  $a_0$  and  $G_0$  are the amplitude and Goertler number at the beginning of the unstable region, and the integration is carried out along a particular growth path.

In all experiments of incompressible flows along concave surfaces, the growth path of the vortex was determined from the conservation of its dimensional wavelength  $\lambda^*$  that was observed in the flow direction. With lack of corresponding information for compressible flows and for comparison purposes, we assume the same criterion to hold. Since the dimensionless wavenumber  $\beta = \beta^* L^*$  varies with  $x^*$  for constant  $\lambda^*$ , the dimensionless wavelength

$$\Lambda = \frac{U_\infty \lambda}{V_\infty} \left( \frac{\lambda}{r} \right)^{1/2} \quad (40)$$

is used instead. In the  $G-\beta$  plane, lines of  $\Lambda = \text{const.}$  are straight with slope  $3/2$ . The locus of maximum growth rates closely coincide with these lines for the corresponding Mach number. We assume that  $a_0$  in Eq.(39) is independent of  $\Lambda$  and  $G$  so that the dependence of  $a$  on  $\Lambda$  and  $G$  will be the same as that of  $a/a_0$ . For different Mach numbers, a series of amplitude ratio curves are calculated by integrating Eq. (39) for constant  $\Lambda$  up to  $G = 20$ . Figure 17 shows a reduction in the maximum value of the amplitude ratio as well as a shift of the most unstable wavelength to higher value as Mach number increases. Fig. 17 shows also an increase in the upper band of the disturbance wavelength that is always attenuated (cut off wavelength) as Mach number increases.

It is a known fact that the stability theory cannot predict which disturbance wavelength will actually appear for a given surface configuration and flow conditions. For incompressible flows along concave surfaces, the wavelength of the disturbance appears to be determined by the particular edge effects of the experimental apparatus (Tani and Sakagami , 1962) or by the oncoming disturbances (Bippes, 1978). Based on incompressible experimental data (Tani and Sakagami 1962; Tani, 1961), Floryan and Saric (1980) suggested that the wavelength selection mechanism (which decide the vortex growth path) may be based on the maximum growth rate of the disturbances. However, the selection process may be very easily affected by the properties of the experimental apparatus that determine the entry location to the locus of the maximum growth rate. For different Mach numbers, we integrate Eq. (39) along the locus of the maximum growth rate. The results are shown in Fig. 18 as function of the Goertler number. The integration is carried up to  $G = 20$  for comparison purposes. The figure

shows a stabilizing effect as Mach number increases in terms of lower values of  $\ln(a/a_0)$ . It is worth to notice that the values of  $\ln(a/a_0)$  at  $G = 20$  for different Mach numbers following the path of maximum growth rates in Fig. 18 are almost identical with the corresponding values at the most unstable wavelengths in Fig. 17.

#### 4.6 Effect of Suction on the Stability Characteristics

It was shown by Goertler (1954) and Hämmerlin (1955) that the curve of neutral stability depends insensibly upon the basic velocity profile in the laminar compressible boundary layer, when the changes in its momentum thickness is very small. However, Kahawita and Meroney (1977) showed that the inclusion of the normal velocity terms change the location of the neutral curve drastically. In section 4.2, the same conclusion was reached for the compressible boundary layer. Terms due to boundary layer growth have large effect near the neutral stability region specially at high Mach numbers. Therefore, it is expected that variation of the velocity profile due to suction (which does not affect the momentum thickness but changes the normal velocity term) may change the critical Goertler number.

The effect of suction of the laminar boundary layer on Goertler instability is examined at  $M_\infty = 0.8$  and 3. The self similar suction parameter  $\gamma$  defined in Eq. (5) is used for this purpose. Figures 19 and 20 show the change in the location of the neutral stability curves for different values of the suction parameter at  $M_\infty = 0.8$  and 3 respectively. It is observed that critical Goertler number first decreases with increasing suction (destabilizes the boundary layer). The boundary layer with a suction given by  $\gamma \approx -0.45$  and -1.3 is the most unstable at  $M_\infty = 0.8$  and 3,

respectively, as far as the critical Goertler number is concerned. By increasing the suction parameter above these levels for each Mach number, the critical Goertler number increases. Fig. 21 shows how the critical Goertler number changes with  $\gamma$  for different Mach numbers. The level of suction that is required for a noticeable increase of the critical Goertler number increases as Mach number increases. This suction level is of higher order of magnitude than the suction required to stabilize Tollmien-Schlichting waves (see Saric and Nayfeh, 1977 for  $M_\infty = 0$ ). This leads to the conclusion that with these levels of suction, Tollmien-Schlichting waves are practically eliminated, and Goertler vortices may dominate the flow.

At  $M_\infty = 3$ , Figs. 10, 22, and 23 show waves of constant growth rates for  $\gamma = 0, -1.2$  and  $-1.6$ . By increasing suction, curves of small growth rates are compressed and moved to higher Goertler numbers. Curves of high growth rates are slightly affected by suction especially at high Mach numbers.

To see the overall effect of suction, the growth of the vortices should be taken into account as they develop downstream. For  $M_\infty = 3$ , Fig. 24 shows the amplitude ratio of the vortices as a function of Goertler number. Integration of the growth rates is performed using Eq. (39) to  $G = 20$  for comparison purposes. It is clear that despite indications of the destabilizing effect of small suction for all Mach numbers regarding the critical Goertler number (see Fig. 20), the overall effect of suction is to stabilize the boundary layer as shown by Fig. 24 for  $M_\infty = 3$  and by Floryan and Saric for  $M_\infty = 0$ . Although a suction corresponding to  $\gamma = -1.2$  which is near to the critical value of the suction parameter at  $M_\infty = 3$ , locally destabilizes the boundary layer in terms of the critical Goertler number, it

reduces the amplitude ratio by about twenty-two percent thus stabilizing the boundary layer.

At different Mach numbers, Fig. 25 displays the amplitude ratio of the vortices at  $G = 20$  over a range of the suction parameter  $\gamma$ . The amplitude ratio of the vortices reduces as suction increases. With increasing Mach number, it becomes more difficult to stabilize the boundary layer (reducing the amplitude ratio of the vortices) unless very high suction is used. Figure 25 shows that at  $M_\infty = 5$  the amplitude ratio is hardly influenced by suction in the range of  $0 < \gamma < 2$ .

At  $M_\infty = 3$ , Fig. 26a-26d show a comparison of the shape of the eigenfunctions  $\hat{u}$ ,  $\hat{v}$ ,  $\hat{w}$ , and  $\hat{\theta}$ , respectively, for different values of the suction parameter  $\gamma$  (normalized with the maximum of  $u$  component). These eigenfunctions are for a neutrally stable disturbance having a wave number  $\beta = 0.3$ . The corresponding Goertler numbers are  $G = 1.1155, 1.7549, 3.5193$  at  $\gamma = -0.6, -1.6, -2.0$ , respectively.

Figure 26 shows that the location of  $\hat{u}_{\max}$ ,  $\hat{v}_{\min}$ ,  $\hat{w}_{\max}$ , and  $\hat{\theta}_{\min}$  move towards the wall as suction increases.

The normal velocity component, if directed away from the wall (the case of no suction), tends to destabilize the flow by encouraging penetration into the free stream where viscous dissipation is small. By increasing suction the thickness of the boundary layer decreases, and the disturbance is confined to a region closer to the wall where dissipative action is strong, thereby increasing the stability of the flow.

#### 4.7 Effect of Cooling on the Stability Characteristics

At  $M_\infty = 3$ , Fig. 27 shows how the location of the neutral curve varies with different cooling rates. The cooling parameter  $\theta_w/\theta_{ad}$  is used for this purpose, where  $\theta_w/\theta_{ad} = 1$  represents no cooling, and  $\theta_w/\theta_{ad} < 1$  re-

presents cooling. Small cooling has a destabilizing influence; however as cooling increases, the neutral curve moves upward indicating a stabilizing influence as far as the critical Goertler number is concerned. For wavenumbers approximately greater than 0.4, Fig. 27 shows that cooling always destabilizes the boundary layer (Goertler number decreases).

It should be noted here that in section 4.3 we arrived at the conclusion that neutral stability curve is dependent on the wall boundary condition of the thermal disturbance. Therefore, one may think that comparing neutral curves in case of cooling, where the wall is considered completely conducting and the wall boundary condition of the thermal disturbance is  $\theta = 0$ , with that in case of no cooling, where the wall is considered ideally insulated and the wall boundary condition of the thermal disturbance is  $\theta_y = 0$ , is somewhat misleading. The neutral stability curve is calculated for a no cooling case with the thermal boundary condition  $\theta = 0$  at  $y = 0$ , and is shown in Fig. 27 for comparison. Previous conclusions regarding effect of cooling on the critical Goertler number are still valid.

At  $M_\infty = 3$ , Fig. 28-30 show contours of constant growth rates for the cooling parameter  $\theta_w/\theta_{ad} = 0.75, 0.25$ , and  $0.15$ , respectively. These figures display the influence of cooling on the vortices at different stages of their growth. Conclusions are summarized in Fig. 31, where the parameter  $(G_{nc} - G_c)/G_{nc}$  is used as ordinate to indicate the stabilizing or destabilizing effect (increase or decrease in critical Goertler number) as cooling increases compared with  $G_{nc}$ , the critical Goertler number at  $\theta_w/\theta_{ad} = 1$  for the corresponding values of the growth rate  $\sigma$ . Fig. 31 shows that at  $M_\infty = 3$ , weak vortices (small growth rates) are more

influenced by cooling. Cooling parameters  $1 > \theta_w/\theta_{ad} > 0.75$  seems to destabilize the boundary layer. As cooling increases ( $\theta_w/\theta_{ad} < 0.75$ ), Fig. 31 shows a stabilizing influence of cooling on weak vortices; however, cooling has almost no influence on strong vortices (high growth rates).

The above conclusions represent a local effect of cooling on the stability limit as well as growth rates of the vortices. It is important to estimate the effect of cooling on the total growth of the vortices by calculating the amplitude ratios. Again, Eq. (39) is used to integrate the growth rates along the locus of maximum growth to  $G = 20$ . At  $M_\infty = 3$ , Fig. 32 shows a comparison of the amplitude ratios for different cooling parameters. The figure shows that stabilizing the boundary layer with respect to Goertler vortices can hardly be achieved by using very high cooling. At  $G = 20$ , the amplitude ratio of the vortices reduces by about 2 % at  $\theta_w/\theta_{ad} = 0.25$  and by 5.6 % at  $\theta_w/\theta_{ad} = 0.15$ . The case of  $\theta_w/\theta_{ad} = 0.75$  shows a destabilizing effect at this Mach number.

Fig. 33 shows the effect of cooling on the amplitude ratio of Goertler vortices for different Mach numbers. The figure clearly demonstrates that moderate cooling has almost no influence on the stability. However, high cooling influences low Mach numbers more than high Mach numbers. At  $\theta_w/\theta_{ad} = 0.25$ , the amplitude ratio is reduced by 13.4% at  $M_\infty = 0.8$ , by 2.8% at  $M_\infty = 3$ , and increased by 2.6% at  $M_\infty = 5$ .

It is clear from Figs. 32 and 33 that the effect of moderate cooling is relatively small considering the strong temperature dependence of the viscosity and density and the corresponding large variation of both in the boundary layer. At  $M_\infty = 3$ , Fig. 34 shows the distribution of viscosity and density of the mean boundary layer flow for differ-

ent cooling parameters. In contrast to the insulated wall, where the density gradient is positive and the viscosity is large at the wall, the density profile in the cooling case has not only positive but negative gradients. The viscosity profile has also two regions where  $\mu > 1$  and  $\mu < 1$ . The negative density gradient may have a stabilizing effect according to the Rayleigh inviscid criterion, but the variation of both density and viscosity in the cooling case are complicated enough to compare with the case of no cooling.

The small effect of moderate cooling shown in Figs. 32 and 33 is in marked contrast to the results for the Tollmien-Schlichting (TS) type instability which is extremely sensitive to wall temperature (see Fig. 7 in Mack, 1975). This is ultimately due to the presence of an inner critical layer in TS disturbances through which the eigenfunction varies rapidly. Therefore, stability characteristics depend critically on the local properties of the mean-flow velocity, viscosity, and density distributions which are very sensitive to the wall temperature. For Goertler instability, however, there is no inner critical layer and the centrifugal force is the controlling factor. This instability depends only on the overall properties of the mean flow, such as the average velocity gradient, which are much less influenced by the wall temperature.

At  $M_\infty = 3$ , Figs. 35a-35d give a comparison of the shape of the eigenfunctions of  $\hat{u}$ ,  $\hat{v}$ ,  $\hat{w}$ , and  $\hat{\theta}$ , respectively, for different values of the parameter  $\theta_w/\theta_{ad}$ . These eigenfunctions are for a neutrally stable disturbance with wavenumber  $\beta = 0.3$ . The corresponding Goertler numbers are  $G = 1.463, 1.301, 1.205$ , and  $1.213$  for  $\theta_w/\theta_{ad} = 1, 0.75, 0.50$  and  $0.25$ , respectively. The values of  $\hat{u}$ ,  $\hat{v}$ ,  $\hat{w}$ , and  $\hat{\theta}$  are normalized with the maximum of  $u$ -component at the corresponding cooling

parameter. The figure shows that the location of  $\hat{u}_{\max}$ ,  $\hat{w}_{\max}$ , and  $\hat{\theta}_{\min}$  move towards the wall as cooling increases. The velocity component  $\hat{v}$  shows a persistence outside the boundary layer.

Comparing the shape of eigenfunctions due to cooling in Fig. 35, with that due to suction in Fig. 25, shows that at  $M_\infty = 3$ , both high suction and high cooling stabilize the boundary layer by confining the disturbance to a highly dissipative region nearer to the wall. Suction may be more effective than cooling as it brings the disturbances more close to the wall.

CHAPTER V  
CONCLUSIONS

A leading order approximation of a compressible stability theory of boundary-layer flow along a concave surface is presented and solved numerically. The compressible boundary layer equations along a flat plate are used to represent the mean flow. The results of the stability analysis are summarized as follows:

1. Instability of the boundary layer with respect to Goertler vortices sets in at higher Goertler number as Mach number increases.
2. The local stability near to the neutral region is dependent on the wall boundary condition imposed on the temperature fluctuation in a compressible boundary layer.
3. At high Mach number, the growth of the vortices is sensitive to small changes in Goertler number.
4. Compressibility has its maximum influence on the vortex when it is weak.
5. Terms due to boundary layer growth have large local effect near the neutral stability region specially at high Mach numbers.
6. Compressibility reduces the maximum amplitude ratio by about 20% as Mach number increases from 0 to 5.
7. With increasing Mach number, the most unstable and cut off wavelengths shift to higher values.
8. Suction may have a local destabilizing effect on the boundary layer as far as the critical Goertler number is concerned, if its level is below a critical value. This critical level of

suction, where local effect becomes stabilizing increases with Mach numbers.

9. In contrast with local suction effects, suction of the boundary layer has always a stabilizing influence on the total growth of Goertler vortices. The amplitude ratios of the vortices reduce with any level of suction used.
10. Suction of the boundary layer is more effective in stabilizing the flow at low Mach numbers than at high Mach numbers. It becomes increasingly difficult as Mach number increases to reduce the amplitude ratios of the vortices unless very high levels of suction are used.
11. Wall cooling, like suction, has a local destabilizing effect on the boundary layer as far as the critical Goertler number is concerned.
12. At low Mach numbers, small cooling applied to the wall ( $\theta_w/\theta_{ad} \geq 0.75$ ) has no influence on the amplitude ratios of Goertler vortices. A noticeable reduction in the amplitude ratio starts with moderate cooling ( $\theta_w/\theta_{ad} \leq 0.5$ ).
13. At high Mach numbers, it seems almost impossible to stabilize the boundary layer using practical rates of wall cooling. The amplitude ratios of the vortices increase and the boundary layer becomes more unstable with small or moderate cooling.
14. Goertler instability is more difficult to influence and control by suction or cooling than Tollmien- Schlitching instability. The reason is that Goertler instability which is referred to as centrifugal type instability, depends on the velocity difference between the inner and outer region of the boundary layer

and not on the shape of the boundary layer profile as in the case of Tollmien-Schlichting instability.

## REFERENCES

- Aihara, Y., 1961, "Stability of the Compressible Boundary Layer Along A Curved Wall Under Goertler-Type Disturbances," Aero. Res. Inst., Tokyo Univ. Rept. No. 362, 31-37
- Aihara, Y., 1962, "Transition in an Incompressible Boundary Layer Along A Concave Wall," Bull. Aero. Res. Inst. Tokyo Univ., 3, 195-240.
- Aihara, Y., 1976, "Nonlinear Analysis of Geortler Vortices," Phys. Fluids 19, 1655-1660.
- Beckwith, I. E. and Holley, B. B., 1981, "Goertler Vortices and Transition in the Wall Boundary Layers of Two Mach 5 Nozzles," NASA TP-1869.
- Bippes, H. and Goertler, H., 1972, "Dreidimensionale Stoerungen in der Grenzschicht an Einer Konkaven Wand," Acta Mechanica 14, 251-267.
- Bippes, H., 1978, "Experimental Study of the Laminar-Turbulent Transition of A Concave Wall in a Parallel Flow," NASA TM-75243. (Translation of "Experimentelle Untersuchung Laminar-Turbulenten Umschlags an Einer Parallel Angestromten Konkaven Wand," Heidelberger Akademie der Wissenschaften, Mathematisch-Naturwissenschaftlich Klasse, Sitzungsberichte, No. 3, 103-180, 1972.)
- Clauser, M. and Clauser, F., 1937, "The Effect of Curvature on the Transition from Laminar to Turbulent Boundary Layer," NACA TN-613.
- DiPrima, R. C. and Stuart, J. T., 1972, "Non-Local Effects in the Stability of Flow Between Eccentric Rotating Cylinders," J. Fluid Mech. 54, pp. 393-415.
- DiPrima, R. C. and Dunn, D. W., 1956, "The Effect of Heating and Cooling on the Stability of Boundary Layer Flow of Liquid Over a Curved Surface," Journal of Aeronautical Sciences, Vol. 23, No. 10, October.

El-Hady, N. M. and Verma, A. K., 1981a, "Growth of Goertler Vortices in Compressible Boundary Layers Along Curved Surfaces," AIAA Paper No. 81-1278, presented at the 14th Fluid and Plasma Dynamic Conference, Palo Alto, CA, June 23-25.

El-Hady, N. M. and Verma, A. K., 1981b, "Goertler Instability in Compressible Boundary Layer With Suction or Cooling," In the proceedings of the Annual Meeting of the Virginia Academy of Science, CDU, Norfolk, May 12-15, Virginia J. of Science.

Floryan, J. M. and Saric, W. S., 1979, "Stability of Goertler Vortices in Boundary Layers With Suction," AIAA Paper No. 79-1497, July.

Floryan, J. M., 1980, "Stability of Boundary Layer Flows Over Curved Walls," Ph.D dissertation, VA Polytechnic Institute and State Univ., Jan.

Floryan, J. M. and Saric, W. S., 1980, "Wavelength Selection and Growth of Goertler Vortices," AIAA Paper No. 80-1376, July.

Ginoux, J. J., 1970, "Streamwise Vortices in Reattaching High-Speed Flows, A Suggested Approach," AIAA Journal, Vol. 9, No. 4, December 15, pp. 759-760.

Goertler, H., 1954, "On the Three-Dimensional Instability of Laminar Boundary Layers on Concave Walls," NACA Tech. Memo. 1375. (Translation of "Über Eine Dreidimensionale Instabilität Laminarer Grenzschichten an Konkaven Wänden," Ges. d. Wiss. Göttingen, Nachr, a.d. Math., Bd. 2, Nr. 1, 1940.)

Gregory, N. and Walker, W. S., 1956, "Part I - The Effect on Transition of Isolated Surface Excrescences in the Boundary Layer," R. & M. No. 2779, British A.R.C.

18. Hammerlin, G., 1956, "Zur Theorie der Dreidimensionalen Instabilitat Laminarer Grenzschichten," ZAMP 7, 156-164.
19. Hammerlin, G., 1961, "Uber die Stabilitat Einer Kompressiblern Strumung Langs Einer Konkaven Wand bei ver Schiedenen Wandtemperaturverhaltnissen," Deutsche Versuchsanstalt fur Luftfahrt, Bericht 176.
20. Herbert, Th., 1976, "On the Stability of the Boundary Layer Along A Concave Wall," Arch. Mech. Stosaw., 28, No. 5, 1039-1055.
21. Hilsenrath, J., Beckett, C. W., Benedict, W. S., Fano, L., Hoge, H. J., Masi, J. F., Nuttall, R. L., Touloukian, Y. S., and Wolley, H. W., 1955, "Tables of Thermal Properties of Gases," Natl. Bur. Std. U.S., Circ. No. 564, U.S. Dept. Commer., Nov. 1.
22. Hughes, W. F. and Gaylord, E. W., c1964, "Basic Equations of Engineering Science," Schaum's Outline Series, McGraw-Hill Book Co., Inc.
23. Hughes, T. H. and Reid, W. H., 1965, "On the Stability of the Asymptotic Suction Boundary-Layer Profile," J. Fluid Mech., 23, pp. 715-735.
24. Kahawita, R. A. and Meroney, R. N., 1977, "The Influence of Heating on the Stability of Laminar Boundary Layers Along Concave Curved Walls," J. Appl. Mech. 44, 11-17.
25. Kobayashi, R., 1972, "Note on the Stability of a Boundary Layer on a Concave Wall With Suction," J. Fluid Mech., Vol. 52, Part 2, pp. 269-272, Mar. 28.
26. Kobayashi, R., 1973, "Stability of Laminar Boundary Layer on a Concave Permeable Wall With Homogeneous Suction," Reports of the Institute of High Speed Mechanics, 27, No. 253, Tohoku Univ., Sendai, Japan, pp. 31-47.
27. Kobayashi, R., 1974, "Taylor-Goertler Instability of a Boundary Layer With Suction or Blowing," AIAA Journal, Vol 12, No. 3, pp. 394-395, Mar.

28. Kobayashi, R. and Kohama, Y., 1977, "Taylor-Goertler Instability of Compressible Boundary Layers," AIAA Journal, Vol 15, No. 12, 1723-1727, Dec.
29. Liepmann, H. W., 1945, "Investigation of Boundary Layer Transition on Concave Walls," NACA WR W-87, (Formerly NACA ACR 4J28).
30. Mack, L. M., 1975, "Linear Stability Theory and the Problem of Supersonic Boundary-Layer Transition," AIAA Journal, Vol. 13, No. 3, 278-289, March.
31. Nayfeh, A. H., 1979, "Effect of Streamwise Vortices on Tollmien-Schlichting Waves," VPI & SJ Rept. No. VPI-E-79.12, March, (Available as NASA CR-162654).
32. Persen, L. N., 1968, "Investigation of Streamwise Vortex System Generated in Certain Classes of Curved Flow," Part I, ARL-68-0134, July.
33. Ragab, S. A. and Nayfeh, A. H., 1980, "Effect of Pressure Gradients on Goertler Instability," AIAA Paper No. 80-1377, July.
34. Rayleigh, (Lord), "On the Dynamics of A Revolving Fluid," Scientific Papers, Vol. VI, pp. 447-453, (1916).
35. Saric, W. S. and Nayfeh, A. H., 1977, "Nonparallel Stability of Boundary Layer Flows With Pressure Gradients and Suction," "Laminar-Turbulent Transition," AGARD-CP-224, pp. 6-1 - 6-21, October.
36. Scott, R. R. and Watts, H. A., 1977, "Computational Solution of Linear Two-Point Boundary-Value Problems via Orthonormalization," SIAM J. Num. Anal., 14, pp. 40-70.
37. Smith, A. M. O., 1955, "On the Growth of Taylor-Goertler Vortices Along Highly Concave Walls," Quart. Appl. Math. XIII, No. 3, 233-262, Oct.
38. Tani, I., 1961, "Some Aspects of Boundary-Layer Transition at Subsonic Speeds," Adv. Aero. Sci. 3, 143-160.

39. Tani, I., and Sakagami, J., 1962, "Boundary Layer Instability at Subsonic Speeds," Proc. Int. Counc. Aero. Sci., Stockholm, (Spartan, Wash. D. S., 1964).
40. Taylor, G. I., "Stability of A Viscous Liquid Contained Between Two Rotating Cylinders," Phil. Trans. Roy. Soc. (London) A, Vol 223, pp. 289-343, Feb. (1923).
41. Van Dyke, M., 1960, "Higher Approximations in Boundary Layer Theory," Lockheed Missiles and Space Div., IMSD - 703097.
42. Van Dyke, M., 1962, "Second-Order Compressible Boundary Layer Theory With Application to Blunt Bodies in Hypersonic Flow," Hypersonic Flow Research, Riddell, F. R. Ed., Academic, New York & London, pp. 37-76.
43. Wortmann, F. X., 1969a, "Experimentelle Untersuchungen Laminarer Grenzschichten bei Instabiler Schichtung," Proc. XI Int. Cong. Appl. Mech., pp. 815-825.
44. Wortmann, F. X., 1964, "Experimental Investigations of Vortex Occurrence at Transition in Unstable Laminar Boundary Layers," AFOSR Rep. 64-1280, AF 61(053)-220.
45. Wortmann, F. X., 1969b, "Visualization of Transition," J. Fluid Mech. 38, 473-480.
46. Zakkay, V. and Calarese, W., 1972, "An Experimental Investigation of Vortex Generation in a Turbulent Boundary Layer Undergoing Adverse Pressure Gradient," NASA CR-2037, June.



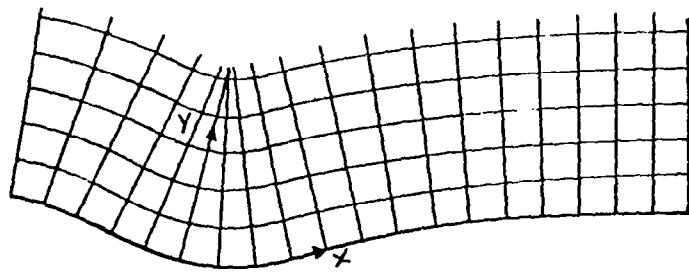


Figure 1     Body oriented coordinate system.

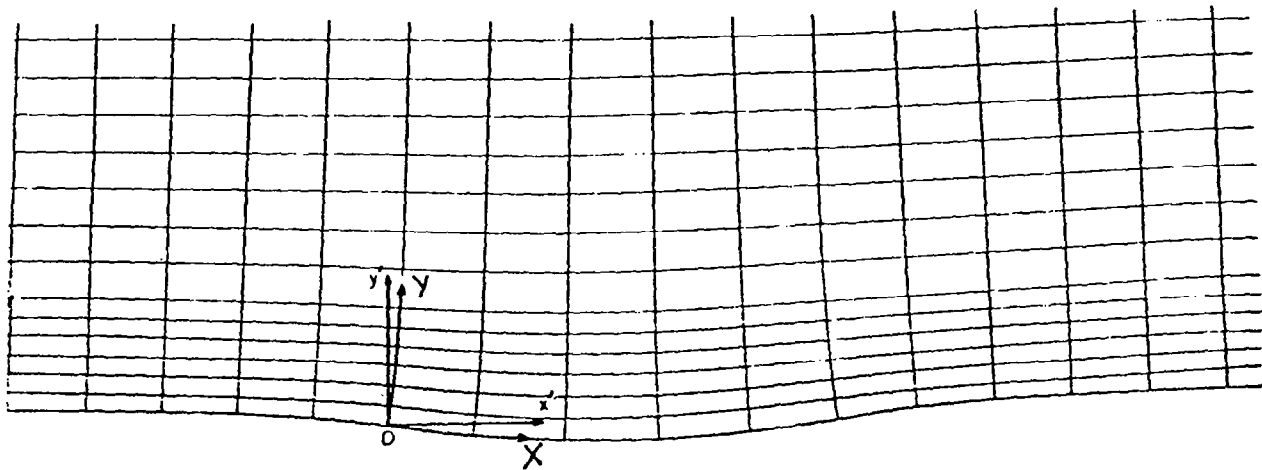


Figure 2     Coordinate system based on streamlines and  
potential lines.

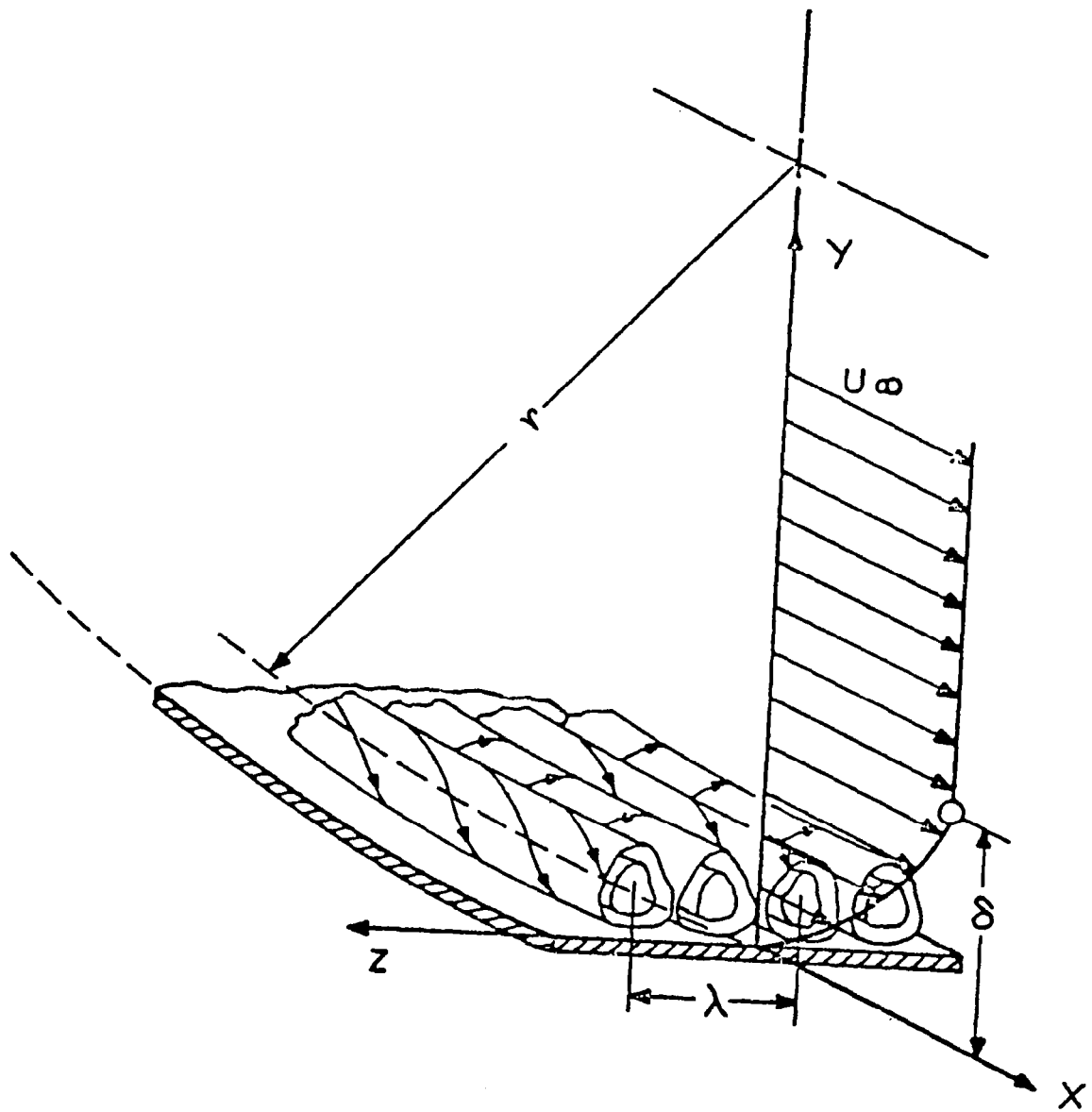


Figure 3 Goertler vortices in a flow along a concave wall.

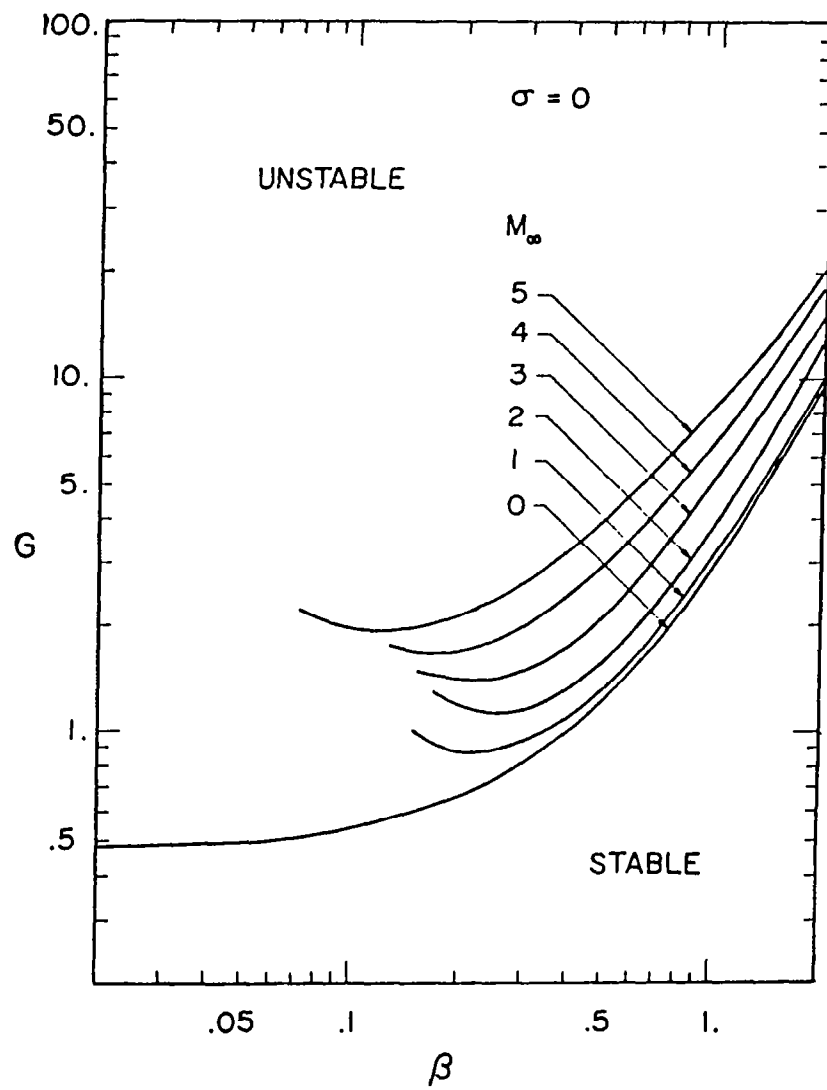


Figure 4 Effect of compressibility on the neutral stability curve.

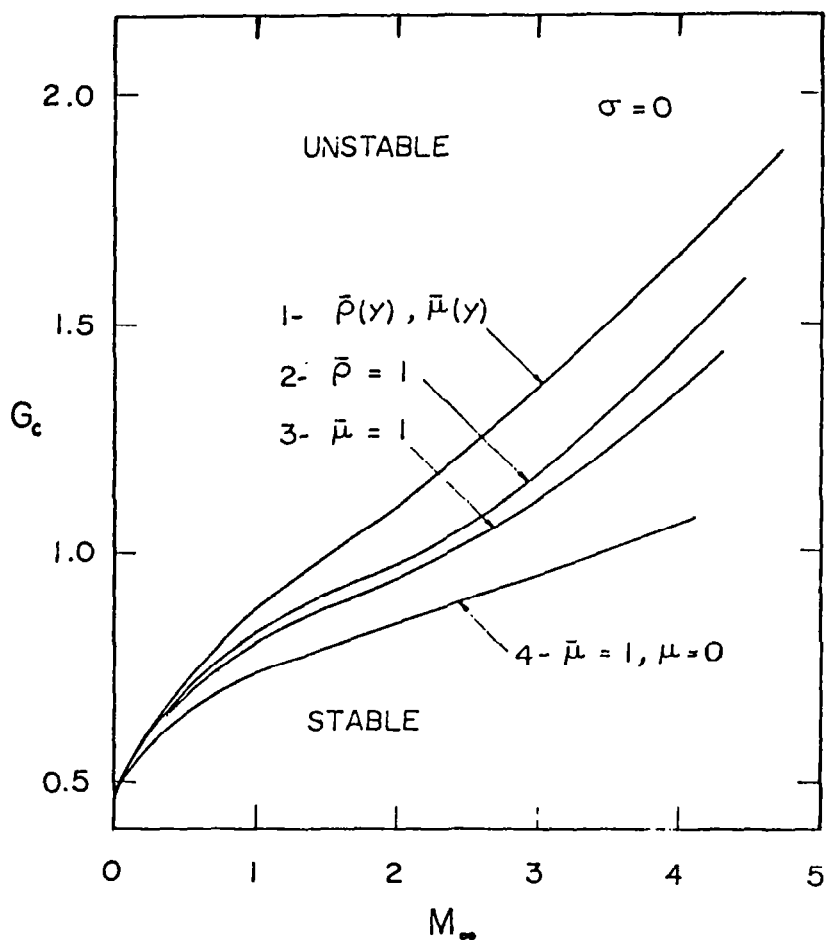


Figure 5 Effect of mean density, mean viscosity, and disturbance viscosity on minimum critical Goertler number, in a compressible boundary layer along an adiabatic flat plate.

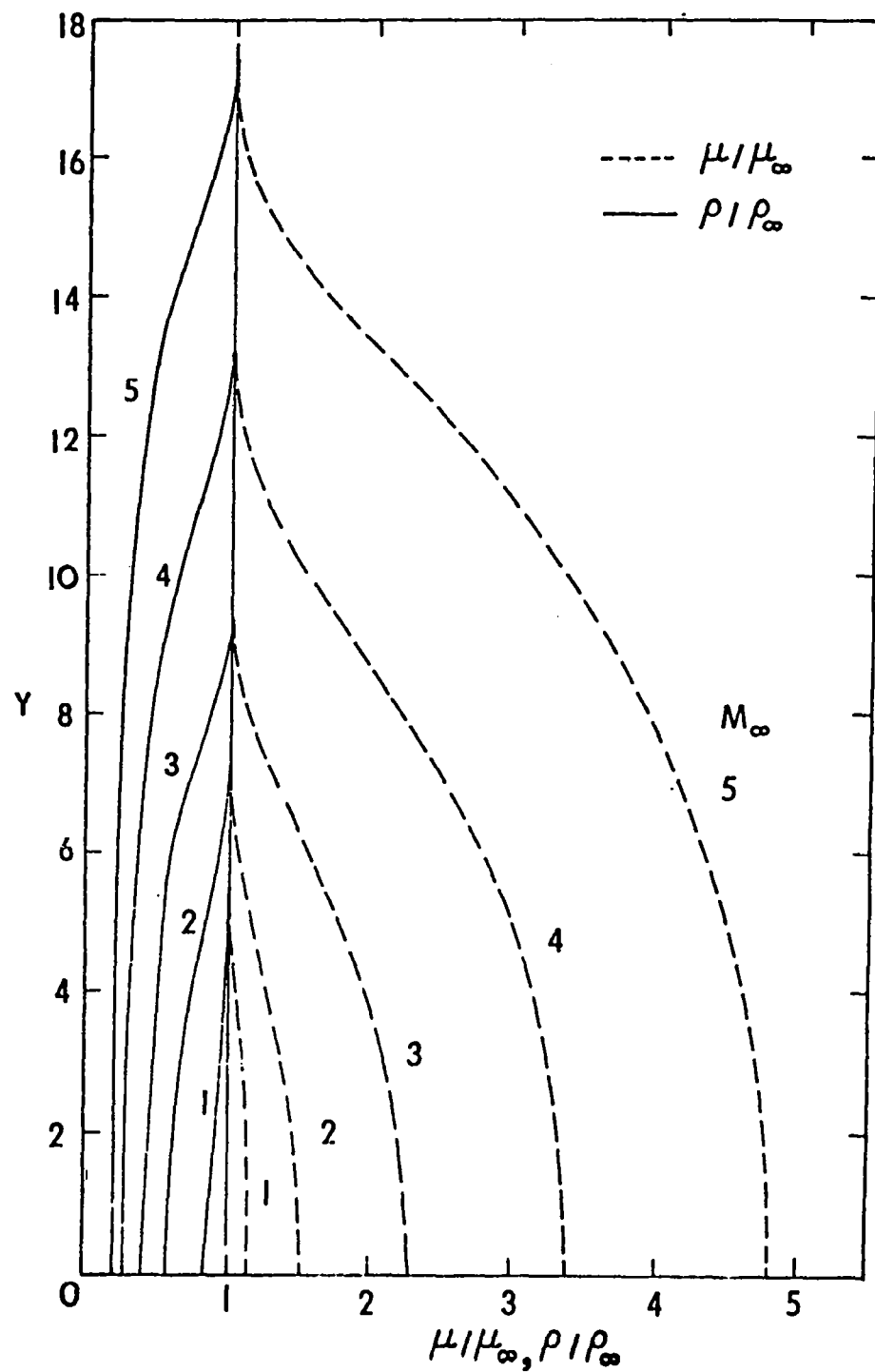


Figure 6. Variation of mean density and viscosity in the Boundary Layer.

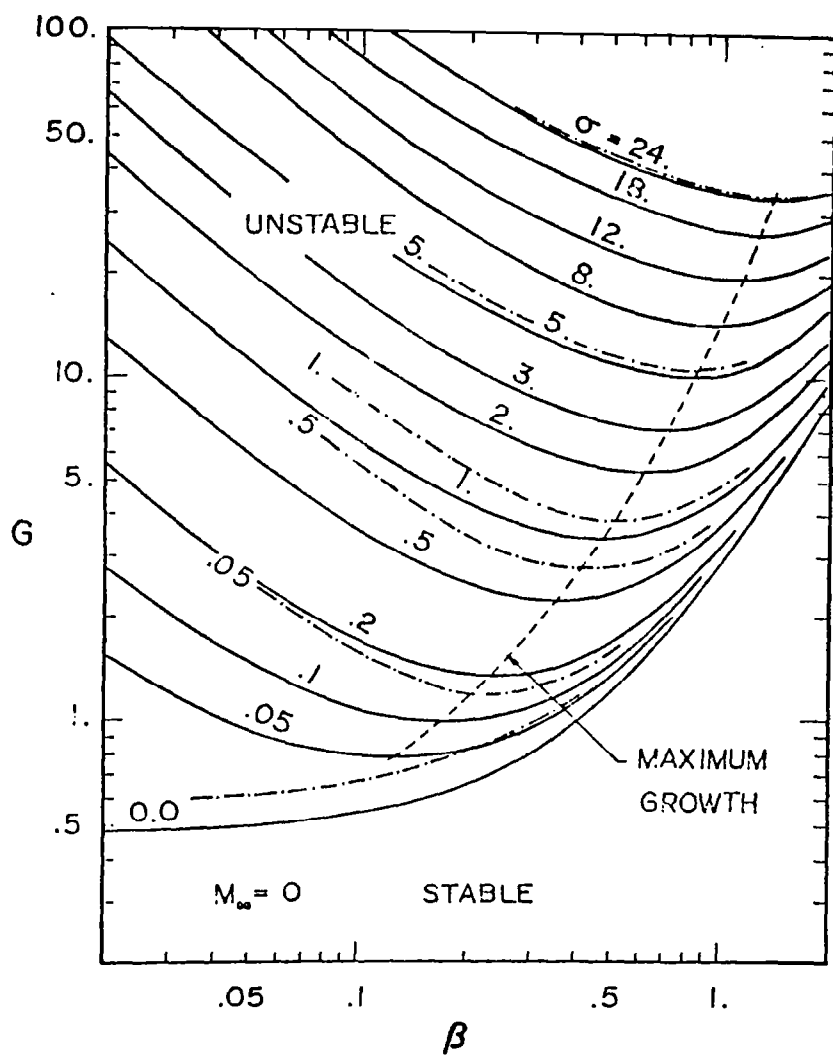


Figure 7 Contours of constant growth rates at Mach number = 0. Terms due to boundary layer growth included —, terms due to boundary layer growth excluded - - -.

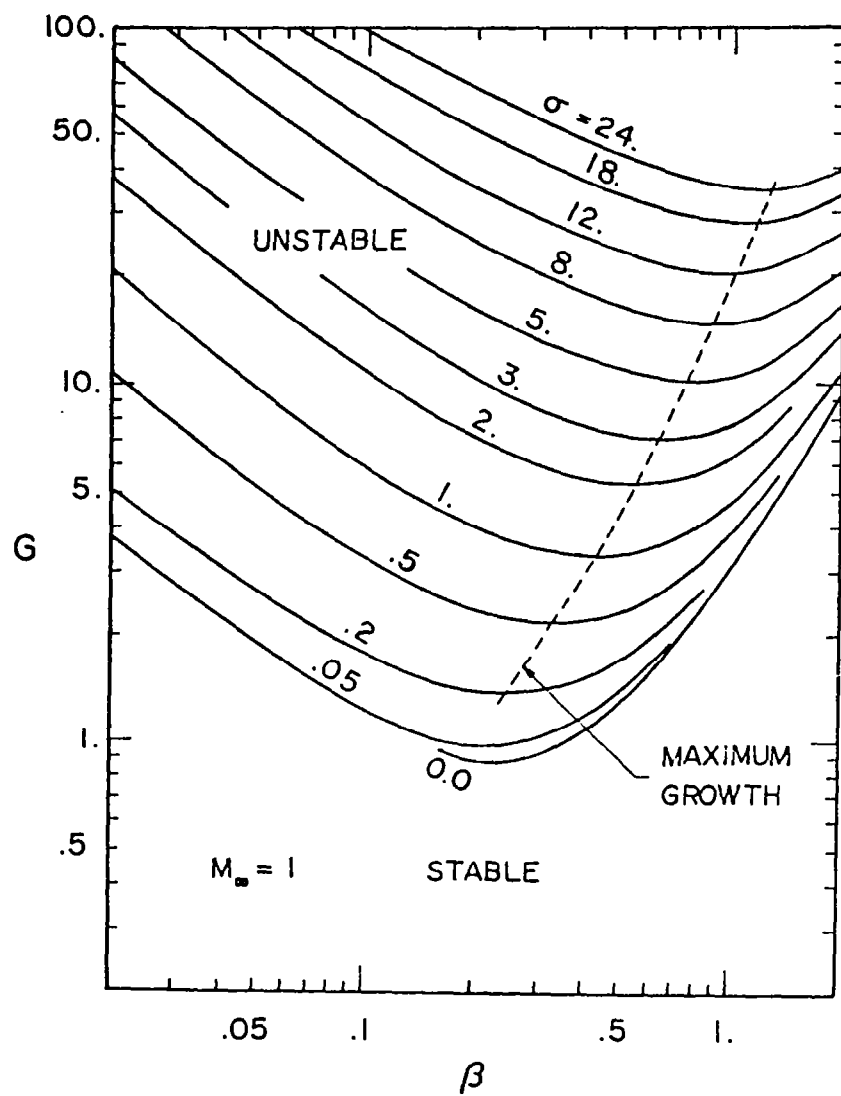


Figure 8 Contours of constant growth rates  
at Mach number = 1.

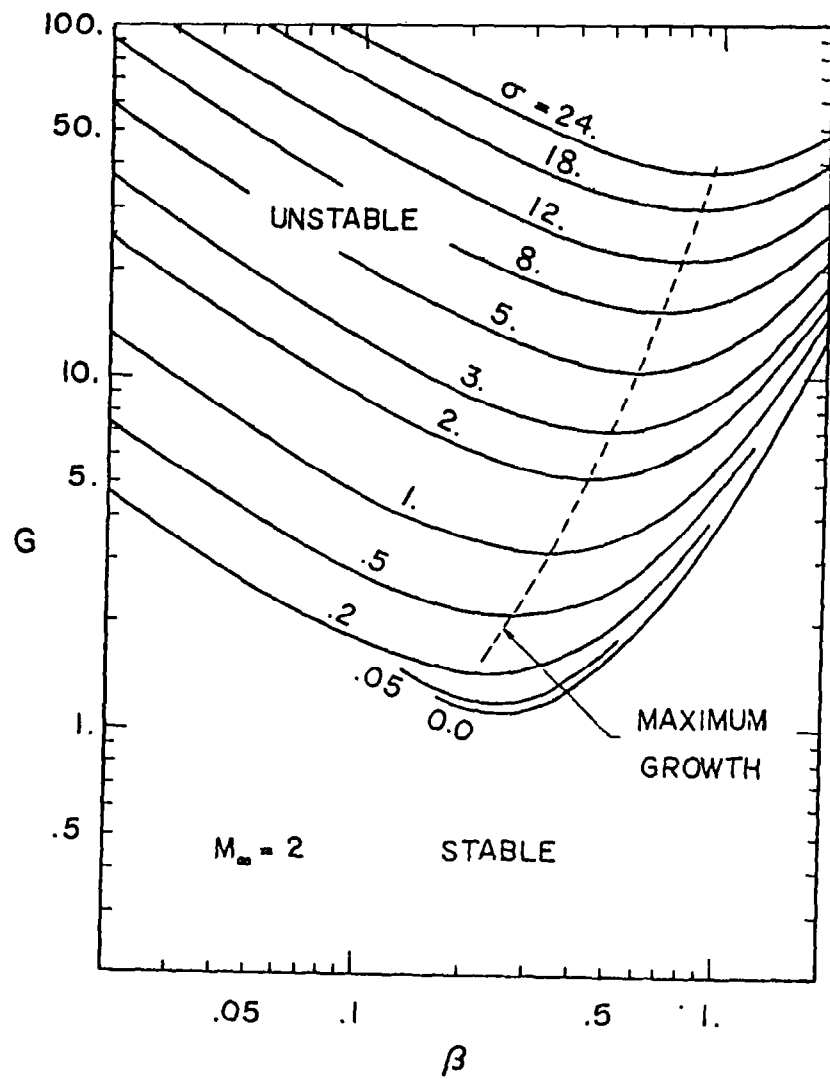


Figure 9 Contours of constant growth rates  
at Mach number = 2.

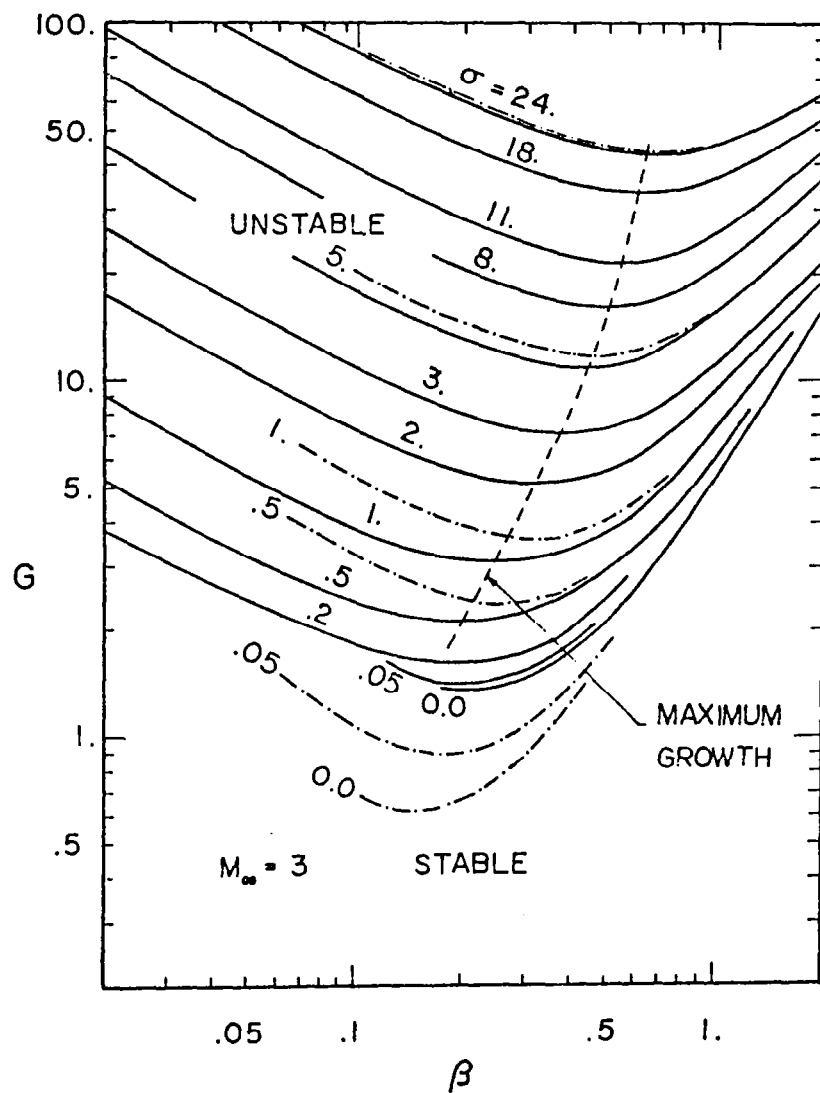


Figure 10 Contours of constant growth rates at Mach number = 3. Terms due to boundary layer growth included       , terms due to boundary layer growth excluded - - -.

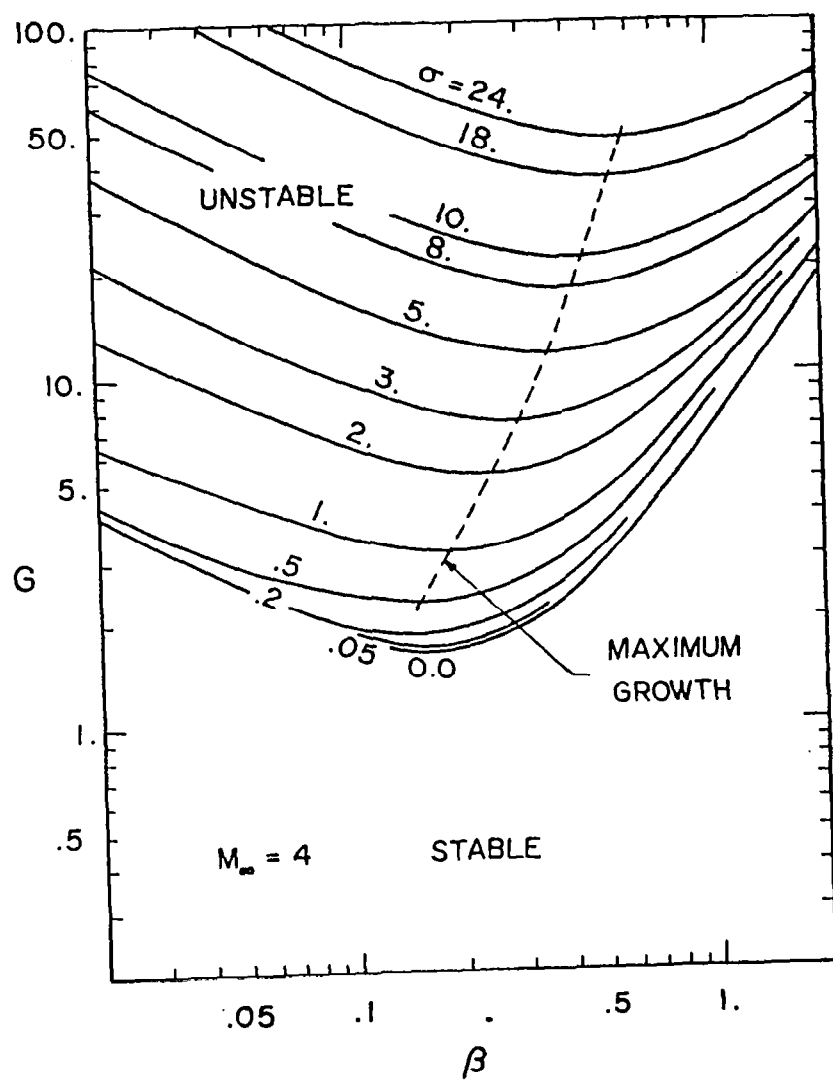


Figure 11 Contours of constant growth rates  
at Mach number = 4.

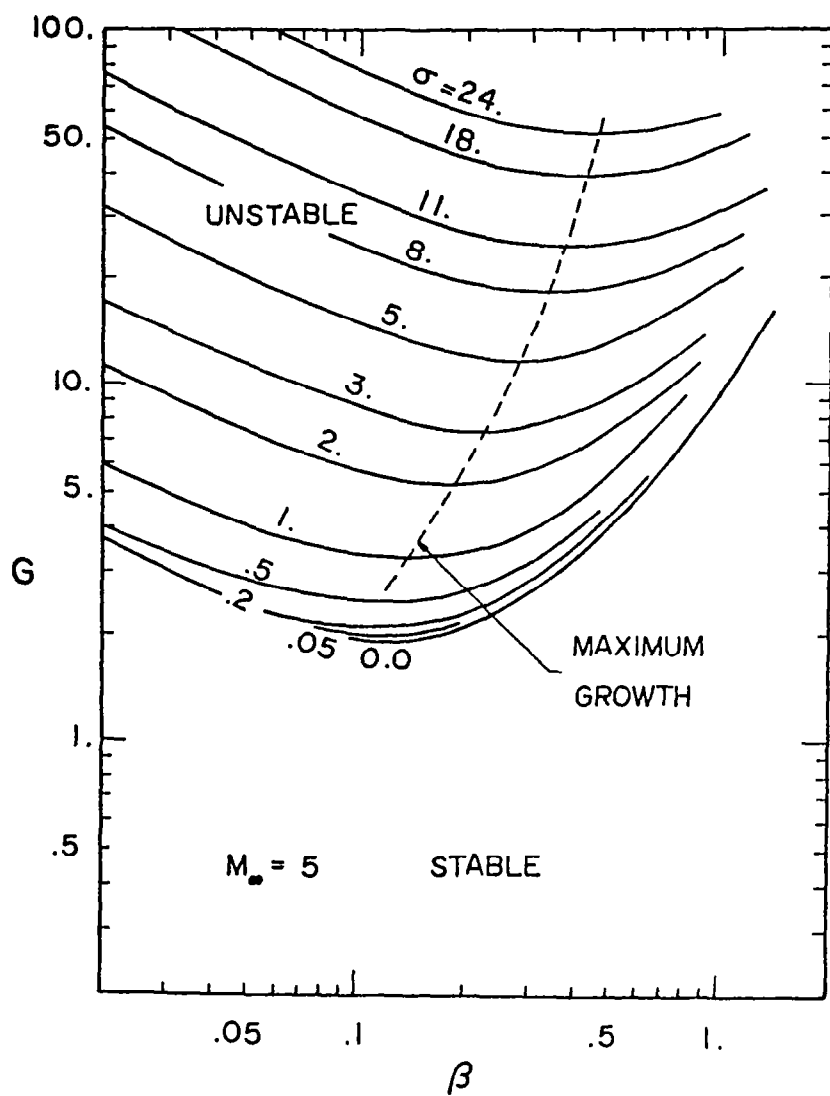


Figure 12 Contours of constant growth rates at Mach number = 5.

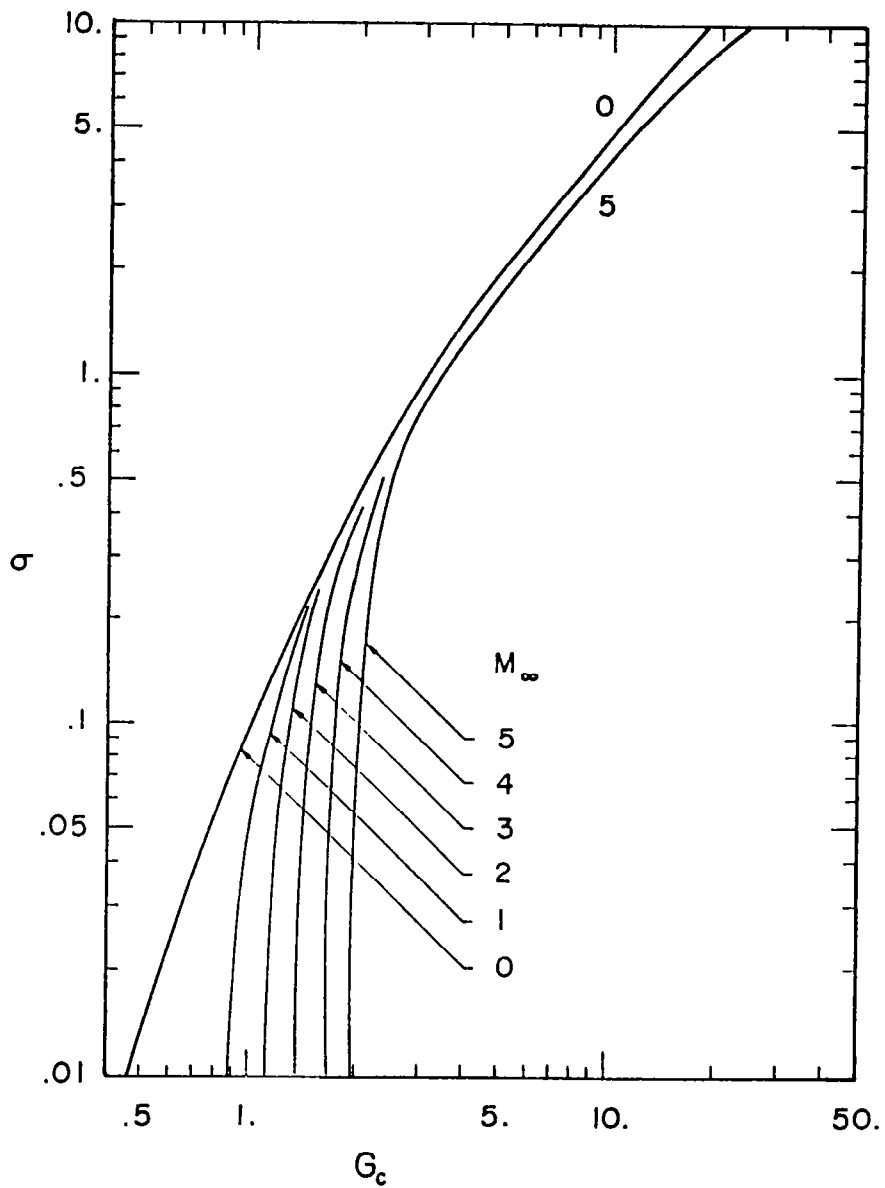


Figure 13 Effect of compressibility on the variation of vortex growth rate with Goertler number.

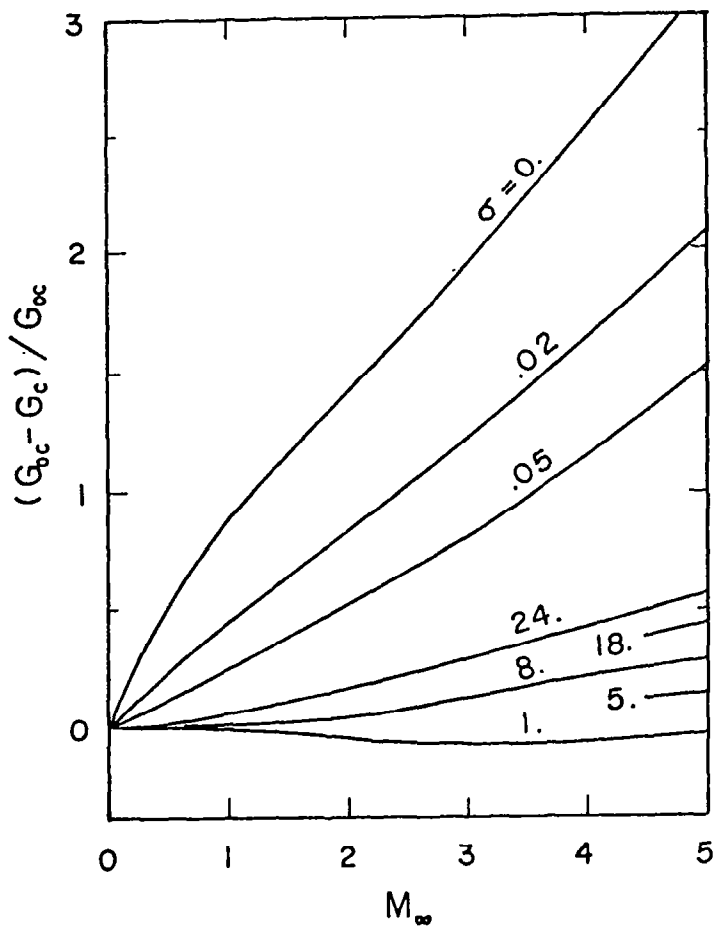


Figure 14 Effect of compressibility on local stability.

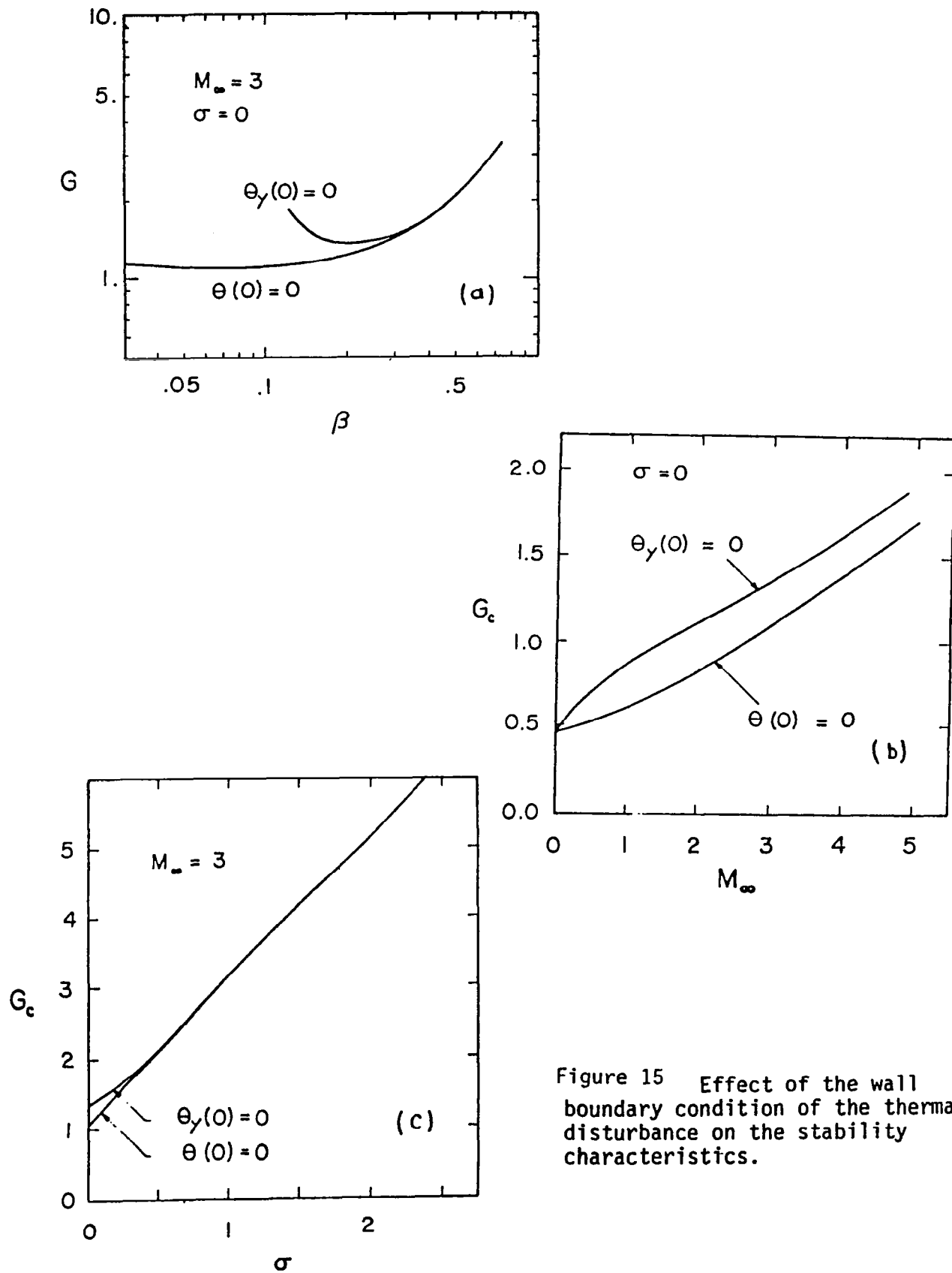


Figure 15 Effect of the wall boundary condition of the thermal disturbance on the stability characteristics.

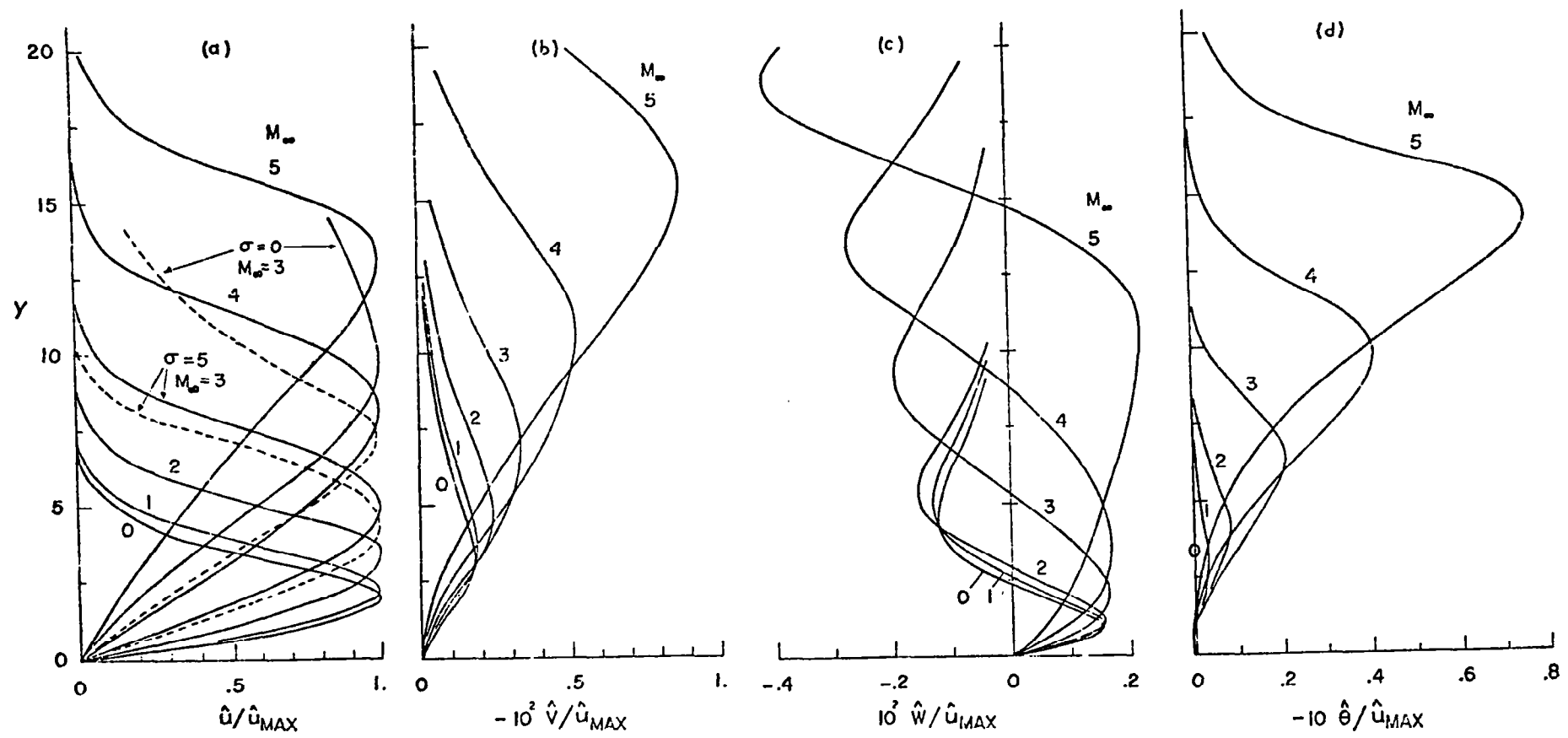


Figure 16 Effect of compressibility on the shape of the eigenfunctions for a disturbance having a wavenumber 0.3 and a growth rate 5. Terms due to boundary-layer growth included —, terms due to boundary-layer growth excluded-----.

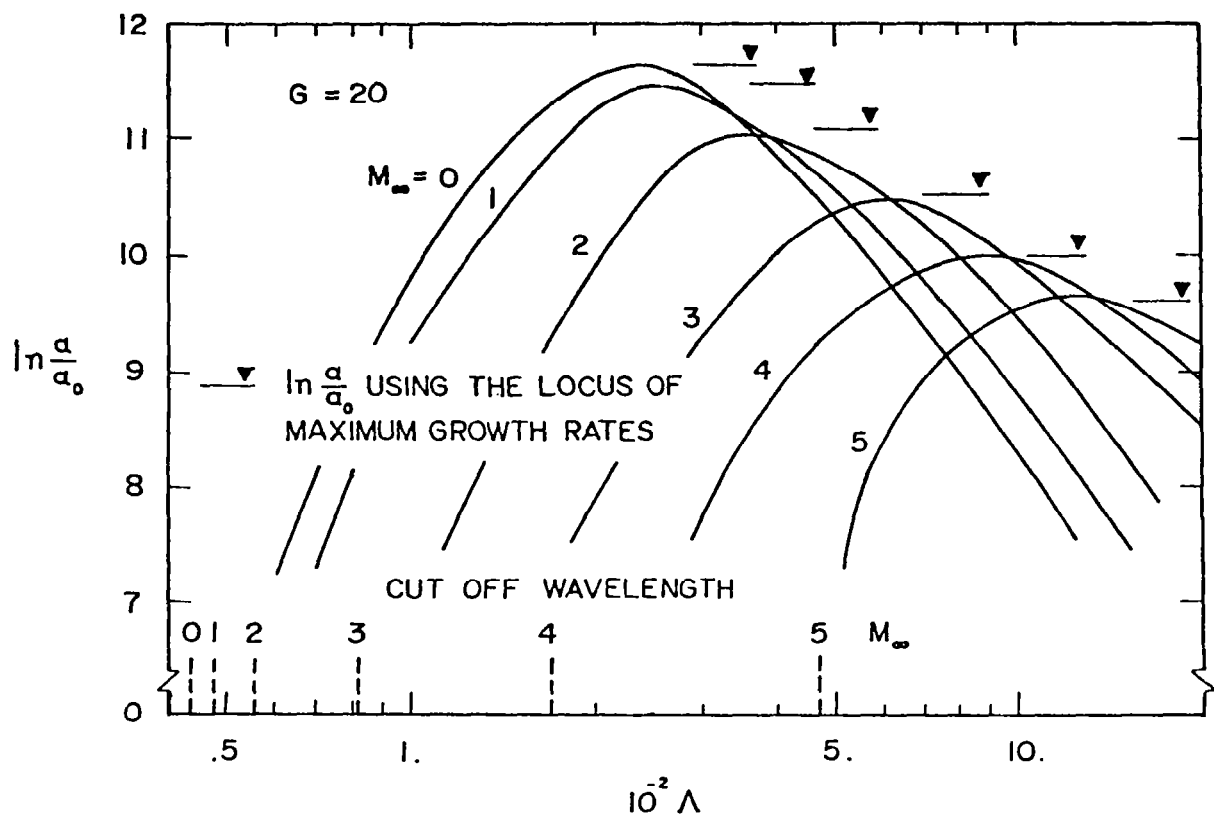


Figure 17 Effect of compressibility on the maximum amplitude ratio calculated along a growth path of constant wavelength  $\Lambda$ .

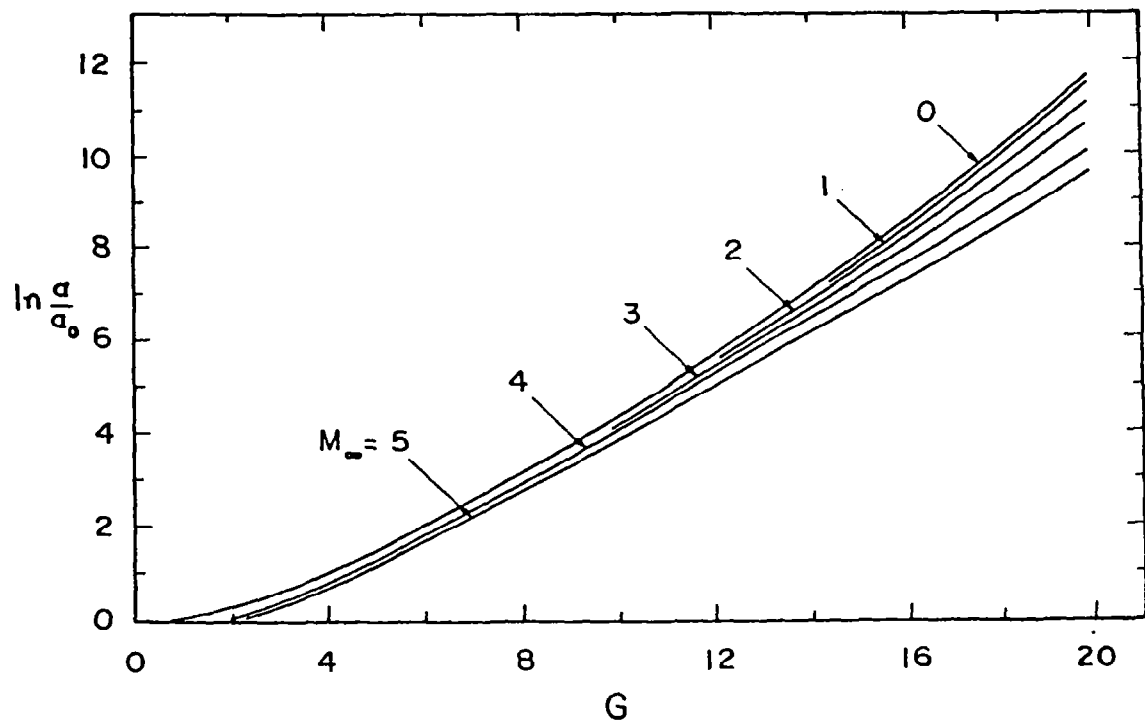


Figure 18 Effect of compressibility on the amplitude ratio calculated along the locus of maximum growth rates.

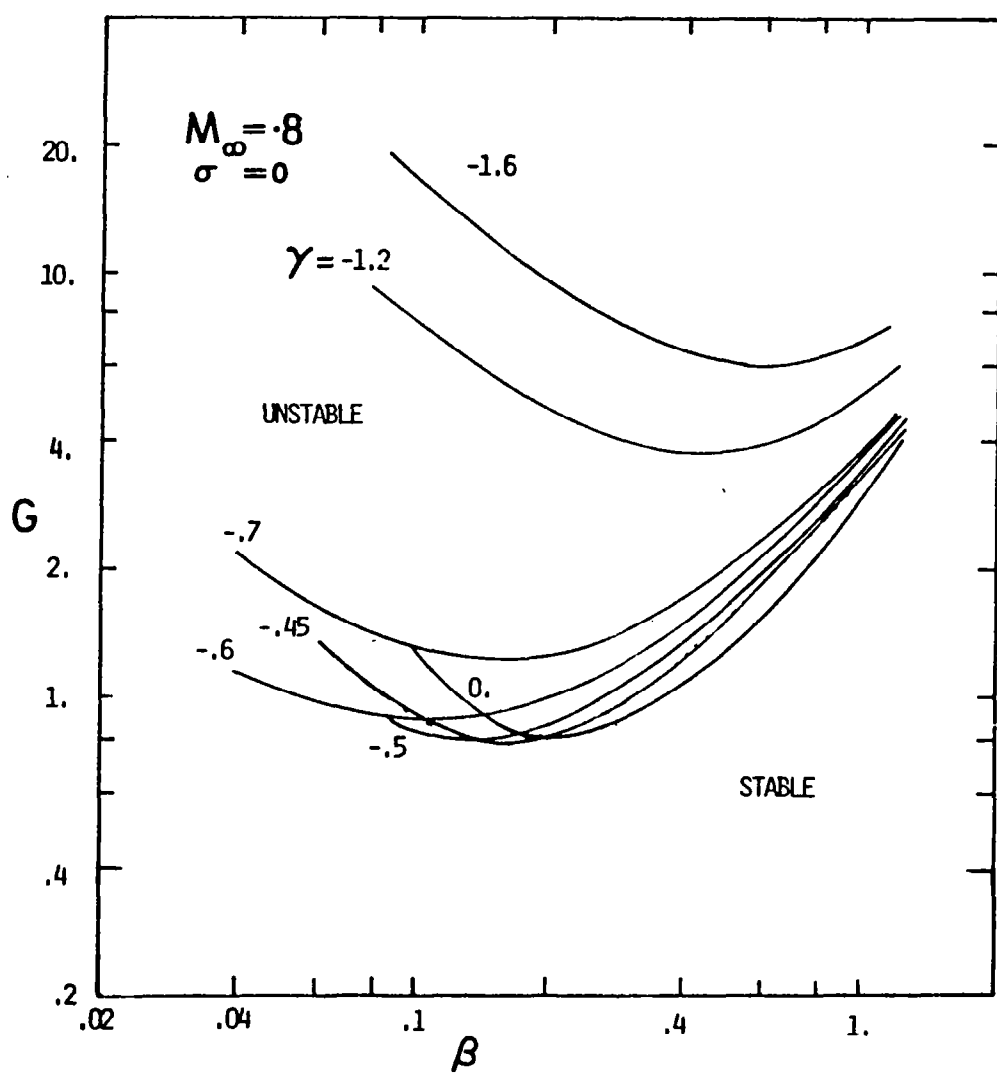


Figure 19 Neutral stability curves for different values of the suction parameter at  $M_{\infty} = 0.8$ .

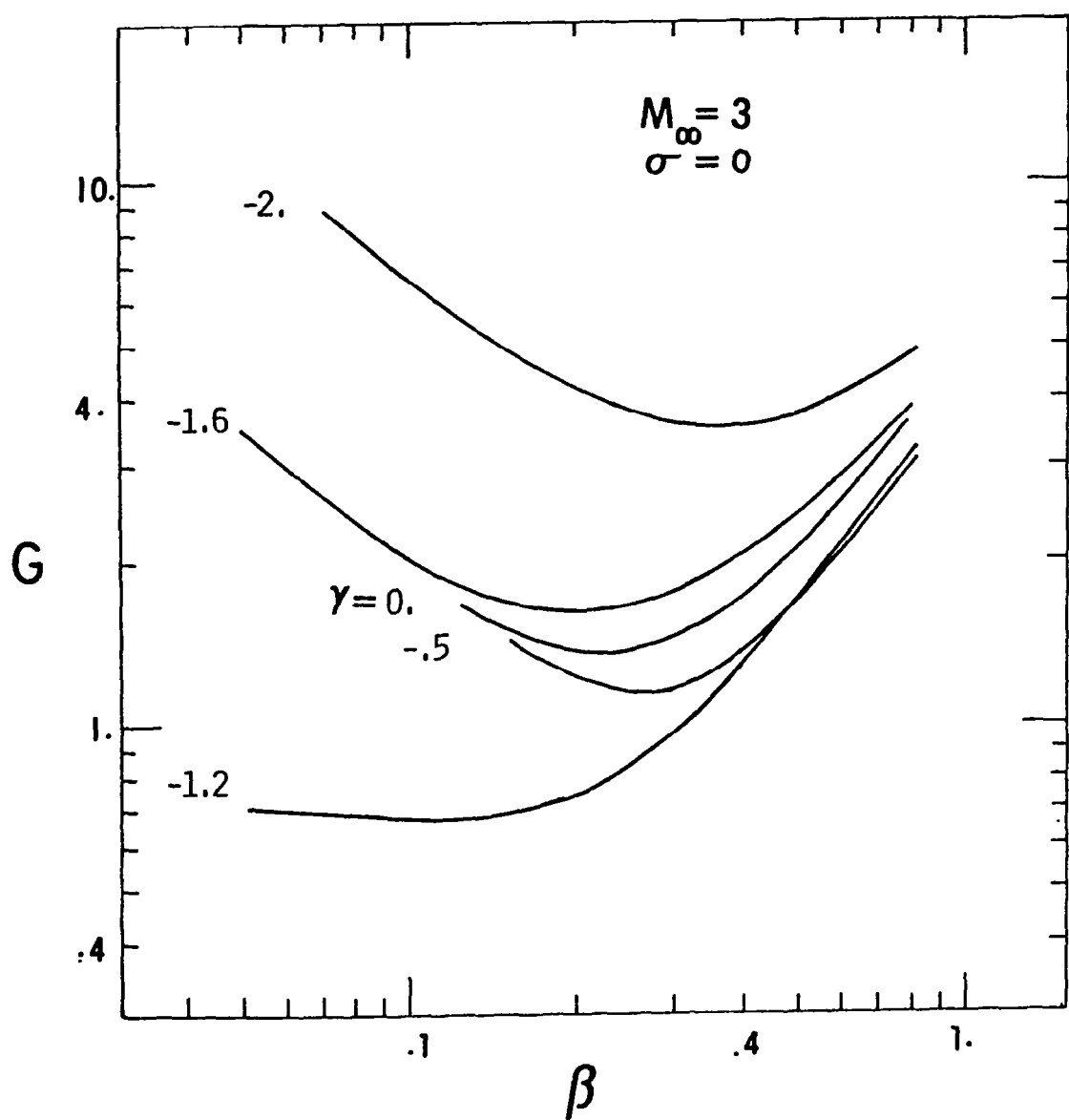


Figure 20 Neutral stability curves for different values of the suction parameter at  $M_{\infty}=0.8$ .

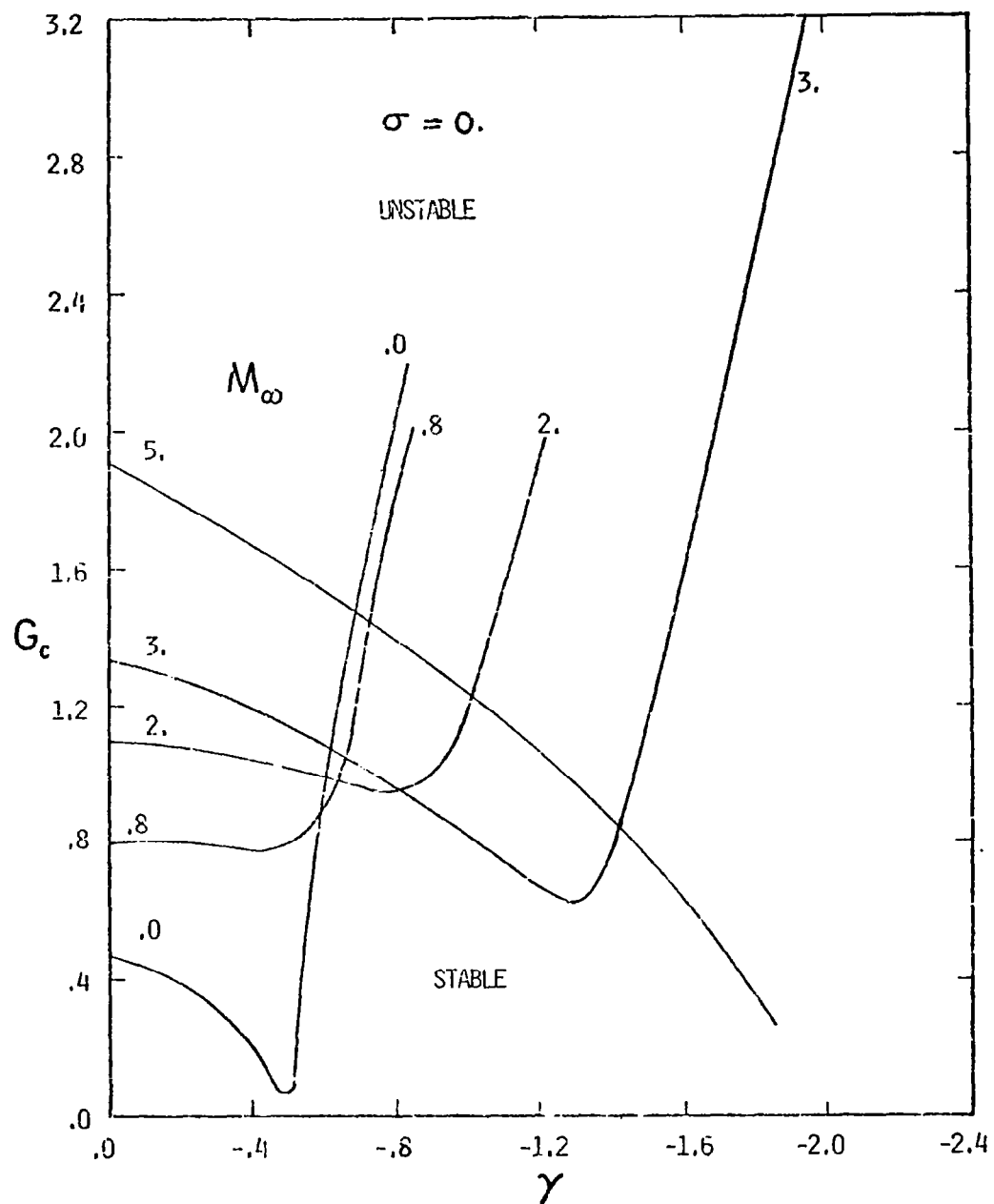


Figure 21 Effect of suction on the critical Goertler number at different Mach numbers.

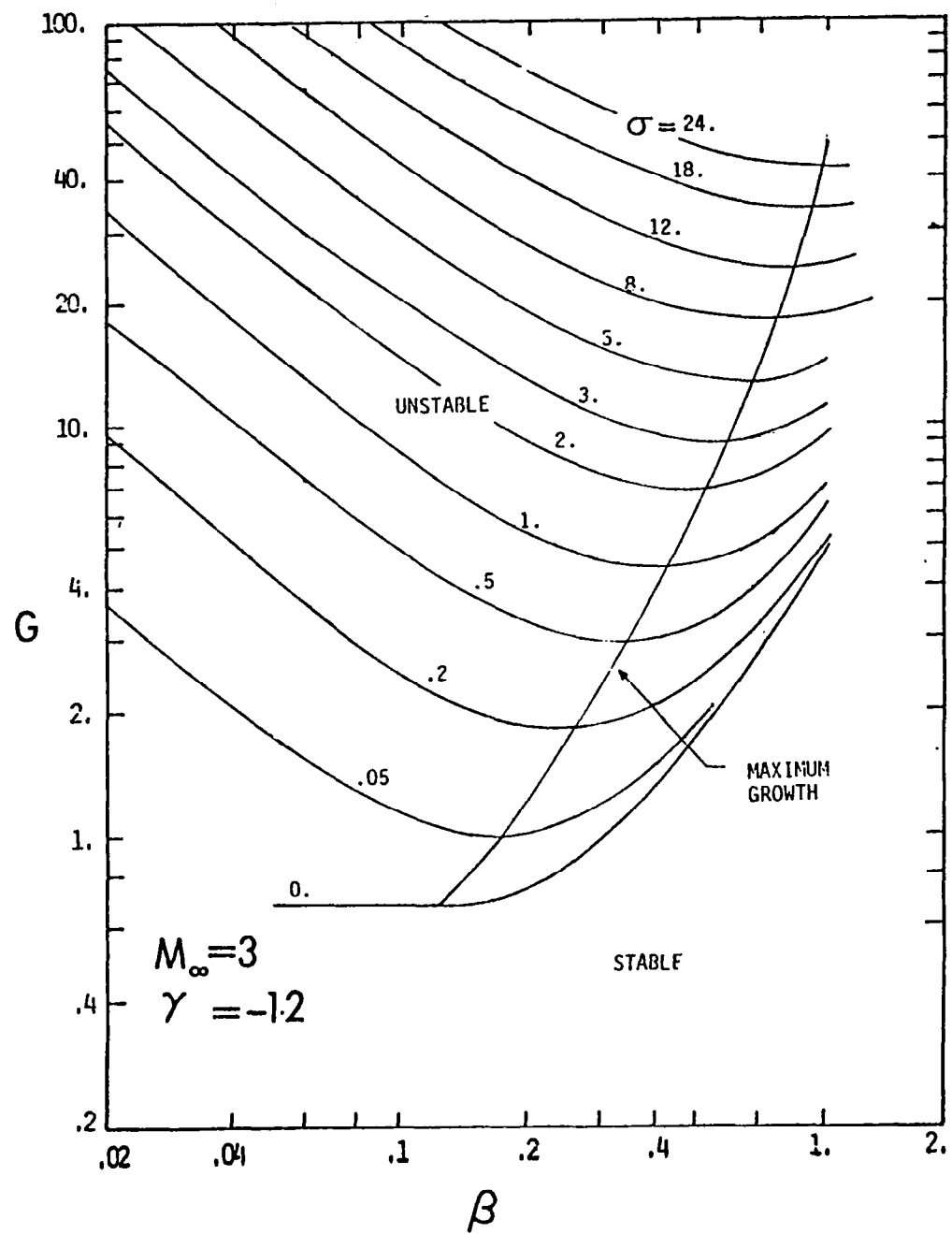


Figure 22 Contours of constant growth rates at  $M_{\infty} = 3$  and suction parameter  $\gamma = -1.2$ .

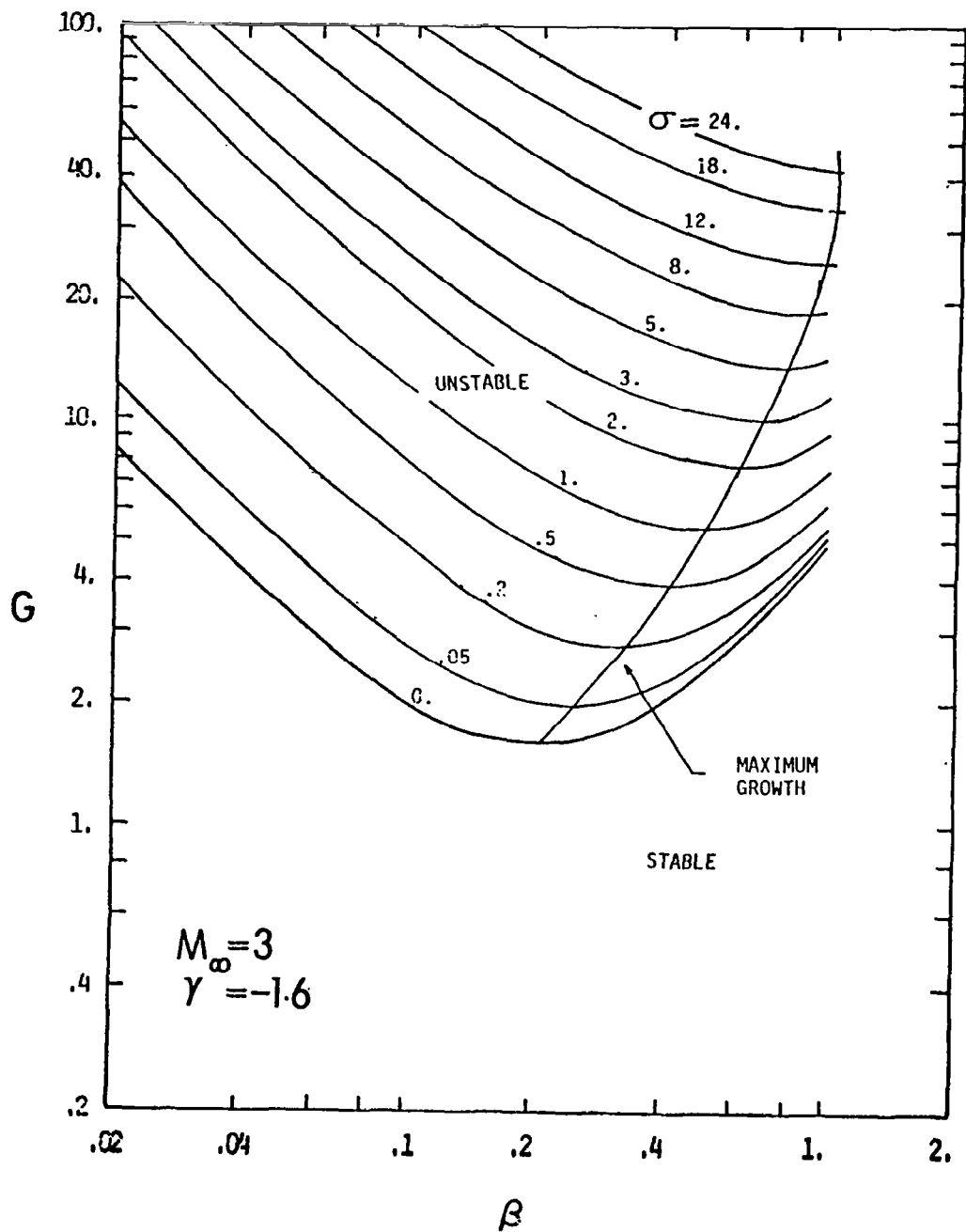


Figure 23 Contours of constant growth rates at  $M_{\infty} = 3$  and suction parameter  $\gamma = -1.6$ .

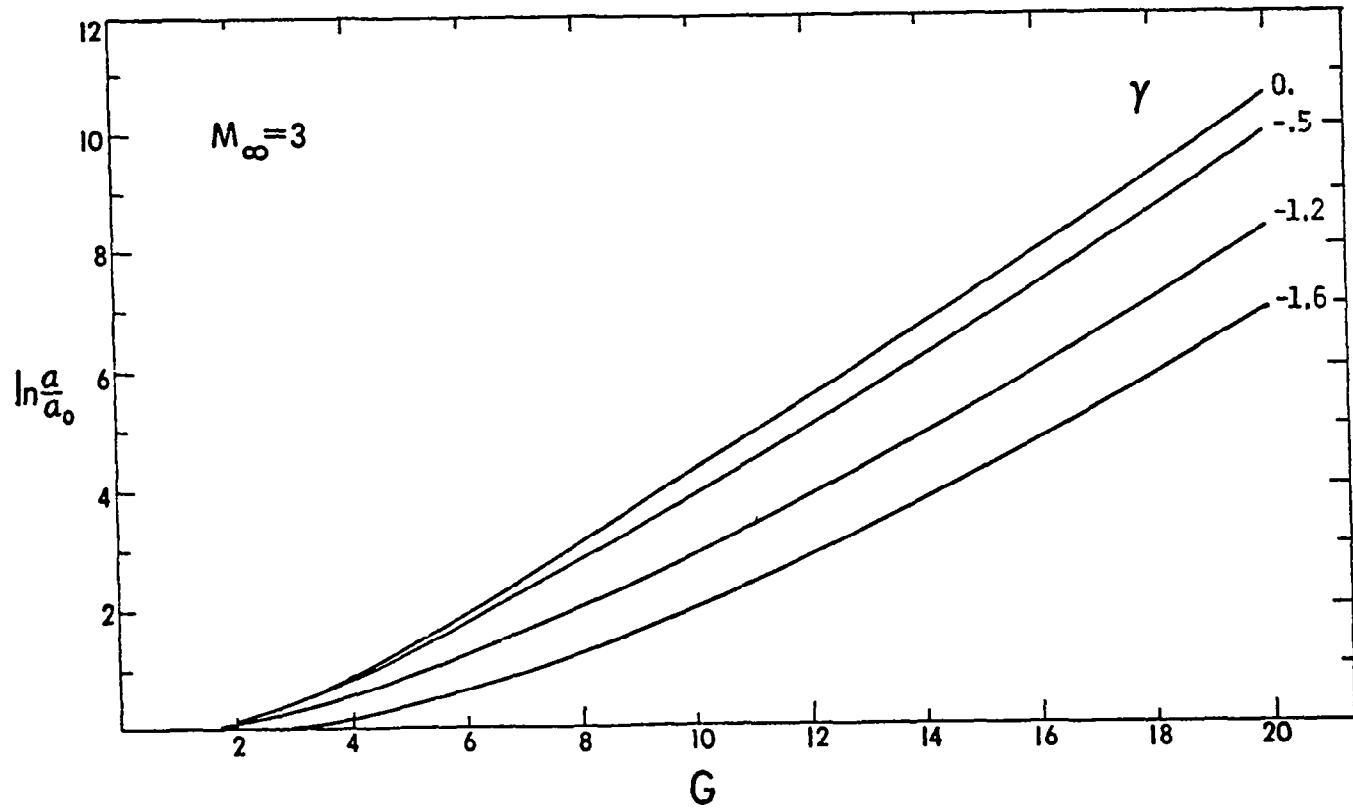


Figure 24 Effect of suction on the amplitude ratio calculated along the locus of maximum growth rates at  $M_\infty = 3$ .

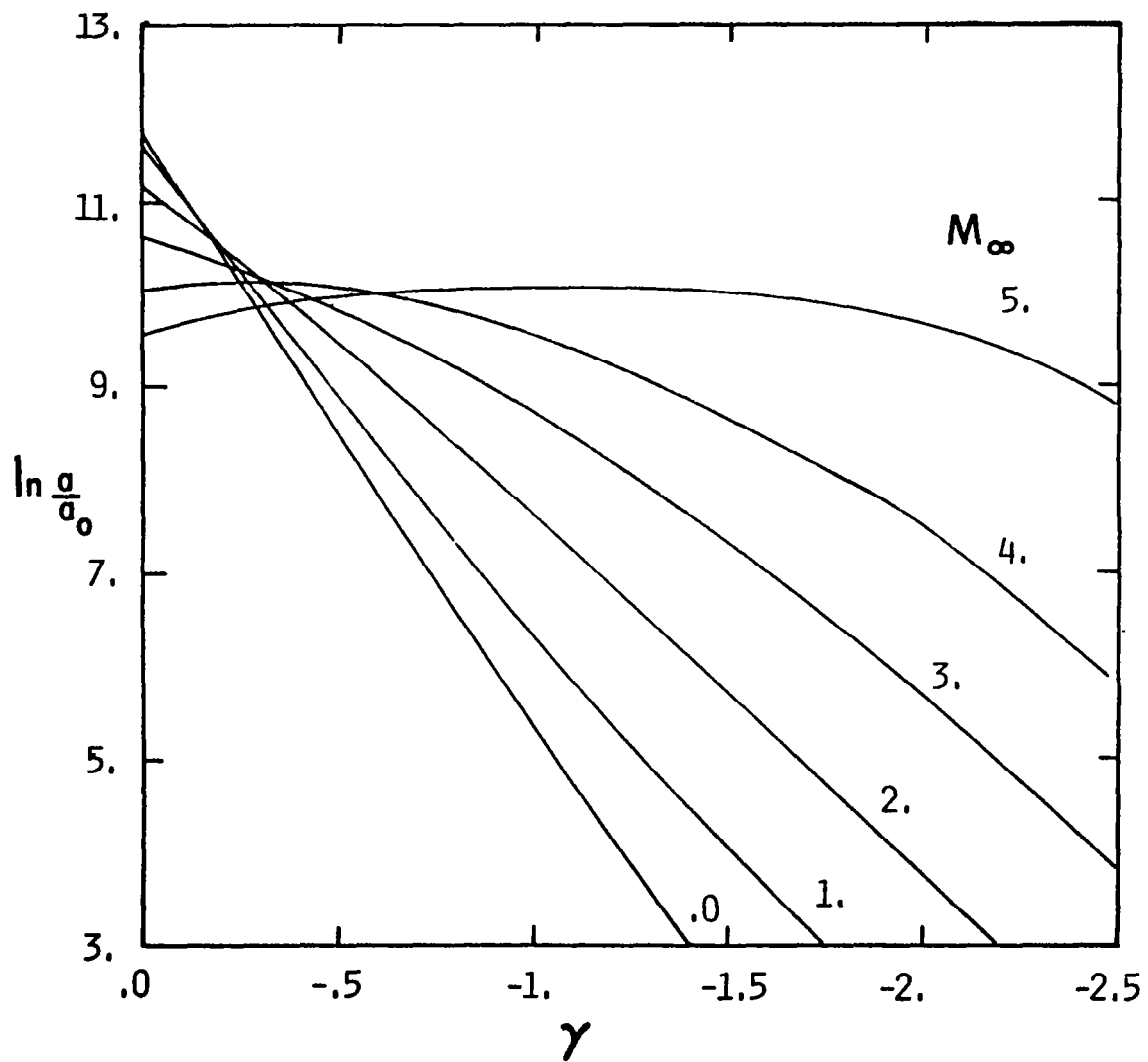


Figure 25 Effect of suction on the amplitude ratio at  
G=20 for different Mach numbers.

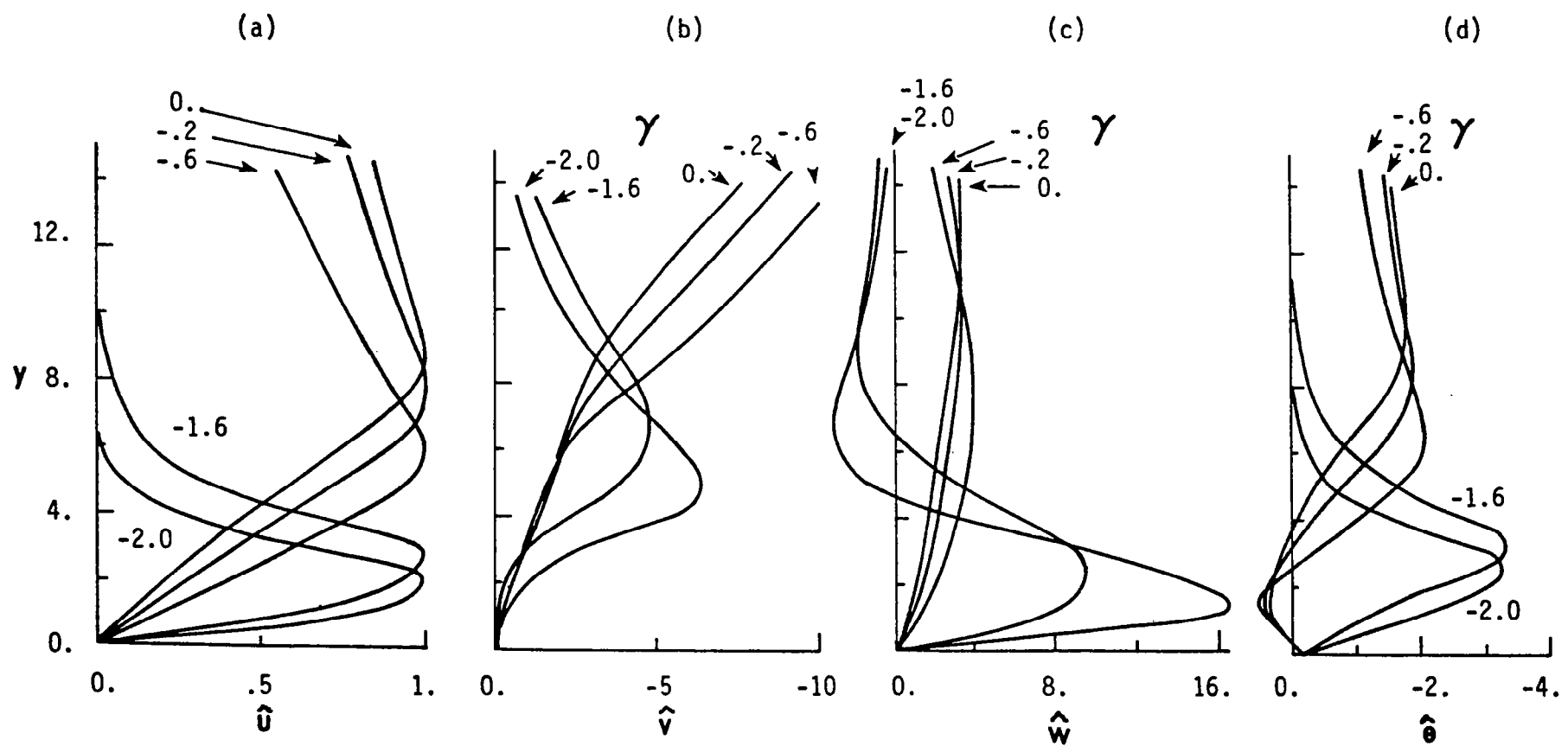


Figure 26 Effect of suction at  $M_\infty=3$  on the shape of the eigenfunctions for a disturbance having wavenumber 0.3 and zero growth rate.

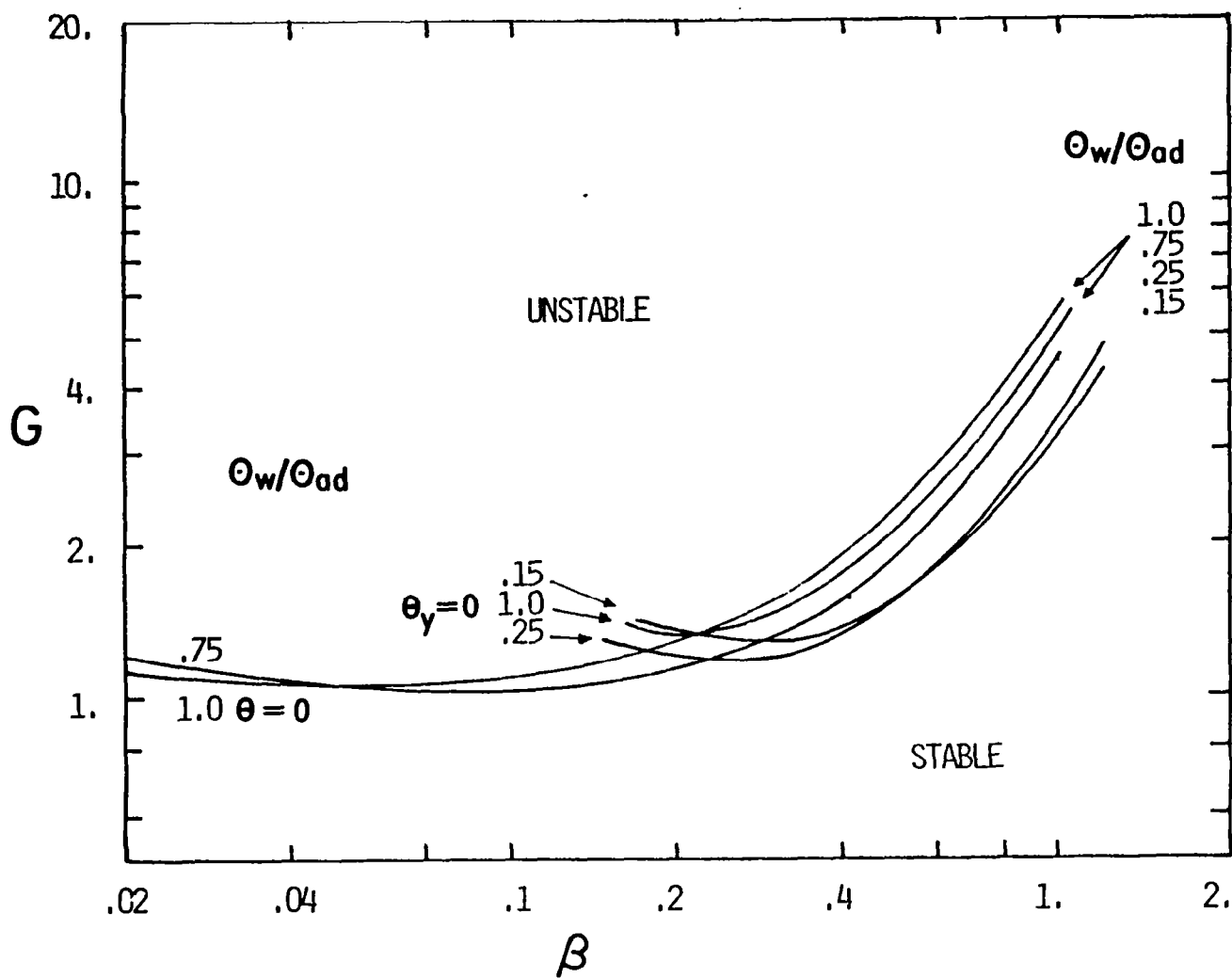


Figure 27 Neutral stability curves for different cooling rates  
at  $M_\infty = 3$ .

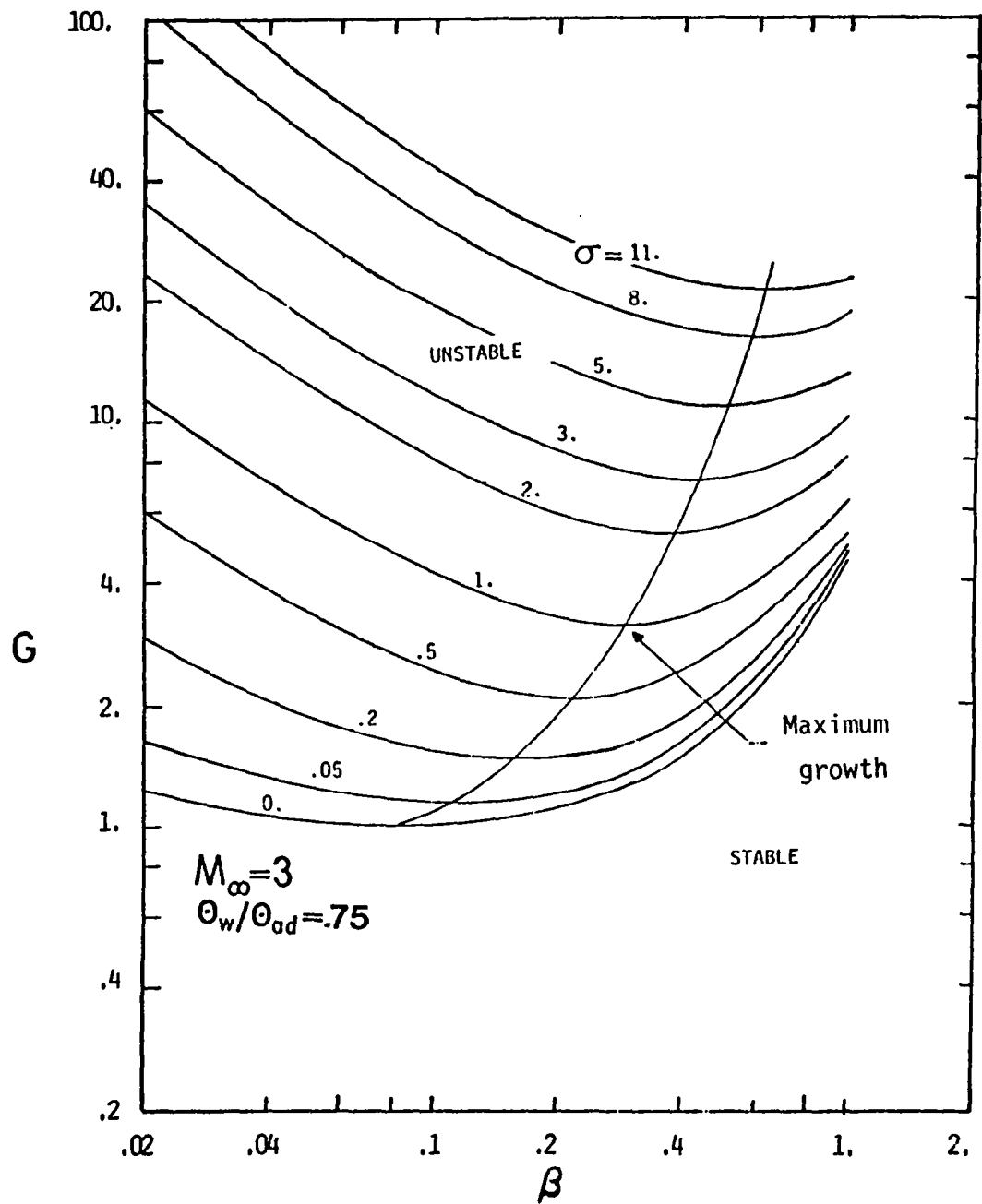


Figure 28 Contours of constant growth rates at  $M_\infty=3$  and  
 $\Theta_w/\Theta_{ad}=0.75$ .

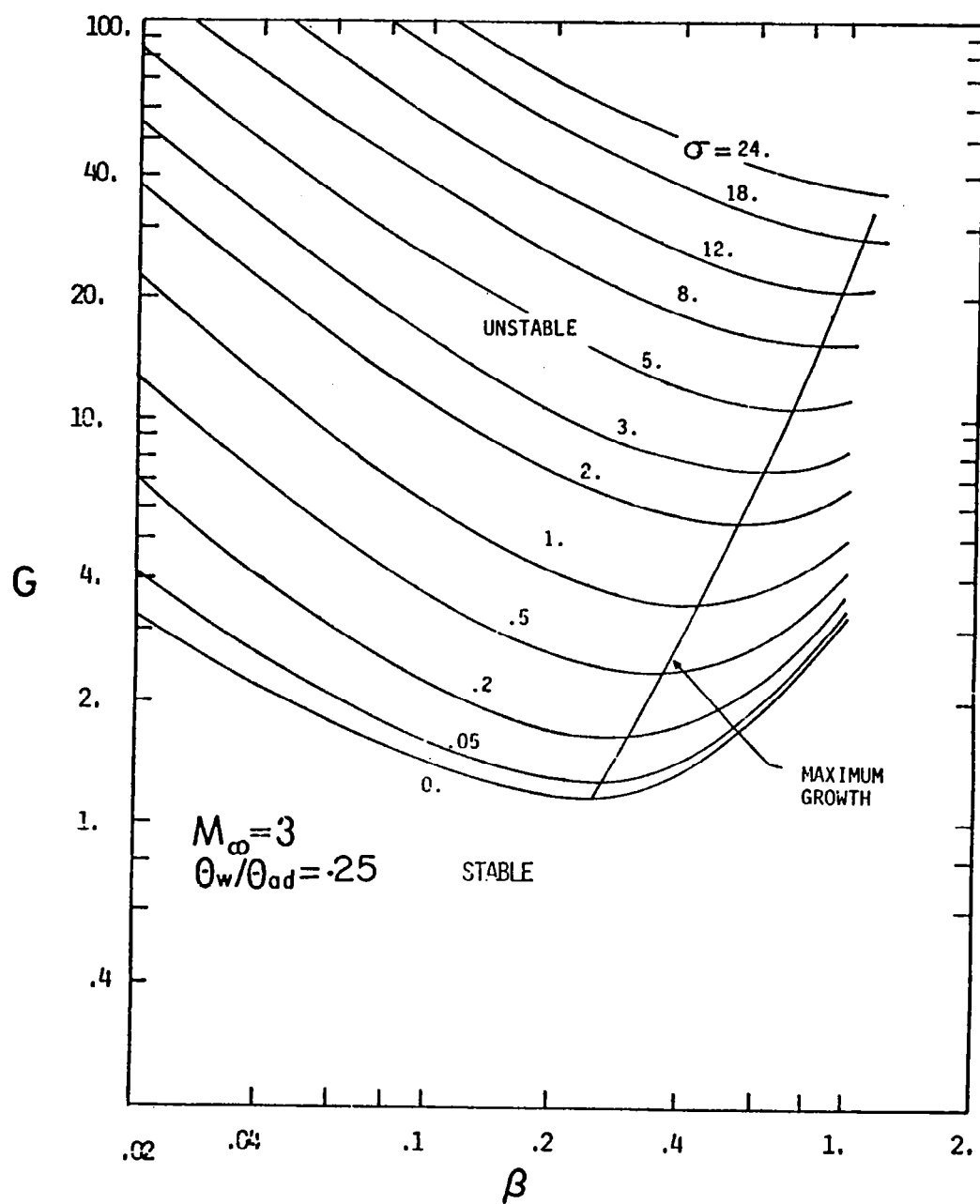


Figure 29 Contours of constant growth rates at  $M_{\infty}=3$  and  $\Theta_w/\Theta_{ad}=0.25$ .

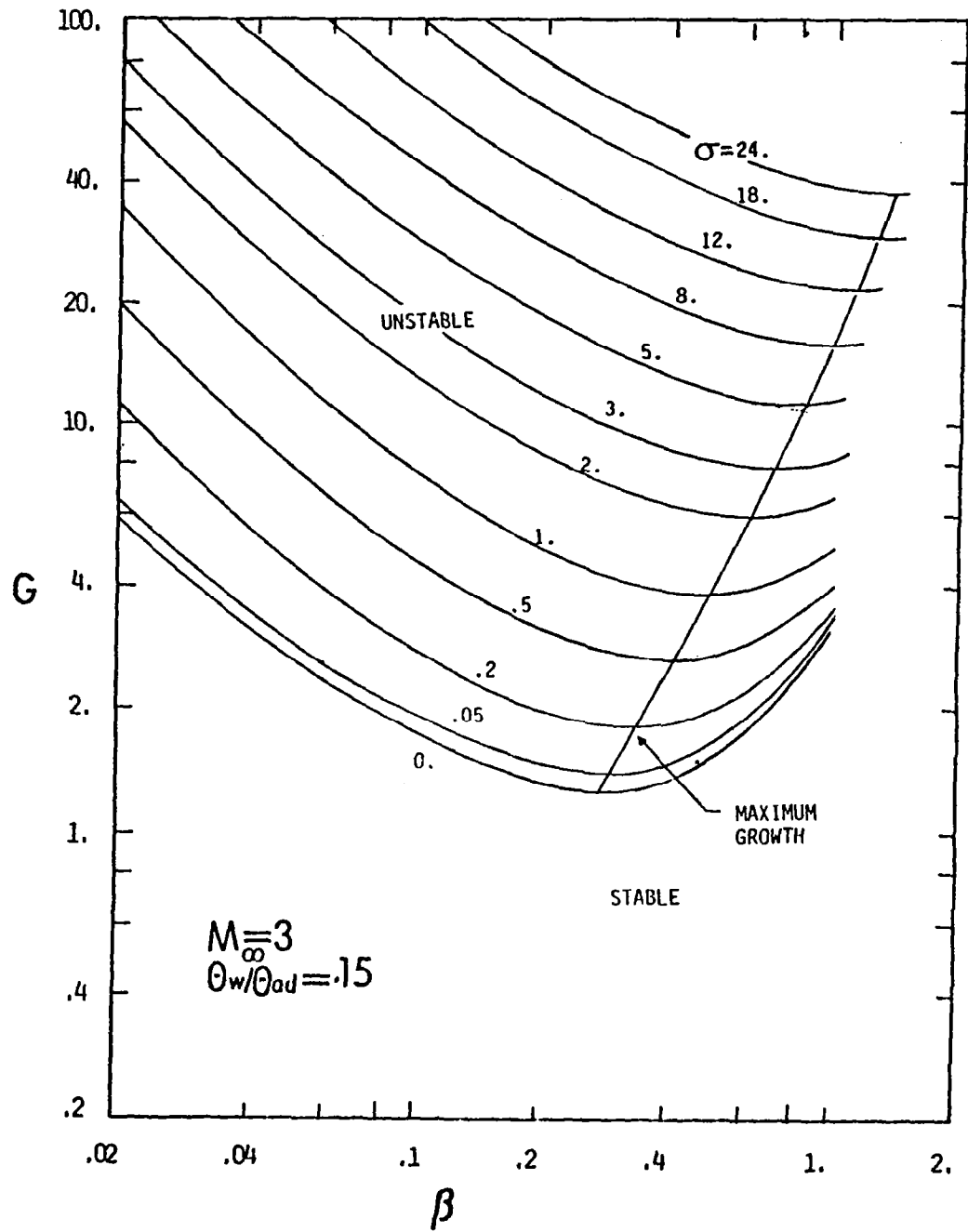


Figure 30 Contours of constant growth rates at  $M_\infty = 3$  and  $\theta_w/\theta_{ad} = 0.15$ .

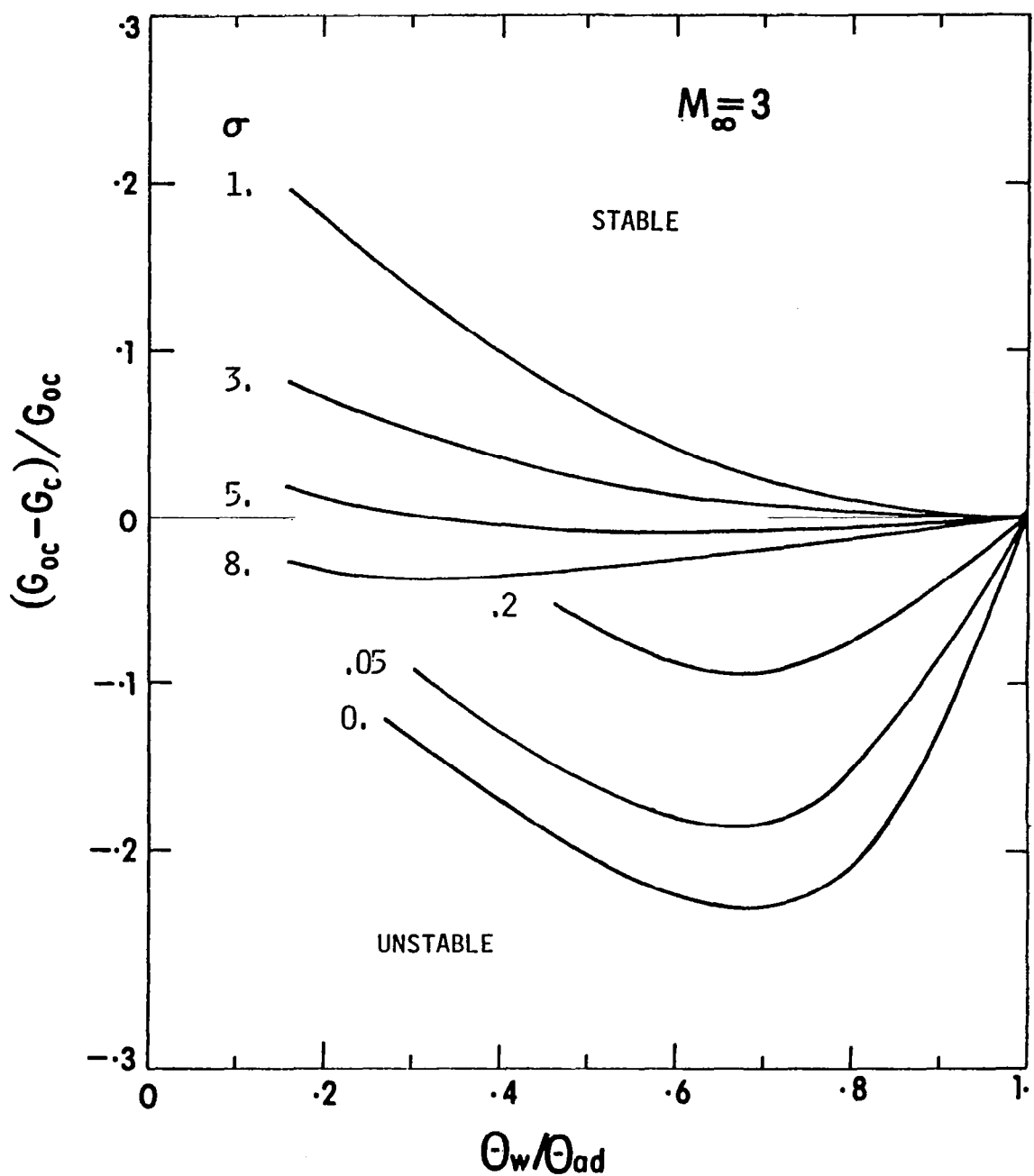


Figure 31 Effect of cooling on local stability.

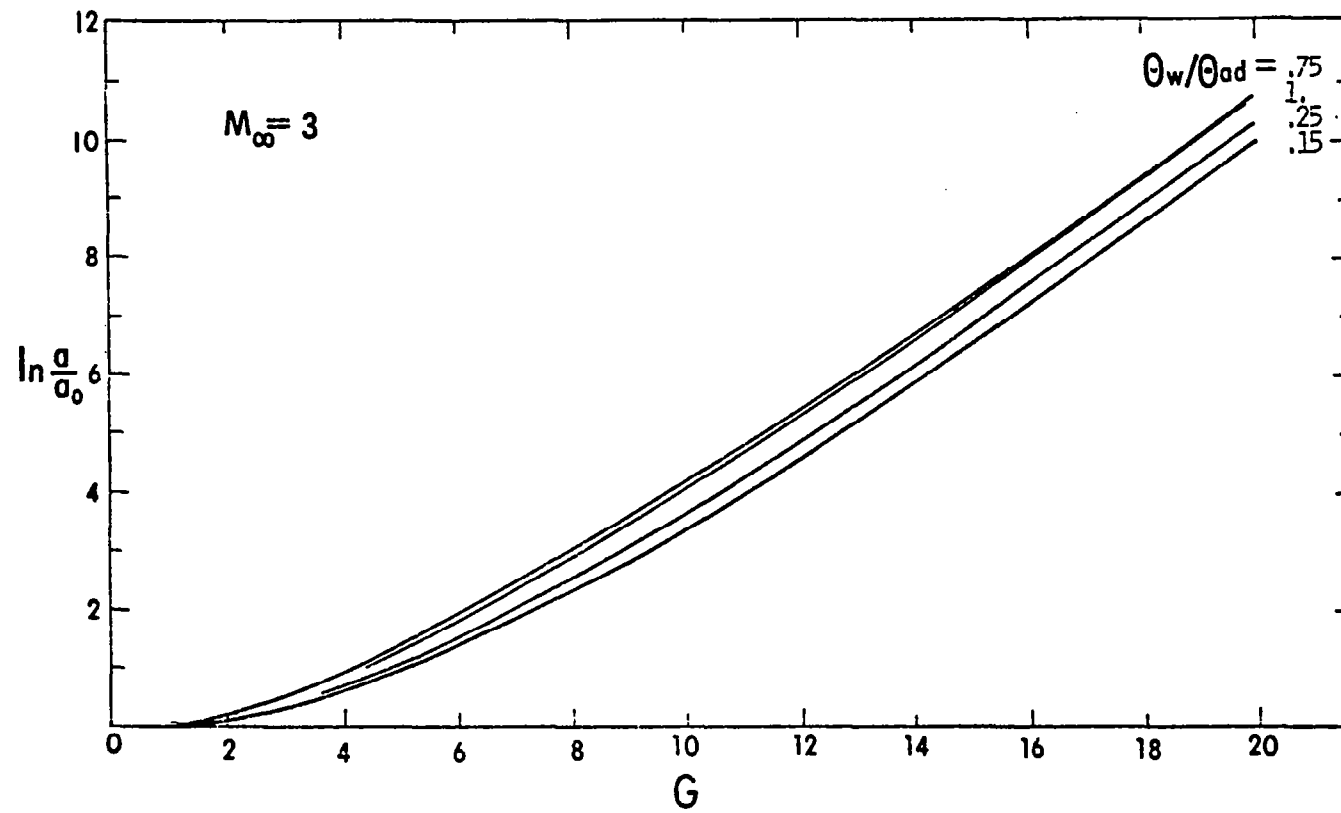


Figure 32 Effect of cooling on the amplitude ratio calculated along the locus of maximum growth rates at  $M_\infty = 3$ .

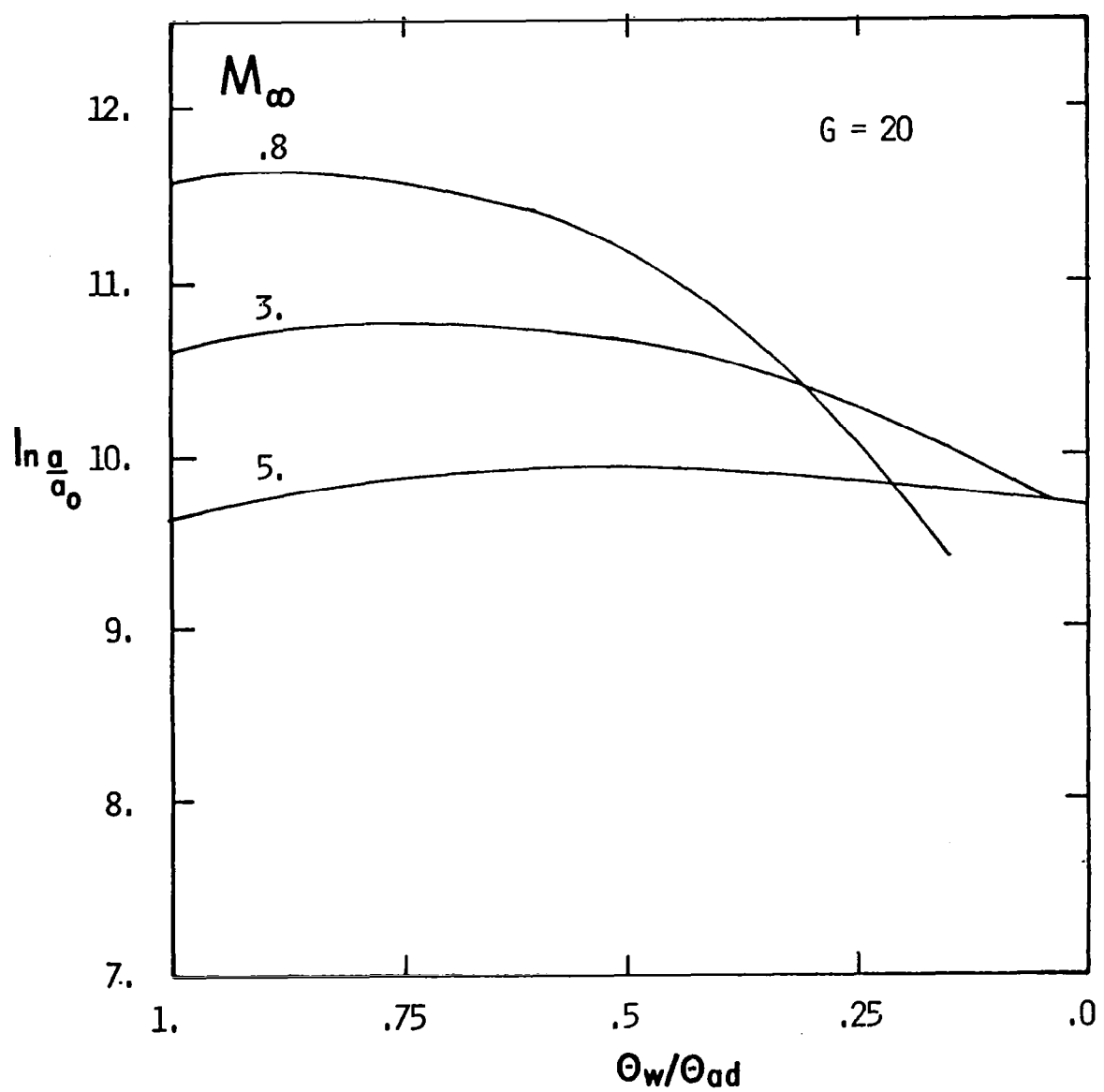


Figure 33 Effect of cooling on the amplitude ratio at  $G=20$   
for different Mach numbers.

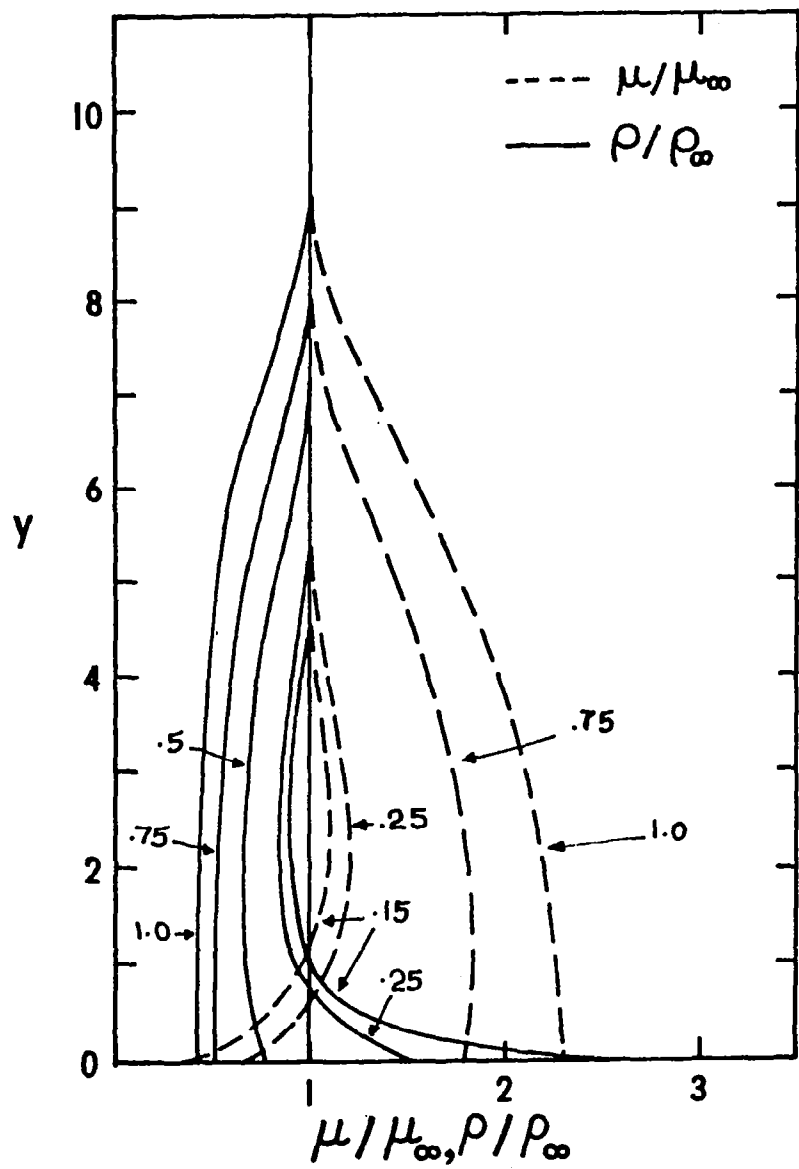


Figure 34 Variation of mean density and viscosity for different cooling rates.

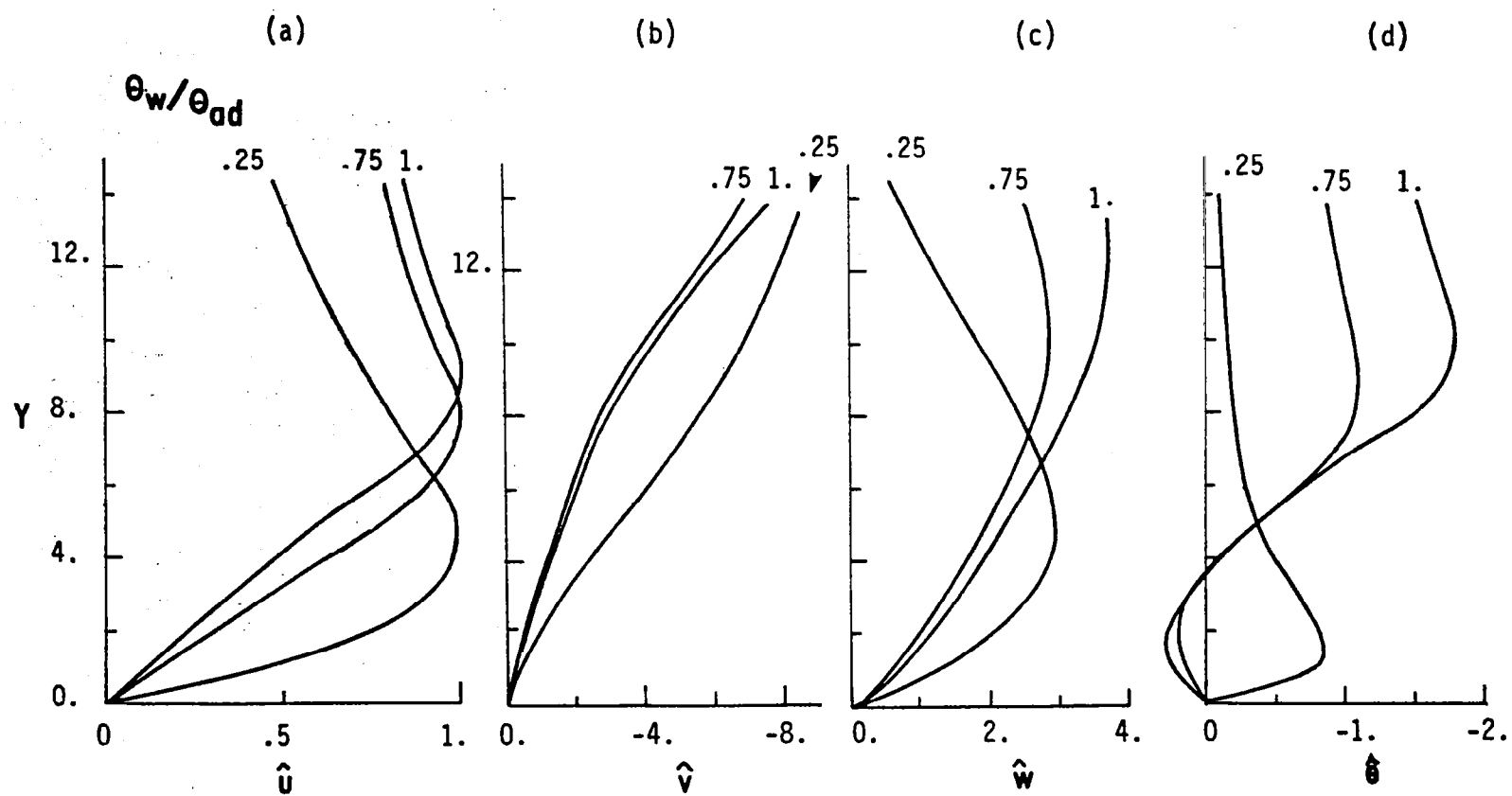


Figure 35 Effect of cooling at  $M_\infty = 3$  on the shape of eigenfunctions  
for a disturbance having a wavenumber 0.3 and zero growth  
rate.

APPENDIX A

This appendix contains the dimensional field equations for compressible flow (see Hughes and Gaylord, 1964) written in the specified system of coordinates  $x, y, z$ . The velocities are given by  $u, v, w$ , and the metric coefficients are  $h, h, l$  in the  $x, y, z$  directions respectively. The Prandtl number  $\Gamma$  and specific heat  $c_p$  are taken constant in the stability analysis. The ratio  $c$  of the second to the first mean flow viscosity coefficients is defined as  $c = 2(e - 1)/3$ ,  $e$  is taken equal to 0.8.

x-momentum

$$\rho \left[ \frac{u}{h} u_x + \frac{v}{h} u_y + w u_z - \frac{v}{h^2} (v h_x - u h_y) \right] = - \frac{1}{h} p_x$$

$$+ \frac{c}{h} (\mu \nabla \cdot v)_x + \frac{1}{h^2} \left[ \{2\mu h(\frac{1}{h} u_x + \frac{v}{h^2} h_y)\}_x \right.$$

$$+ \{\mu h \left[ (\frac{v}{h})_x + (\frac{u}{h})_y \right]\}_y + \{\mu h^2 (u_z + \frac{1}{h} w_x)\}_z \left. \right]$$

$$+ \frac{\mu}{h^2} \left[ (\frac{v}{h})_x + (\frac{u}{h})_y \right] h_y - \frac{2\mu}{h^2} \left[ \frac{1}{h} v_y + \frac{u}{h^2} h_x \right] h_x$$

y-momentum

$$\rho \left[ \frac{u}{h} v_x + \frac{v}{h} v_y + w v_z + \frac{u}{h^2} (v h_x - u h_y) \right] = - \frac{1}{h} p_y$$

$$+ \frac{c}{h} (\mu \nabla \cdot v)_y + \frac{1}{h^2} \left[ \{\mu h \left[ (\frac{v}{h})_x + (\frac{u}{h})_y \right]\}_x \right.$$

$$+ \{2\mu h(\frac{1}{h} v_y + \frac{u}{h^2} h_x)\}_y + \{\mu h^2 (\frac{1}{h} w_y + v_z)\}_z \left. \right]$$

$$+ \frac{\mu}{h^2} \left[ (\frac{v}{h})_x + (\frac{u}{h})_y \right] h_x - \frac{2\mu}{h^2} \left[ \frac{1}{h} u_x + \frac{v}{h^2} h_y \right] h_y$$

z-momentum

$$\rho \left[ \frac{u}{h} w_x + \frac{v}{h} w_y + w w_z \right] = - p_z + c(\mu \nabla \cdot v)_z \\ + \frac{1}{h^2} \left[ \{\mu h(u_z + \frac{1}{h} w_x)\}_x + \{\mu h(\frac{1}{h} w_y + v_z)\}_y \right. \\ \left. + \{2\mu h^2 w_z\}_z \right]$$

Energy

$$\rho c_p \left( \frac{u}{h} \theta_x + \frac{v}{h} \theta_y + w \theta_z \right) = \frac{u}{h} p_x + \frac{v}{h} p_y + w p_z \\ + (c+2)\mu \left[ \left( \frac{1}{h} u_x + \frac{v}{h^2} h_y \right)^2 + \left( \frac{1}{h} v_y + \frac{u}{h^2} h_x \right)^2 + w_z^2 \right] \\ + \mu \left[ \left( \frac{1}{h} w_y + v_z \right)^2 + \left( u_z + \frac{1}{h} w_x \right)^2 + \left( \left( \frac{v}{h} \right)_x + \left( \frac{u}{h} \right)_y \right)^2 \right. \\ \left. + 2c \left\{ \left( \frac{1}{h} u_x + \frac{v}{h^2} h_y \right) \left( \frac{1}{h} v_y + \frac{u}{h^2} h_x \right) + \left( \frac{1}{h} u_x \right. \right. \right. \\ \left. \left. \left. + \frac{v}{h^2} h_y \right) w_z + \left( \frac{1}{h} v_y + \frac{u}{h^2} h_x \right) w_z \right\} \right] \\ + \frac{c_p}{h^2 \Gamma} \left[ (\mu \theta_x)_x + (\mu \theta_y)_y + h^2 (\mu \theta_z)_z \right]$$

Continuity

$$(h\rho u)_x + (h\rho v)_y + h^2 (\rho w)_z = 0$$

where

$$\nabla \cdot v = \frac{1}{h^2} \left[ (hu)_x + (hv)_y + h^2 w_z \right]$$

APPENDIX B

The two-dimensional compressible boundary layer equations for zero pressure gradient together with the equation of state for a perfect gas are reduced to the following set of ordinary differential equations.

$$(\mu U_y)_y + gU_y - \gamma U_y \quad (B1)$$

$$(\frac{\mu}{\Gamma} \theta_y)_y + g\theta_y + 2\mu(U_y)^2 - \gamma\theta_y = 0 \quad (B2)$$

$$g_y - \frac{1}{2} \rho U = 0 \quad (B3)$$

$$U = 0, g = 0, \text{ and } \theta_y = 0 \text{ or}$$

$$\theta = \theta_w \text{ at } y = 0 \quad (B4)$$

$$U \rightarrow 1, \theta \rightarrow 0 \text{ as } y \rightarrow y_e \quad (B5)$$

by using the transformation

$$y = (U_e^*/v_e^* x^*)^{\frac{1}{2}} \int_0^{y^*} (\rho^*/\rho_e^*) dy^* \quad (B6)$$

as well as a stream function to satisfy the continuity equations. Here  $\theta = (i^* - i_e^*)/(i_{oe}^* - i_e^*)$ , where  $i^*$ ,  $i_0^*$  are the fluid enthalpy and stagnation enthalpy respectively, and e denotes conditions at the edge of the boundary layer. Equations B1-B5 are integrated numerically with the thermodynamic and transport properties of the perfect gas computed at each integration step. The variation of perfect gas properties with temperature are taken from (Hilsenrath, Beckett, et al., 1955).

APPENDIX C

This appendix contains the nonzero elements of eigenvector matrix D for the case when  $\lambda_2$  and  $\lambda_6$  are repeated.

J = 1,5

$$D_{3J} = -\beta/\lambda_J$$

$$D_{4J} = \beta[\sigma + \beta^2 + \lambda_J(v_e - \lambda_J)]/\lambda_J^2$$

$$D_{7J} = 1.0$$

$$D_{8J} = \lambda_J$$

J = 2,6

$$D_{3J} = -\beta/\lambda_J$$

$$D_{7J} = 1.0$$

$$D_{8J} = \lambda_J$$

J = 3,7

$$D_{1J} = \beta(v_e - 2\lambda_J)(1 - \lambda_J^2/\beta^2)/(2G^2 + v_{xe})\lambda_J$$

$$D_{2J} = \lambda_J D_{1J}$$

$$D_{3J} = 1.0$$

$$D_{4J} = (v_e - 2\lambda_J)/\beta$$

$$D_{7J} = 1.0/\lambda_J - \lambda_J/\beta - \sigma D_{1J}/\beta$$

$$D_{8J} = 1 + \lambda_J D_{7J}$$

J = 4,8

$$D_{3J} = [\lambda_J(\sigma + \lambda_J v_e) - \frac{(G^2\beta^2 + v_{xe}\beta^2)}{\sigma + \beta^2 + \lambda_J(v_e - \lambda_J)}] \frac{1}{(\lambda_J^2 - \beta^2)}$$

$$D_{4J} = -\lambda_J[\sigma + \beta^2 + \lambda_J(v_e - \lambda_J)]D_{3J}/\beta^2$$

$$D_{5J} = 1.0$$

$$D_{6J} = J$$

$$D_{7J} = -\lambda_J D_{3J}/\beta + (\sigma + \lambda_J v_e)/\beta$$

$$D_{8J} = \lambda_J D_{7J}$$

APPENDIX D

This appendix contains the nonzero elements of the eigenvectors matrix D for the special case  $\sigma = \beta V_e$  where  $\lambda_1, \lambda_2, \lambda_3$ , and  $\lambda_4$  are repeated.

$J = 1, 5$

$$D_{7J} = -\lambda_J/\beta$$

$$D_{8J} = -\beta$$

$J = 2, 6$

$$D_{1J} = 1$$

$$D_{2J} = \lambda_J$$

$$D_{3J} = 1$$

$$D_{5J} = 2$$

$$D_{6J} = 2\lambda_J$$

$$D_{7J} = -\lambda_J/\beta$$

$$D_{8J} = -\beta$$

$J = 3, 7$

$$D_{3J} = 1$$

$$D_{4J} = 2$$

$$D_{7J} = -(1 + \lambda_J)/\beta$$

$$D_{8J} = -\lambda_J(\lambda_J + 2)/\beta$$

$J = 4, 8$

$$D_{3J} = 1$$

$$D_{4J} = \lambda_J(2\lambda_J + 3)/\beta^2$$

$$D_{5J} = 4/G^2$$

$$D_{6J} = 4\lambda_J/G^2$$

$$D_{7J} = -(1 + \lambda_J)/\beta \quad D_{8J} = -(1 + \lambda_J)^2/\beta$$

APPENDIX E

This appendix contains the nonzero elements of the eigenvectors matrix for the Adjoint Problem (34).

$$J = 1, 3$$

$$D_{1J} = \frac{-1}{\lambda_J} \left[ \frac{\beta}{\lambda_J} (\sigma V_e - 2G^2 - V_{xe}) - \frac{\sigma(\sigma + \beta^2)}{\beta} + (\sigma + \beta^2) D_{2J} \right]$$

$$D_{2J} = \left[ \frac{\beta}{\lambda_J} (\sigma V_e - 2G^2 - V_{xe}) - \frac{\sigma^2}{\beta} \right] \frac{1}{(\lambda_J V_e - \sigma)}$$

$$D_{3J} = (\sigma + \beta^2)/\beta$$

$$D_{4J} = \beta/\lambda_J$$

$$D_{5J} = -\frac{1}{\lambda_J} \left[ (\sigma \Gamma_e + \beta^2) D_{6J} + (c + 2)\sigma\beta + \frac{\alpha^2}{\beta} + \frac{\beta}{\lambda_J} (G^2 + V_{xe} - V_e\sigma + (c + 2)V_e(\Gamma_e\sigma + \beta^2)) \right]$$

$$D_{6J} = \frac{1}{\Gamma_e(\sigma - V_e\lambda_J)} \left[ \lambda_J \left( \frac{2V_e\sigma}{\beta} - \frac{G^2}{\beta} - \frac{V_{xe}}{\lambda} \right) - \beta V_e^2 - \frac{\sigma^2}{\beta} + (c + 2)\Gamma_e V_e (\Gamma_e\sigma - \frac{\sigma\lambda_J}{\beta}) \right]$$

$$D_{7J} = -V_e$$

$$J = 3, 7$$

$$D_{1J} = \frac{1}{\lambda_J} \left[ (\sigma + \beta^2) \left( \frac{1}{\lambda_J} - 1.0 \right) + (\sigma \lambda_J + 2G^2 + V_{xe}) D_{4J} \right]$$

$$D_{2J} = 1.0$$

$$D_{3J} = \frac{(\sigma + \beta^2)}{\lambda_J} D_{4J}$$

$$D_{4J} = \frac{(V_e + 2\lambda_J)}{(2G^2 + V_{xe})}$$

$$D_{5J} = -\frac{1}{\lambda_J} \left[ (\Gamma_e\sigma + \beta^2) D_{6J} + [(c + 2)V_e(\Gamma_e\sigma + \beta^2) + G^2 + V_{xe} + (c + 2)\lambda_J\sigma] D_{4J} \right]$$

$$D_{6J} = \frac{[G^2 + V_{xe} - (c + 2)V_e(\Gamma_e V_e + \lambda_J^2 - \Gamma_e\sigma - \beta^2)] D_{4J}}{(\Gamma_e V_e + \lambda_J^2 - \Gamma_e\sigma - \beta^2)}$$

$$D_{7J} = \frac{\beta - \lambda_J(v_e + \lambda_J)}{\lambda_J} D_{4J}$$

$$D_{8J} = \frac{\lambda_J}{\beta} D_{4J}$$

$$J = 4, 8$$

$$D_{5J} = -(\Gamma_e v_e + \lambda_J)$$

$$D_{6J} = 1.0$$

## APPENDIX F

FORTRAN PROGRAM FOR STABILITY ANALYSIS.

THIS PROGRAM CALLS SUBROUTE JOCK (LINE A 430) WHICH

IS A VARIABLE STEP SIZE INTEGRATOR WRITTEN BY SCOTT AND WATTS (1977).

PROGRAM STATIC(INPUT,OUTPUT,TAPE5=INPUT,TAPF6=OUTPUT,TAPF10)	A 1
REAL K(8,8),KK(8,8),KNT,KNTB,KTB,MACH,MU,MUP	A 2
DIMENSION Z(8,101), A(4,8), ALPHA(4), B(4,8), BETA(4), KARRAY(7),	A 3
IC(8,8), CCC(8,8), FF(8,8), DD(8,8), XL(8)	A 4
DIMENSION WORK(10000), IWORK(150)	A 5
DIMENSION PV(8), IK(30), CD(8)	A 6
COMMON /AAA/ KNT,BET,VELF,GG,MACH,CC,PX,PY	A 7
COMMON /BBB/ XSAVE,KL,INDEX	A 8
COMMON /CCC/ V(101),VP(101),VPP(101),DUX(101),DUPX(101),DVX(101),D	A 9
ITX(101),DTPX(101),DMUX(101),DALFX(101)	A 10
COMMON /DDD/ Y(101),U(101),UP(101),UPP(101),T(101),TP(101),TPP(101)	A 11
,PRANDL(101),MU(101),MUP(101),ALFA(101),ALFAP(101)	A 12
COMMON /FFF/ IE,MOD	A 13
COMMON /EEE/ ACC,FACT	A 14
NAMELIST /GORTLR/ GG,KNT,BFT,ACC,MOD,ITR,INDEX,NIT,ILM,FACT	A 15
C*****	A 16
C	A 17
C MOD INDICATES DIFFERENT MODELS	A 18
C MOD=1 WITHOUT TERMS DUE TO BOUNDARY LAYER GROWTH	A 19
C MOD=2 WITH TERMS DUE TO BOUNDARY LAYER GROWTH	A 20
C ITR INDICATES ITERATION APPLIED TO	A 21
C ITR=1 GG KNT=CONSTANT	A 22
C ITR=2 KNT GG=CONSTANT	A 23
C INDEX INDICATES TYPE OF PROBLEM	A 24
C INDEX=1 HOMOGENEOUS PROBLEM	A 25
C INDEX=2 ADJOINT HOM. PROBLEM	A 26
C NOTE- INDEX=1,2 ARE VALID FOR MOD=2 ONLY	A 27
C NIT=MAX. NO. OF ITERATION	A 28
C IN IS NO OF ITFRATIONS	A 29
C IM=0 CONVERGENCE	A 30
C IE=NO OF POINTS IN THE Y DIRECTION	A 31

C	IM=1 NO CONVERGENCE	A 32
C	IL IS COUNTER FOR THE NO OF POINTS ON PLOT	A 33
C	ILM IS MAX NO OF POINTS ON THE PLOT	A 34
C	GG=GOERTLER NUMBER	A 35
C	KNT= WAVE NUMBER	A 36
C	MACH= MACH NUMBER	A 37
C	MU = VISCOSITY	A 38
C	XL(I)= EIGENVALUE ARRAY	A 39
C	C(8,8)=CONSTANT COEFFICIENT MATRIX	A 40
C	K(8,8)=EIGENVECTOR MATRIX	A 41
C	BET =GROWTH RATE	A 42
C	VELF =NORMAL VELOCITY COMPONENT OUTSIDE THE B.L.	A 43
C	CC =CONSTANT=0.4/3.	A 44
C	ACC =ACCURACY	A 45
C	FACT =A PARAMETER WHICH DETERMINES THE STEP SIZE IN NEWTON-RAPHSON ITERATIVE METHOD.SEE SUBROUTINE	A 46
C	ITRN.	A 47
C	SUFFIX P DENOTES DERIVATIVES WITH RESPECT TO Y COORDINATE.	A 48
C	SUFFIX X DENOTES DERIVATIVE WITH RESPECT TO X COORDINATE.	A 49
C	THUS UP AND UPP ARE FIRST AND SECOND DERIVATIVES WITH RESPECT TO Y AND DVX AND DTX ARE THE X DERIVATIVE OF THE NORMAL COMPONENT OF VELOCITY AND TEMPERATURE	A 50
C	PRANDL=PRANDTL NUMBER	A 51
C	ALFA =DERIVATIVE OF MEAN VISCOSITY WITH MEAN TEMPERATURE.	A 52
C	*****	A 53
C	READ (10) ETA,MACH,IE	A 54
C	READ (10) (Y(I),I=1,IE)	A 55
C	READ (10) (U(I),I=1,IE)	A 56
C	READ (10) (UP(I),I=1,IE)	A 57
C	READ (10) (UPP(I),I=1,IE)	A 58
C	READ (10) (T(I),I=1,IE)	A 59
C	*****	A 60
C	READ (10) (Y(I),I=1,IE)	A 61
C	READ (10) (U(I),I=1,IE)	A 62
C	READ (10) (UP(I),I=1,IE)	A 63
C	READ (10) (UPP(I),I=1,IE)	A 64
C	READ (10) (T(I),I=1,IE)	A 65
C	READ (10) (Y(I),I=1,IE)	A 66
C	READ (10) (U(I),I=1,IE)	A 67

READ (10) (TP(I),I=1,IE)	A 68
READ (10) (TPP(I),I=1,IE)	A 69
READ (10) (PRANDL(I),I=1,IE)	A 70
READ (10) (MU(I),I=1,IE)	A 71
READ (10) (MUP(I),I=1,IE)	A 72
READ (10) (ALFA(I),I=1,IE)	A 73
READ (10) (ALFAP(I),I=1,IE)	A 74
READ (10) (DUX(I),I=1,IE)	A 75
READ (10) (DUPX(I),I=1,IE)	A 76
READ (10) (DTX(I),I=1,IE)	A 77
READ (10) (DTPX(I),I=1,IE)	A 78
READ (10) (DMUX(I),I=1,IE)	A 79
READ (10) (DALFX(I),I=1,IF)	A 80
READ (10) (V(I),I=1,IE)	A 81
READ (10) (VP(I),I=1,IE)	A 82
READ (10) (VPP(I),I=1,IE)	A 83
READ (10) (DVX(I),I=1,IE)	A 84
C*****	A 85
C	A 86
C INPUT PARAMETERS	A 87
C	A 88
C*****	A 89
PX=0.0	A 90
PY=0.0	A 91
CC=-0.4/3.0	A 92
CC1=CC+1.	A 93
CC2=CC+2.	A 94
PR1=PRANDL(1)	A 95
VELF=V(1)	A 96
IL=0	A 97
READ (5,GORTLR)	A 98
1 IF (EOF(5)) 45,1	A 99
CONTINUE	A 100
WRITE (6,GORTLR)	A 101

2	CONTINUE	A 102
	IF (ABS(BET).EQ.ABS(KNT*VELF)) STOP	A 103
	IN=0	A 104
	WRITE (6,56)	A 105
3	CONTINUE	A 106
	IM=0	A 107
	C*****	A 108
	C PARALLEL AND NON PARALLEL BRANCHING	A 109
	C*****	A 110
	IF (MOD.NE.1) GO TO 5	A 111
	DO 4 I=1,IE	A 112
	V(I)=0.0	A 113
	VP(I)=0.0	A 114
	VPP(I)=0.0	A 115
	DVX(I)=0.0	A 116
	DUX(I)=0.0	A 117
	DUPX(I)=0.0	A 118
	DTX(I)=0.0	A 119
	DTPX(I)=0.0	A 120
	DMUX(I)=0.0	A 121
	DALFX(I)=0.0	A 122
4	CONTINUE	A 123
	VELF=V(1)	A 124
5	CONTINUE	A 125
	C*****	A 126
	C CONSTANT COEFFICIENT MATRIX	A 127
	C*****	A 128
	DO 6 I=1,8	A 129
	DO 6 J=1,8	A 130
6	C(I,J)=0.0	A 131
	C(1,2)=1.0	A 132
	C(2,1)=KNT**2+BET	A 133
	C(2,2)=VELF	A 134
	C(3,1)=-BET	A 135
	C(3,5)=BET	A 136
	C(3,6)=VELF	A 137
	C(3,7)=-KNT	A 138

```

C(4,1)=-2.0*GG**2+BET*VELF-DVX(1) A 139
C(4,2)=-BET A 140
C(4,3)=-KNT**2-BET A 141
C(4,5)=GG**2+DVX(1)-VFLF*BET+CC2*VELF*(PR1*BFT+KNT**2) A 142
C(4,6)=CC2*(BET+PR1*VELF**2)-VELF**2 A 143
C(4,7)=KNT*VELF A 144
C(4,8)=-KNT A 145
C(5,6)=1.0 A 146
C(6,5)=KNT**2+BET*PR1 A 147
C(6,6)=PR1*VELF A 148
C(7,8)=1.0 A 149
C(8,4)=-KNT A 150
C(8,5)=CC1*KNT*BET A 151
C(8,6)=CC1*KNT*VELF A 152
C(8,7)=KNT**2+BET A 153
C(8,8)=VELF A 154
IF (MOD.EQ.1.AND.BET.EQ.0.0) GO TO 20 A 155
KNTB=(VELF**2+4.0*(BET+KNT**2))**0.5 A 156
KTB=((PRANDL(1)*VELF)**2+4.0*(BET*PRANDL(1)+KNT**2))**.5 A 157
***** C 158
C EIGENVALUES A 159
***** C 160
XL(1)=-KNT A 161
XL(2)=-0.5*(-VELF+KNTB) A 162
XL(3)=-0.5*(-VELF+KNTB) A 163
XL(4)=-0.5*(PRANDL(1)*(-VELF)+KTB) A 164
XL(5)=KNT A 165
XL(6)=0.5*(VELF+KNTB) A 166
XL(7)=0.5*(VELF+KNTB) A 167
XL(8)=0.5*(PRANDL(1)*VELF+KTB) A 168
IF (INDFX.EQ.2) GO TO 13 A 169
PS=2.0*GG**2+DVX(1) A 170
PP=(GG*KNT)**2+DVX(1)*KNT**2 A 171
C A 172
DO 12 J=1,8 A 173
XLL=XL(J)*XL(J) A 174
GO TO (7,8,9,10,7,8,9,10), J A 175

```

```

C*****EIGENVECTOR MATRIX ELEMENTS*****
C
C
7   K(1,J)=0.0
    K(2,J)=0.0
    K(3,J)=-KNT/XL(J)
    K(4,J)=KNT*((BET+KNT**2)+XL(J)*(VELF-XL(J)))/XLL
    K(5,J)=0.0
    K(6,J)=0.0
    K(7,J)=1.0
    K(8,J)=XL(J)
    GO TO 11
8   K(1,J)=0.0
    K(2,J)=0.0
    K(3,J)=-KNT/XL(J)
    K(4,J)=0.0
    K(5,J)=0.0
    K(6,J)=0.0
    K(7,J)=1.0
    K(8,J)=XL(J)
    GO TO 11
9   X1=(KNT*(VELF-2.0*XL(J))*(1.0-(XL(J)/KNT)**2))/(PS*XL(J))
    K(1,J)=X1
    K(2,J)=XL(J)*X1
    K(3,J)=1.0
    K(4,J)=(VELF-2.0*XL(J))/KNT
    K(5,J)=0.0
    K(6,J)=0.0
    K(7,J)=1.0/XL(J)-XL(J)/KNT-BET*X1/KNT
    K(P,J)=1.0+XL(J)*K(7,J)
    GO TO 11
10  X4=BFT+KNT**2+XL(J)*(VELF-XL(J))
    K(1,J)=0.0
    K(2,J)=0.0
    K(3,J)=(XL(J)*(BET+XL(J)*VELF)-(PP/X4))/(XL(J)**2-KNT**2)

```

```

K(4,J)=-X4*XL(J)*K(3,J)/(KNT**2)+(BET+XL(J)*VELF)*((CC+1.0)+X4/KNT A 212
1**2) A 213
K(5,J)=1.0 A 214
K(6,J)=XL(J) A 215
K(7,J)=-XL(J)*K(3,J)/KNT+(BET+XL(J)*VELF)/KNT A 216
K(8,J)=XL(J)*K(7,J) A 217
11 CONTINUE A 218
12 CONTINUE A 219
GO TO 29 A 220
C
13 CONTINUE A 221
C*****ADJOINT PROBLEM EIGFN-VECTORS***** A 222
C*****ADJOINT PROBLEM EIGFN-VECTORS***** A 223
C*****ADJOINT PROBLEM EIGFN-VECTORS***** A 224
C*****ADJOINT PROBLEM EIGFN-VECTORS***** A 225
BKN=BET+KNT**2 A 226
BPK=BET*PR1+KNT**2 A 227
DO 19 J=1,8 A 228
GO TO (14,15,16,17,14,15,16,17), J A 229
C
14 CONTINUE A 230
K(2,J)=(KNT*(BET*VELF-2.0*GG**2-DVX(1))/XL(J)-BET**2/KNT)/(XL(J)*V A 232
ELF-BET) A 233
K(1,J)=-(KNT/XL(J))*(BET*VELF-2.0*GG**2-DVX(1))-BET*BKN/KNT+BKN*K A 234
1(2,J))/XL(J) A 235
K(3,J)=BKN/KNT A 236
K(4,J)=KNT/XL(J) A 237
K(6,J)=(XL(J)*(2.0*VELF*BET/KNT-GG**2/KNT-DVX(1)/KNT)-KNT*VELF**2- A 238
1BET**2/KNT+CC2*PR1*VELF*(VELF*KNT-BET*XL(J)/KNT))/(PR1*(BET-VELF*X A 239
2L(J))) A 240
K(5,J)=-(BPK*K(6,J)+CC2*BET*KNT+BET**2/KNT+(KNT/XL(J))*(-VELF*BET+ A 241
1CC2*VELF*BPK+GG**2+DVX(1)))/XL(J) A 242
K(7,J)=-VELF A 243
K(8,J)=1.0 A 244
GO TO 18 A 245
15 K(1,J)=-(VFLF+XL(J)) A 247
K(2,J)=1.0 A 248

```

```

K(3,J)=0.0 A 249
K(4,J)=0.0 A 250
K(5,J)=0.0 A 251
K(6,J)=0.0 A 252
K(7,J)=0.0 A 253
K(8,J)=0.0 A 254
GO TO 18 A 255
C A 256
16   BPR=(PR1*VELF+XL(J))*XL(J)-BPK A 257
      K(4,J)=-(VELF+2.*XL(J))/(2.0*GG**2+DVX(1)) A 258
      K(2,J)=1.0 A 259
      K(1,J)=(BKN*(1./XL(J)-1.0)+(BET*XL(J)+2.0*GG**2+DVX(1))*K(4,J))/XL A 260
      1(J) A 261
      K(3,J)=(BKN/XL(J))*K(4,J) A 262
      K(6,J)=(GG**2+DVX(1)-CC2*VELF*BPR)*K(4,J)/BPR A 263
      K(5,J)=-(BPK*K(6,J)+(CC2*VELF*BPK+GG**2+DVX(1)+CC2*XL(J)*BET)*K(4, A 264
      1J))/XL(J) A 265
      K(7,J)=(KNT-XL(J)*(VELF+XL(J))/KNT)*K(4,J) A 266
      K(8,J)=(XL(J)/KNT)*K(4,J) A 267
      GO TO 18 A 268
C A 269
17   K(1,J)=0.0 A 270
      K(2,J)=0.0 A 271
      K(3,J)=0.0 A 272
      K(4,J)=0.0 A 273
      K(5,J)=-(PR1*VELF+XL(J)) A 274
      — K(6,J)=1.0 A 275
      K(7,J)=0.0 A 276
      K(8,J)=0.0 A 277
18   CONTINUE A 278
19   CONTINUE A 279
C A 280
      GO TO 29 A 281
20   CONTINUE A 282
C***** A 283
C EIGENVECTORS FOR RFT=0 & MOD=1 A 284
C FOUR REPEATED EIGENVALUES A 285
C***** A 286

```

```

C      WRITE (6,100) XL1,XL2,XL3,XL4,XL5,XL6,XL7,XL8          A 287
      DO 21 J=1,4                                         A 288
21    XL(J)=-KNT                                         A 289
      DO 22 J=5,8                                         A 290
22    XL(J)=KNT                                         A 291
C
      DO 28 J=1,8                                         A 292
      GO TO (23,24,25,26,23,24,25,26), J                 A 293
C
23    K(1,J)=0.0                                         A 294
      K(2,J)=0.0                                         A 295
      K(3,J)=1.0                                         A 296
      K(4,J)=0.0                                         A 297
      K(5,J)=0.0                                         A 298
      K(6,J)=0.0                                         A 299
      K(7,J)=-XL(J)/KNT                                A 300
      K(8,J)=-KNT                                       A 301
      GO TO 27                                         A 302
C
24    K(1,J)=1.0                                         A 303
      K(2,J)=XL(J)                                       A 304
      K(3,J)=1.0                                         A 305
      K(4,J)=0.0                                         A 306
      K(5,J)=2.0                                         A 307
      K(6,J)=2.0*XL(J)                                  A 308
      K(7,J)=-XL(J)/KNT                                A 309
      K(8,J)=-KNT                                       A 310
      GO TO 27                                         A 311
C
25    K(1,J)=0.0                                         A 312
      K(2,J)=0.0                                         A 313
      K(3,J)=1.0                                         A 314
      K(4,J)=2.0                                         A 315
      K(5,J)=0.0                                         A 316
      K(6,J)=0.0                                         A 317
      K(7,J)=-(1.0+XL(J))/KNT                           A 318
      K(8,J)=-XL(J)*(XL(J)+2.0)/KNT                   A 319
                                                A 320
                                                A 321
                                                A 322
                                                A 323

```

```

      GO TO 27                                A 324
C
26   K(1,J)=0.0                               A 325
      K(2,J)=0.0                               A 326
      K(3,J)=1.0                               A 327
      K(4,J)=XL(J)*(2.0*XL(J)+3.0)/KNT**2    A 328
      K(5,J)=4.0/GG**2                          A 329
      K(6,J)=4.0*XL(J)/GG**2                   A 330
      K(7,J)=-(1.0+XL(J))/KNT                 A 331
      K(8,J)=-(1.0+XL(J))**2/KNT              A 332
      K(8,J)=-(1.0+XL(J))**2/KNT              A 333
27   CONTINUE                                 A 334
28   CONTINUE                                 A 335
29   CONTINUE                                 A 336
      DO 30 L=1,8                             A 337
      DO 30 I=1,8                             A 338
30   KK(I,L)=K(I,L)                           A 339
C     WRITE (6,100) ((K(I,L),L=1,8),I=1,8)    A 340
      CALL MATINV (8,8,K,0,CD,C,DETR,CS,PV,IK) A 341
C     WRITE (6,203) DETR                      A 342
C     WRITE(6,100) ((K(I,L),L=1,8),I=1,8)     A 343
      KARRAY(1)=20                            A 344
      KARRAY(2)=8                            A 345
      KARRAY(3)=8                            A 346
      KARRAY(4)=8                            A 347
      KARRAY(5)=8                            A 348
      KARRAY(6)=8                            A 349
      KARRAY(7)=8                            A 350
      CALL MATOPS (KARRAY,K,C,FF)             A 351
      CALL MATOPS (KARRAY,KK,K,DD)            A 352
      CALL MATOPS (KARRAY,FF,KK,CCC)          A 353
C     WRITE (6,100) ((C(I,L),L=1,8),I=1,8)    A 354
C     WRITE (6,100) ((DD(I,L),L=1,8),I=1,8)    A 355
C     WRITE (6,100) ((FF(I,L),L=1,8),I=1,8)    A 356
C*****ELEMENTS OF INVERTED MATRIX           A 357
C*****ELEMENTS OF INVERTED MATRIX           A 358
C*****ELEMENTS OF INVERTED MATRIX           A 359

```

```

A(1,1)=K(5,1)          A 360
A(1,2)=K(5,2)          A 361
A(1,3)=K(5,3)          A 362
A(1,4)=K(5,4)          A 363
A(1,5)=K(5,5)          A 364
A(1,6)=K(5,6)          A 365
A(1,7)=K(5,7)          A 366
A(1,8)=K(5,8)          A 367
A(2,1)=K(6,1)          A 368
A(2,2)=K(6,2)          A 369
A(2,3)=K(6,3)          A 370
A(2,4)=K(6,4)          A 371
A(2,5)=K(6,5)          A 372
A(2,6)=K(6,6)          A 373
A(2,7)=K(6,7)          A 374
A(2,8)=K(6,8)          A 375
A(3,1)=K(7,1)          A 376
A(3,2)=K(7,2)          A 377
A(3,3)=K(7,3)          A 378
A(3,4)=K(7,4)          A 379
A(3,5)=K(7,5)          A 380
A(3,6)=K(7,6)          A 381
A(3,7)=K(7,7)          A 382
A(3,8)=K(7,8)          A 383
A(4,1)=K(8,1)          A 384
A(4,2)=K(8,2)          A 385
A(4,3)=K(8,3)          A 386
A(4,4)=K(8,4)          A 387
A(4,5)=K(8,5)          A 388
A(4,6)=K(8,6)          A 389
A(4,7)=K(8,7)          A 390
A(4,8)=K(8,8)          A 391
DO 31 I=1,4            A 392
DO 31 J=1,8            A 393
B(I,J)=0.0              A 394
IF (INDEX.EQ.2) GO TO 32 A 395

```

```

C***** C***** C***** C***** C***** C***** C***** C***** C***** C*****
C      OUTER BOUNDARY CONDITION FOR REGULAR PROBLEM A 396
C***** C***** C***** C***** C***** C***** C***** C***** C***** C*****
      B(1,1)=1.0 A 397
      B(2,3)=1.0 A 398
      B(3,5)=1.0 A 399
      B(4,7)=1.0 A 400
      GO TO 33 A 401
32      CONTINUF A 402
C***** C***** C***** C***** C***** C***** C***** C***** C*****
C      OUTER BOUNDARY CONDITION FOR ADJOINT PROBLEM A 403
C***** C***** C***** C***** C***** C***** C***** C***** C*****
      B(1,2)=1.0 A 404
      B(2,4)=1.0 A 405
      B(3,5)=1.0 A 406
      B(4,8)=1.0 A 407
33      CONTINUE A 408
      DO 34 I=1,4 A 409
      ALPHA(I)=0.0 A 410
34      BETA(I)=0.0 A 411
C***** C***** C***** C***** C***** C***** C***** C***** C*****
C      PARAMETERS FOR JOCK A 412
C***** C***** C***** C***** C***** C***** C***** C***** C*****
      NY=IE A 413
      IFLAG=0 A 414
      AE=ACC A 415
      RE=ACC A 416
      IWORK(1)=10 A 417
      IWORK(11)=1 A 418
      DO 35 I=1,10 A 419
35      WORK(I)=Y(9*I+1) A 420
      XSAVE=0.0 A 421
      KL=1 A 422
C
      CALL JOCK (Z,8,8,Y,NY,A,4,ALPHA,4,B,4,BETA,4,0,RF,AE,IFLAG,WORK,10 A 423
      1000,IWORK,150,0) A 424

```

	IF (INDEX.EQ.2) GO TO 36	A 432
	MNV=IWORK(1)	A 433
	MNW=IWORK(2)	A 434
	AD=Z(2,NY)	A 435
	DA=Z(7,NY)/AD	A 436
	GO TO 37	A 437
36	CONTINUE	A 438
	MNV=IWORK(1)	A 439
	MNW=IWORK(2)	A 440
	AD=Z(1,NY)	A 441
	DA=Z(8,NY)/AD	A 442
37	CONTINUE	A 443
	IF (ITR.NE.1) GO TO 38	A 444
	CALL ITRN (GG,KNT,DA,IN,IM,ITR,IFLAG,MNV,MNW)	A 445
	GO TO 39	A 446
38	CALL ITRN (KNT,GG,DA,IN,IM,ITR,IFLAG,MNV,MNW)	A 447
39	CONTINUE	A 448
	IF (IN.EQ.NIT) GO TO 60	A 449
	IF (IM.EQ.1) GO TO 3	A 450
	IF (INDEX.EQ.2) GO TO 40	A 451
	NN=2	A 452
	GO TO 41	A 453
40	NN=1	A 454
41	CONTINUE	A 455
	DO 42 J=1,NY	A 456
	DO 42 L=1,8	A 457
42	Z(L,J)=Z(L,J)/Z(NN,NY)	A 458
	WRITE (6,53)	A 459
	DO 43 J=1,NY,5	A 460
43	PRINT 58, Y(J),(Z(L,J),L=1,8)	A 461
C	WRITE(6,70)	A 462
C	WRITE (6,100)((KK(I,L),L=1,8),I=1,8)	A 463
C	WRITE(6,81)	A 464
C	WRITE(6,100)((CCC(I,L),L=1,8),I=1,8)	A 465
	WRITE (6,59)	A 466
	WRITE (6,54) (XL(I),I=1,8)	A 467
	PRINT 55, IN	A 468

C	NUMORT=IWORK(1)	A 469
	PRINT 57, KNT,GG,BET	A 470
C	WRITE (6,100) Z(1,NY)	A 471
	GO TO 44	A 472
	STOP	A 473
44	CONTINUE	A 474
45	CONTINUE	A 475
	IF (0.2.LT.KNT.AND.0.5.GE.KNT) GO TO 46	A 476
	IF (KNT.LE.0.2) GO TO 47	A 477
	IF (KNT.GE.1.0) GO TO 48	A 478
	IF (0.5.LT.KNT.AND.1.0.GT.KNT) GO TO 49	A 479
46	KNT=KNT-0.050	A 480
	GG=GG-0.20	A 481
	GO TO 52	A 482
47	KNT=KNT-0.02	A 483
	GG=GG+0.1	A 484
	GO TO 52	A 485
48	KNT=KNT-0.20	A 486
	GG=GG-0.3	A 487
	GO TO 52	A 488
49	IF (BET.LE.2.0) GO TO 50	A 489
	KNT=KNT-0.05	A 490
	GO TO 51	A 491
50	KNT=KNT-0.05	A 492
51	GG=GG-0.3	A 493
52	CONTINUE	A 494
	IL=IL+1	A 495
	IF (IL.GE.ILM) STOP	A 496
	GO TO 2	A 497
	STOP	A 498
C		A 499
53	FORMAT (//,15HEIGEN FUNCTIONS,//)	A 500
54	FORMAT (8X,8E15.6)	A 501
55	FORMAT (//,10X,17HNO OF ITERATIONS=,I2,//)	A 502
		A 503



```

X1=X1+DEL          B 31
IN=IN+1            B 32
IM=1               B 33
RETURN             B 34
B 35
C
6   FORMAT (8X,I3,2X,E15.6,4X,F8.5,4X,F8.5,4X,E15.6,4X,F10.5,4X,I4,8X,
1I4,8X,I4)        B 36
END                B 37
B 38-
C
SUBROUTINE FMAT (X,S,SP,IGOFX,E,EP)
REAL KNT,MACH,MU,MUP
DIMENSION S(1), SP(1), E(1), EP(1)
COMMON /AAA/ KNT,BET,VELF,GG,MACH,CC,PX,PY
COMMON /BBB/ XSAVE,KL,INDEX
C*****
C EIGHT FIRST ORDER EQUATIONS FOR REGULAR AND ADJOINT PROBLEM
C AND THEIR COEFFICIENTS
C*****
CC1=CC+1.0          C 6
CC2=CC+2.0          C 7
GAM=1.4             C 8
C
EC=(GAM-1.0)*MACH**2          C 9
IF (XSAVE.EQ.X) GO TO 1        C 10
IF (XSAVE.LT.X) KL=1           C 11
XSAVE=X                 C 12
CALL PROF (X,U,UP,UPP,T,TP,TPP,PRANDL,MU,MUP,ALFA,ALFAP,DUX,DTX,DM
1UX,DALFX,V,VP,DVX,VPP,DUPX,DTPX,KL)          C 13
PR=PRANDL             C 14
TPTX=TP*V+DTX*U         C 15
A44P=4.0*TP*TPTX/T**3-2.0*(TPP*V+DTPX*U+TP*VP+DTX*UP)/T**2-TP*(DUX
1+VP)/T**2+(DUPX+VPP)/T+UP*BET/T-U*BET*TP/T**2          C 16
C
C IN ABOVE LINE TERM -U*TP/T**2 WAS DELETED AT THE END          C 17
C
A21=KNT**2+(BET*U+DUX)/(T*MU)          C 18
A22=(V/T-MUP)/MU                         C 19
A23=UP/(MU*T)                           C 20
A24=0.0                                  C 21

```

```

A25=-((U*DUX+V*UP)/T**2+ALFA*UPP+ALFAP*UP)/MU C 29
A26=-ALFA*UP/MU C 30
A27=0.0 C 31
A28=0.0 C 32
C 33
C
A31=-(BET-DTX/T) C 34
A32=0.0 C 35
A33=TP/T C 36
A34=0.0 C 37
A35=U*BET/T+(DUX+VP)/T-2.0*TPTX/T**2 C 38
A36=V/T C 39
A37=-KNT C 40
A38=0.0 C 41
C 42
C
A41=-DVX/T-2.0*U*GG**2/T-(DTX/T)*(V/T-CC2*MUP)+BET*(V/T-2.0*MUP)+M C 43
1U*CC2*(TP*(DTX/T-BET)/T+PR*V*(DTX/T-EC*PX)/(MU*T)+DTPX/T-TP*DTX/T* C 44
2*2) C 45
A45=(V/T-CC2*MUP)*(2.0*TPTX/T**2-(DUX+VP)/T-U*BET/T)+MU*CC2*((PR*V C 46
1/(MU*T))*(U*BET/T+MU*KNT**2/PR-TPTX/T**2-EC*ALFA*UP**2-TP*ALFAP/PR C 47
2-ALFA*TPP/PR)-(TP/T)*(2.0*TPTX/T**2-(DUX+VP)/T-U*BET/T)+A44P)+ALFA C 48
3*(CC1*DUX+CC2*VPP+BET*UP)+(U*DVX+V*VP+(U*GG)**2)/(T**2)+DALFX*UP+ C 49
4ALFAP*(CC*DUX+CC2*VP) C 50
C
IN THE ABOVE LINE U*GG**2 WAS MODIFIED AS (U*GG)**2 C 51
C 52
C 53
C
A48=-KNT*MU C 54
A46=-V*(V/T-CC2*MUP)/T+MU*CC2*(TP*V/T**2-2.0*TPTX/T**2+(DUX+VP)/T+ C 55
1U*BET/T+PR*V*(V/T-MUP/PR-ALFA*TP/PR)/(T*MU)+VP/T-V*TP/T**2)+ALFA*( C 56
2CC*DUX+CC2*VP) C 57
A47=KNT*V/T-2.0*KNT*MUP-MU*CC2*KNT*TP/T C 58
A42=CC1*MU*BET+DMUX+MU*CC2*(DTX/T-BET-2.0*PR*V*EC*UP/T) C 59
A43=-U*BET/T-MU*KNT**2-VP/T-(TP/T)*(V/T-CC2*MUP)+MU*CC2*(PR*V*(TP/ C 60
1T-FC*PY)/(MU*T)+TPP/T) C 61
A44=0.0 C 62
C 63
A61=PR*(DTX/T-EC*PX)/MU C 64
A62=-2.0*PR*EC*UP C 65

```

```

A63=PR*(TP/T-EC*PY)/MU C 66
A64=0.0 C 67
A65=PR*(U*BET/T+MU*KNT**2/PR-TPTX/T**2-EC*ALFA*UP**2-ALFA*TPP/PR-A C 68
1LFAP*TP/PR)/MU C 69
A66=PR*(V/T-MUP/PR-ALFA*TP/PR)/MU C 70
A67=0.0 C 71
A68=0.0 C 72
C 73
C
A81=DMUX*KNT/MU+CC1*KNT*DTX/T C 74
A82=0.0 C 75
A83=KNT*MUP/MU+KNT*CC1*TP/T C 76
A84=-KNT/MU C 77
A85=ALFA*KNT*CC*(DUX+VP)/MU-KNT*CC1*(2.0*TPTX/T**2-(DUX+VP)/T-U*BE C 78
1T/T) C 79
A86=KNT*CC1*V/T C 80
A87=U*BET/(T*MU)+KNT**2 C 81
A88=V/(T*MU)-MUP/MU C 82
C
WRITE (6,100) A44P,A41,A45,A46,A61,A81,A85 C 83
C 84
C
CONTINUE C 85
IF (INDEX.EQ.2) GO TO 2 C 86
SP(1)=S(2) C 87
SP(2)=A21*S(1)+A22*S(2)+A23*S(3)+A24*S(4)+A25*S(5)+A26*S(6)+A27*S( C 88
17)+A28*S(8) C 89
SP(3)=A31*S(1)+A32*S(2)+A33*S(3)+A34*S(4)+A35*S(5)+A36*S(6)+A37*S( C 90
17)+A38*S(8) C 91
SP(4)=A41*S(1)+A42*S(2)+A43*S(3)+A44*S(4)+A45*S(5)+A46*S(6)+A47*S( C 92
17)+A48*S(8) C 93
SP(5)=S(6) C 94
SP(6)=A61*S(1)+A62*S(2)+A63*S(3)+A64*S(4)+A65*S(5)+A66*S(6)+A67*S( C 95
17)+A68*S(8) C 96
SP(7)=S(8) C 97
SP(8)=A81*S(1)+A82*S(2)+A83*S(3)+A84*S(4)+A85*S(5)+A86*S(6)+A87*S( C 98
17)+A88*S(8) C 99
RETURN C 100

```

```

2 CONTINUE
SP(1)=-A21*S(2)-A31*S(3)-A41*S(4)-A61*S(6)-A81*S(8) C 101
SP(2)=-S(1)-A22*S(2)-A32*S(3)-A42*S(4)-A62*S(6)-A82*S(8) C 102
SP(3)=-A23*S(2)-A33*S(3)-A43*S(4)-A63*S(6)-A83*S(8) C 103
SP(4)=-A24*S(2)-A34*S(3)-A44*S(4)-A64*S(6)-A84*S(8) C 104
SP(5)=-A25*S(2)-A35*S(3)-A45*S(4)-A65*S(6)-A85*S(8) C 105
SP(6)=-A26*S(2)-A36*S(3)-A46*S(4)-A66*S(6)-A86*S(8)-S(5) C 106
SP(7)=-A27*S(2)-A37*S(3)-A47*S(4)-A67*S(6)-A87*S(8) C 107
SP(8)=-A28*S(2)-A38*S(3)-A48*S(4)-A68*S(6)-A88*S(8)-S(7) C 108
RETURN C 109
C RETURN C 110
C
END C 111
SUBROUTINE GVEC (X,G)
DIMENSION G(8) D 1
RETURN D 2
END D 3
D 4-
SUBROUTINE PROF (YARG,SU,SUP,SUPP,ST,STP,STPP,SPRAND,SMU,SMUP,SALF E 1
1A,SALFP,SUX,STX,SMUX,SALFX,SV,SVP,SVX,SVPP,SUPX,STPX,KL) E 2
REAL INTER,MU,MUP E 3
COMMON /DDD/ Y(101),U(101),UP(101),UPP(101),T(101),TP(101),TPP(101 E 4
1),PRANDL(101),MU(101),MUP(101),ALFA(101),ALFAP(101) E 5
COMMON /FFF/ IE,MOD E 6
COMMON /CCC/ V(101),VP(101),VPP(101),DUX(101),DUPX(101),DVX(101),D E 7
1TX(101),DTPX(101),DMUX(101),DALFX(101) E 8
***** E 9
C SUBROUTINE TO CALCULATE VALUES OF U,MU,T ETC AND THEIR E 10
C DERIVATIVES AT A PARTICULAR Y LOCATION BY INTERPOLATION E 11
C***** E 12
DO 1 J=KL,IE E 13
I=J E 14
IF (YARG.GT.Y(J)) GO TO 2 E 15
IF (YARG.EQ.Y(J)) GO TO 3 E 16
1 CONTINUE E 17
2 MIN=I-3 E 18
IF (I.LE.3) MIN=1 E 19
IF (I.GE.(IE-2)) MIN=IE-6 E 20
SU=INTER(Y,U,YARG,6,MIN) E 21
SUP=INTER(Y,UP,YARG,6,MIN) E 22
SUPP=INTER(Y,UPP,YARG,6,MIN) E 23

```

ST=INTER(Y,T,YARG,6,MIN)	E 24
STP=INTER(Y,TP,YARG,6,MIN)	E 25
STPP=INTER(Y,TPP,YARG,6,MIN)	E 26
SPRAND=INTER(Y,PRANDL,YARG,6,MIN)	E 27
SMU=INTER(Y,MU,YARG,6,MIN)	E 28
SMUP=INTER(Y,MUP,YARG,6,MIN)	E 29
SALFA=INTER(Y,ALFA,YARG,6,MIN)	E 30
SALFP=INTER(Y,ALFAP,YARG,6,MIN)	E 31
IF (MOD.EQ.1) GO TO 4	E 32
SUX=INTER(Y,DUX,YARG,6,MIN)	F 33
SV=INTER(Y,V,YARG,6,MIN)	E 34
SVX=INTER(Y,DVX,YARG,6,MIN)	E 35
SVP=INTER(Y,VP,YARG,6,MIN)	E 36
SVPP=INTER(Y,VPP,YARG,6,MIN)	E 37
SUPX=INTER(Y,DUPX,YARG,6,MIN)	F 38
STX=INTER(Y,DTX,YARG,6,MIN)	E 39
SMUX=INTER(Y,DMUX,YARG,6,MIN)	E 40
SALFX=INTER(Y,DALFX,YARG,6,MIN)	E 41
STPX=INTER(Y,DTPX,YARG,6,MIN)	E 42
KL=I	E 43
RETURN	E 44
3 SU=U(I)	E 45
SUP=UP(I)	EE 46
SUPP=UPP(I)	EE 47
ST=T(I)	E 48
STP=TP(I)	EE 49
STPP=TPP(I)	EE 50
SPRAND=PRANDL(I)	E 51
SMU=MU(I)	E 52
SMUP=MUP(I)	F 53
SALFA=ALFA(I)	E 54
SALFP=ALFAP(I)	E 55
IF (MOD.EQ.1) GO TO 4	E 56
SUPX=DUPX(I)	E 57
STX=DTX(I)	E 58
STPX=DTPX(I)	E 59
SMUX=DMUX(I)	E 60

```

SALFX=DALFX(I) E 61
SV=V(I) E 62
SUX=DUX(I) E 63
SVX=DVX(I) E 64
SVP=VP(I) E 65
SVPP=VPP(I) F 66
KL=I F 67
RETURN E 68
CONTINUE E 69
SV=0.0 E 70
SVP=0.0 E 71
SVPP=0.0 E 72
SVX=0.0 F 73
SUX=0.0 E 74
SUPX=0.0 F 75
STX=0.0 E 76
STPX=0.0 E 77
SMUX=0.0 E 78
SALFX=0.0 E 79
KL=I E 80
RETURN E 81
END E 82-
REAL FUNCTION INTER(X,Y,XARG,IDEGL,MIN) G 1
DIMENSION X(151), Y(151) G 2
1 FACTOR=1.0 G 3
MAX=MIN+IDEGL G 4
DO 2 J=MIN,MAX G 5
IF (XARG.NE.X(J)) GO TO 2
INTER=Y(J) G 6
RETURN G 7
2 FACTOR=FACTOR*(XARG-X(J)) G 9
YEST=0.0 G 10
DO 4 I=MIN,MAX G 11
TERM=Y(I)*FACTOR/(XARG-X(I)) G 12
DO 3 J=MIN,MAX G 13
3 IF (I.NE.J) TERM=TERM/(X(I)-X(J)) G 14
4 YEST=TERM+YEST G 15
INTER=YEST G 16
RETURN G 17
END G 18-

```

1. Report No. NASA CR-3544	2. Government Accession No.	3. Recipient's Catalog No.	
4. Title and Subtitle  GOERTLER INSTABILITY IN COMPRESSIBLE BOUNDARY LAYERS ALONG CURVED SURFACES WITH SUCTION AND COOLING		5. Report Date April 1982	
7. Author(s)  Nabil El-Hady and Alok K. Verma		6. Performing Organization Code	
9. Performing Organization Name and Address  Old Dominion University Norfolk, VA 23508		8. Performing Organization Report No.	
12. Sponsoring Agency Name and Address  National Aeronautics and Space Administration Washington, DC 20546		10. Work Unit No.	
		11. Contract or Grant No. NSG-1645	
		13. Type of Report and Period Covered Contractor Report	
		14. Sponsoring Agency Code	
15. Supplementary Notes  Langley Technical Monitor: William D. Harvey Final Report			
16. Abstract  The Goertler instability of the laminar compressible boundary layer flows along concave surfaces is investigated. The linearized disturbance equations for the three-dimensional, counter-rotating streamwise vortices in two-dimensional boundary layers are presented in an orthogonal curvilinear coordinate. The basic approximation of the disturbance equations, that includes the effect of the growth of the boundary layer, is considered and solved numerically. The effect of compressibility on critical stability limits, growth rates, and amplitude ratios of the vortices is evaluated for a range of Mach numbers for 0 to 5. The effect of wall cooling and suction of the boundary layer on the development of Goertler vortices is investigated for different Mach numbers.			
17. Key Words (Suggested by Author(s))  Boundary layer Stability Transition		18. Distribution Statement  FEDD Distribution  Subject Category - 34	
19. Security Classif. (of this report) Unclassified	20. Security Classif. (of this page) Unclassified	21. No. of Pages 120	22. Price

Available: NASA's Industrial Applications Centers

NASA-Langley, 1982